Interactions and Photocatalytic Reactions of Organochlorine Compounds at the Nanoparticulate TiO_2 Surface: A FTIR Study

Von der Naturwissenschaftlichen Fakultät

der Gottfried Wilhelm Leibniz Universität Hannover

zur Erlangung des Grades

Doktor der Naturwissenschaften

Dr. rer. nat.

genehmigte Dissertation

von

Elias Tauchert, Mestre

geboren am 01.03.1982 in Cunha Porã – Brasilien

2012

Referent:	Prof. Dr. Thomas Scheper
	Institut für Technische Chemie
	Gottfried Wilhelm Leibniz Universität Hannover
Korreferent:	Prof. Dr. Jürgen Caro
	Institut für Physikalische Chemie
	Gottfried Wilhelm Leibniz Universität Hannover
Tag der Promotion:	02.03.2012

Erklärung

Ich versichere, dass ich diese Dissertation selbständig verfasst habe und alle benutzen Hilfsmittel und Quellen sowie evtl. zur Hilfeleistung herangezogene Institutionen vollständig angegeben wurden. Diese Dissertation wurde nicht als Diplomarbeit oder ähnliche Prüfungsarbeit verwendet.

Hannover, im Dezember 2011

Danksagung

Ich danke Herrn Prof. Dr. Thomas Scheper und Herrn Prof. Dr. Detlef Bahnemann für die Möglichkeit am Institut für Technische Chemie meine Promotion anfertigen zu können und für die Bereitstellung des interessanten, hochaktuellen Themas.

Herrn Prof. Dr. Detlef Bahnemann und Frau Dr. Cecilia Mendive Hansmann danke ich besonders für die Unterstützung und Förderung während der Promotion sowie den Möglichkeiten zur Teilnahme an zahlreichen Tagungen und Workshops.

Der Conselho Nacional de Pesquisa e Desenvolvimento Científico do Brasil (CNPq) für die finanzielle Untertützung.

Herrn Prof. Dr. Thorsten M. Gesing danke ich für die XRD-Messungen (Institut für Mineralogie).

Weiterhin danke ich allen Arbeitskollegen des AK Bahnemann für die sehr gute Zusammenarbeit und die anregenden Diskussionen und Hilfestellungen. Ich danke meiner Bachelorete Imme Kretschmer, und meinen Austauschstudenten Javier Segarra, Hee Sook Song und Jwa für ihre Arbeiten und damit zu meiner Arbeit geleisteten Beiträge.

Ich danke allen Mitarbeitern des Institutes für Technische Chemie für die sehr gute Zusammenarbeit und die wunderschöne Zeit am Institut. Ganz besonders den Bibliothek Kollegen für die schöne Zeit im dritten Stock.

Ich danke Steffi, Anne S., Jonathan, Anne N. und Sonia für das Korrekturlesen, und für die Zeit die ich mit euch verbringen konnte.

Ganz besonders danke ich Willian G. Menezes für die Unterstützung während der letzten Jahre.

Ich danke meiner Familie und meinen Freunden für die moralische Unterstützung während des gesamten Zeitraumes der Arbeit, besonders meinen geschwister Cristiani und Diogo, und meinem Eltern Marli und Ercio. Besonderen dank auch an Vovó Lorena, Ede, Carla, Claudio, Alana, Sérgio Janis, Marta, Fabienne, Ismet, Ana V., Mike und Estabrak.

Table of Contents

List of Figures

List of Tables

Abbreviations

%	Percent
ºC	Degree Celsius
µL	Micro liter
µm	Micrometer
µmol	Micromole
µg	Microgram
2,4-D	2,4-Dichlorophenoxyacetic acid
Å	Angstrom
ATR	Attenuated Total Reflection
BET	Brunauer, Emmett and Teller
Cm	Centimeter
DCA	Dichloroacetic acid
DRIFT	Diffuse Reflectance Infrared Fourier Transform spectroscopy
et. al.	et alii
etc.	et cetera
eV	electron Volt
FTIR	Fourier Transform Infrared spectroscopy
FWHM	Full Width at Half Maximum
g	Gramm
h	hour
IR	Infrared
IRE	Internal Reflection Element
L	Liter
m	meter
mA	miliampère
AA	Acetic acid
MCA	Monochloroacetic acid
min	minute
mL	milliliter
mm	millimeter
mmol	millimol
N	number of exchangeable OH groups at the titanium dioxide surface

mΩ	milliOhm
nm	nanometer
PMMA	Poly-MethylMethAcrylate polymer
rpm	rounds per minute
s	seconds
TCA	trichloroacetic acid
UV	Ultraviolet
XRD	X-Ray diffraction
zpc	zero proton condition
λ	wavelenght

Abstract

The adsorption and the photocatalytic degradation of dichloroacetic acid and its homologues, mono- and trichloroacetic acids as well as acetic acid, from the aqueous phase on TiO_2 nanoparticles have been investigated. Due to its environmental importance, an analogous study has been performed employing the pesticide 2,4-dichlorophenoxyacetic acid. The investigations have been performed using the Attenuated Total Reflection - Fourier Transformed Infrared (ATR-FTIR) spectroscopy. Films of TiO_2 have been deposited onto a ZnSe crystal. The oxide/solution interface investigation has been performed in two systems, i.e., a flow cell and a batch reactor. These reactors have been attached to a support containing the crystal.

Due to the bad fitting of the Langmuir isotherm model observed for the adsorption curves of dichloroacetic acid, a new model to describe the adsorption has been proposed. This model considers the formation of structures at the TiO_2 surface, which involves different adsorption sites and adsorption modes. The so called modified Langmuir model considers the formation of complexes involving adjacent molecules.

The adsorption of dichloroacetic acid on the TiO_2 in the dark occurs in a two steps process. Firstly, with the formation of a bond via the carboxylate group, which forms mono- or bidentate structures on the oxide surface. These structures flip at the surface and interact with the surface through the CCl_2H group. The stabilization of the complexes involves also adjacent structures. The newly formed complexes are able to interact with molecules from the solution bulk as well, increasing the adsorption potential of the powders. It is assumed that different adsorption sites at the TiO_2 surface are involved in the adsorption process.

Due to the low intensity of the spectral signals recorded for dichloroacetic acid it is almost impossible to propose a detailed photodegradation mechanism. However, employing high bulk concentrations new adsorption possibilities have been observed during the irradiation periods. This are probably related to the disaggregation of the TiO_2 agglomerates, which expose different facets of the particle surface for the adsorption of new molecules. Anatase exhibits more intense changes in the spectral behavior than rutile, because of its lower particle size and higher degree of aggregation.

The adsorption of acetic and trichloroacetic acid on TiO_2 is not as strong as monochloroacetic acid. Monochloroacetic acid is the only molecule still showing spectral signals after longer adsorption times. Apparently, there is no correlation between the molecular structures of the acids and their adsorption and photodegradation behavior.

The adsorption experiments involving 2,4-dichlorophenoxyacetic acid demonstrate an intense dependence on the pesticide concentration. The assignment of the bands observed in these studies indicates at least two types of interaction between the TiO_2 surface and the molecule. One at low bulk concentrations, with the formation of adsorption structures interacting only weakly with the surface. The second possibility takes place at high concentrations, with the formation of structures which are closely packed and stabilized by interactions with adjacent molecules.

Keywords: Attenuated Total Reflection - Fourier Transformed Infrared, adsorption, 2,4-dichlorophenoxyacetic acid, dichloroacetic acid.

Zusammenfasung

In der vorliegenden Arbeit wurden die Adsorption und die photokatalytische Reaktion von Dichloressigsäure, sowie von Essigsäure, Monochloressigsäure und Trichloressigsäure in wässrigen Lösungen auf der Oberfläche von TiO_2 Nanopartikeln untersucht. Aufgrund seiner Bedeutung für die Umwelt, wurden diese Untersuchungen ebenfalls mit dem Pestizid 2,4-Dichlorphenoxyessigsäure durchgeführt. Für die Untersuchungen wurde abgeschwächte Totalreflexion - Fourier-transformierten Infrarot Spektroskopie verwendet. Beschichtungen von TiO_2 wurden auf einem ZnSe-Kristall abgelagert. Die Untersuchungen der Oxid/Lösung-Schnittstelle wurden in zwei Systemen durchgeführt: in einer Messzelle und in einen Batch-Reaktor. Diese Reaktoren wurden auf dem ZnSe-Kristallhalter fixiert.

Aufgrund der schlechten Übereinstimmung der experimentell ermittelten Daten der Adsorptionsisothermen mit dem Modell von Langmuir, wurde ein neues Modell, dass „modified-Langmuir-modell“ entwickelt. Bei diesem neu entwickelten Modell wird angenommen, dass verschiedene Adsorptionsplätze belegt werden und über die Bildung von Oberflächenkomplexen unterschiedliche Adsorptionsstrukturen gebildet werden.

Der Mechanismus der Adsorption von Dichloressigsäure auf einer TiO_2-Oberfläche besteht aus zwei-Schritten. Der erste Schritt, ist die Bindung von Dichloressigsäure über die Carboxyl- gruppe, die einzähnige oder zweizähnige Strukturen auf der Oxidoberfläche bildet. Diese Strukturen drehen sich um, und interagieren durch die CCl_2H Gruppe mit der Oberfläche. Die Stabilisierung der Komplexe umfasst auch angrenzende Strukturen. Die neu gebildeten Komplexe sind in der Lage, auch mit in der Lösung vorhandenen Molekülen zu interagieren. Es wird davon ausgegangen, dass verschiedene Adsorptionsplätze der TiO_2-Oberfläche an der Adsorption beteiligt sind.

Aufgrund der geringeren Signalintensität des für Dichloressigsäure aufgezeichneten Spektrums, ist es nahezu unmöglich einen detaillierten photokatalytischen Abbaumechanismus vorzuschlagen. Allerdings werden bei Beleuchtung, von Lösungen mit höheren Säurekonzentrationen, neue Adsorptionsmöglichkeiten wahrgenommen, welche vermutlich im Zusammenhang mit den verschiedenen Kristallflächen der Partikel stehen. Die neuen Kristallflächen werden durch Auflösen der TiO_2 Agglomerate freigegeben. Anatas weist wegen seiner geringeren Partikelgröße und seinem höheren Aggregationsgrad eine intensivere Veränderung im spektralen Verhalten auf, als Rutil.

Die Adsorption von Essigsäure und Trichloressigsäure an TiO_2 ist nicht so stark wie die von Monochloressigsäure. Monochloressigsäure ist das einzige Molekül, das auch nach längeren Adsorptionszeiten noch spektrale Signale zeigt. Offensichtlich gibt es keine Korrelation zwischen den molekularen Strukturen der Säuren und deren Adsorptions- und photochemischen Verhalten.

Die Adsorption Experimente mit 2,4-Dichlorphenoxyessigsäure zeigen eine intensive Abhängigkeit der Pestizid Konzentrationen. Die Zuordnung der in diesen Studien beobachteten Banden zeigt mindestens zwei Arten der Interaktion zwischen der TiO_2-Oberfläche und des Molekül. Bei niedrigen Konzentrationen tritt die Bildung von Adsorption-Strukturen, die schwach mit der Oberfläche interagieren, auf. Die zweite Möglichkeit, die bei hohen Konzentrationen stattfindet, ist die Bildung von dicht gepackten Strukturen, die über Wechselwirkungen mit benachbarten Molekülen stabilisiert werden.

Schlagworte: abgeschwächte Totalreflexion - Fourier-transformierten Infrarot Spektroskopie, Adsorption, 2,4-Dichlorphenoxyessigsäure, Dichloressigsäure.

1 Introduction

During the last decades a significant increase of the world's population has been observed creating a lot of consequences concerning the social structure as well as different sectors of the world's economy. From agriculture to industry, all the economical sectors are constantly looking for new technologies to supply the growing demand.

Various modifications have been established to cultivation methods of agricultural products in order to provide adequate grains and sufficient food, to meet the increasing demand. One of the most important modifications in cultivation processes is the use of chemical substances to prevent the increasing impact of plagues. These substances are also known as agrochemicals or pesticides and posses due to their chemical nature, a high pollution potential, derived in part from their characteristics: such as their resistivity to natural degradation, their high mobility in the environment, and their toxicity (especially for organochlorine and organophosphates). The corresponding residues contain recalcitrant substances, which are very difficult to treat using large scale processes employed for the wastewater treatment of industrial plants.

By enhancing the production of goods according to the growing rate of population, unfortunately, environmental pollution und damage caused by the use of agrochemicals increases as well.

Therefore, new technologies for the treatment of these resistant compounds are required. One of the most promising processes is the heterogeneous photocatalysis using TiO_2. This process shows an elevated mineralization rate of organic molecules with the possibility to use solar radiation, even allows a reduction of the treatment costs. Due to its resistivity to chemical attack or photo corrosion, its low cost and especially the low consumption of energy TiO_2 has been found to be a very attractive photocatalyst [1].

Dealing with the development of semiconductors that can degrade these compounds effectively, the understanding of the degradation paths is extremely relevant. The importance of the adsorption for this process is still dubious [2], therefore, one of the main points of this work is to understand which role the adsorption of monocarboxylated acids on TiO_2 plays for the photocatalytic degradation process.

2 Fundamentals

2.1 Environmental Problem

2.1.1 Agrochemicals

The need to increase food production, especially in the 20th century, has led to the improvement of technologies for the production of crops. Special significance has been given to the mechanization of the agricultural equipment, to the use of fertilizers as well as to the use of chemicals, known as agrochemicals, to control various pests and weeds. All of the factors mentioned above have contributed to a substantial increase of the production of crops, thus reducing the likelihood of food scarcity on the planet.

Agrochemicals contribute significantly to this progress. They are applied in the control of various pests that devastate plantations, reducing the losses caused by the attack of insects and fungus or the presence of weeds, making the use of mechanical instrumentation easy. This makes it cheaper and more practical to plant, handle and harvest crops.

Unfortunately, the indiscriminate use of agrochemicals is a threat to farmers, the environment and the population in general, mainly because of the inherent toxicity of these compounds, and because of the products generated by their biotransformation through the metabolism of microorganisms present in the environment. Often the compounds formed here are more toxic than the initial species [3]. Additionally, these structures can be biomagnified, causing huge alterations of the diverse trophic levels, leading in some cases, to mutagenic and carcinogenic effects [4]. The persistence of the agrochemicals in the environment, where they remain in some cases for months or years [5], also appreciably increases their adverse side effect.

The growing use of agrochemicals implies also an increase in their industrial production, and like for other industrial activities, these production plants generate enormous amounts of effluents contaminated not only with agrochemicals but also with intermediates of their production [6].

Some of the most commonly used agrochemicals worldwide are chlorinated compounds (diuron, pentachlorophenol and 2,4-dichlorophenoxyacetic acid) [7] which are highly toxic. Furthermore, chlorophenolic structures often occur as intermediates during their production or their degradation processes [3]. Chlorinated compounds have been considered to be responsible for some serious environmental contamination phenomena, because of their toxicity, their recalcitrance towards natural degradation and their persistence in the environment, where they tend to undergo biomagnifications [8]. These compounds are frequently found in the soil and in surface and/or underground water [9].

Some countries have established limiting values for discarding effluents to the environment, as well as for drinking water. In the European Union the limits for agrochemical concentrations in drinking water, as established through the EEC Directive 80/778, is 0.1 $\mu g \cdot L^{-1}$ for each individual agrochemical and 0.5 $\mu g \cdot L^{-1}$ for the total amount of pesticides [10].

2.1.1.1 2,4-Dichlorophenoxyacetic Acid (2,4-D)

2,4-Dichlorophenoxyacetic acid is possibly the most widely investigated herbicide concerning its impact for environmental pollution, its structure is shown in Figure 1. It has a complex vibrational spectrum with contributions of different molecular groups; including the carboxylate moiety and groups related with the aromatic ring and the substituted chlorine atoms.

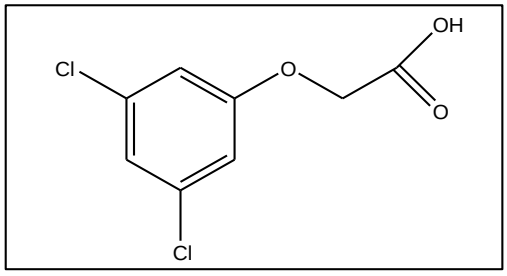

Figure 1: Molecular structure of 2,4-Dichlorophenoxyacetic acid (2,4-D).

2,4-D is one of the most commonly used herbicides worldwide. This herbicide belongs to a larger class of substances known as the phenoxyl herbicides, which have provided control

of broadleaf weeds in both agricultural fields and non-cropland grasses for the past 50 years. Farmers rely profoundly on the use of herbicides and pesticides to maximize crop yields. This dependence on 2,4-D and other herbicides by the agricultural industry will not decline, guaranteeing the continued application of these compounds in large amounts (millions of Kg per year). This massive reliance on herbicides has led to measurable herbicide levels in natural bodies of water, which supply the human population with fresh drinking water [11, 12].

An amount of the contamination of natural waterways originates from agricultural field runoff, since many herbicides and pesticides exhibit solubility in water. 2,4-D readily dissolves and dissipates in surface waters but can also be transported through the atmosphere during airborne application. When herbicides reach the water supply, natural degradation processes, such as UV light induced degradation or biodegradation by microorganisms, may initiate the breakdown of these compounds. The persistence of the compounds varies according to many factors of the water environment: UV light, pollutant concentration, level of microorganisms, oxygen level, temperature, and so forth [13-15]. The half-life of 2,4-D can be as short as 4-10 days; however, 2,4-D and its natural degradation products may also persist for several weeks [16].

Although the toxicity risks of 2,4-D are not completely known, the World Health Organization has established a guideline value of 30 $\mu g \cdot L^{-1}$ for drinking water. Measurable levels of herbicides are continually detected in natural waters, evincing that the herbicide usage has surpassed the ability of the ecological systems to degrade these organic contaminants [16].

However, 2,4-D pollution levels in the environment are significantly reduced due to the advancement in treatments methods and steadily increasingly stringent regulations. Due to its environmental importance the investigation of new degradation processes for the elimination of 2,4-D has been intense in the last decades, and also the use of AOPs like photocatalysis has been studied [9, 17-19]. Since both, the initial 2,4-D concentration and the properties of the TiO_2 catalyst significantly influence the degradation kinetics and the mineralization efficiency [18, 19], an investigation concerning the photocatalytic decomposition of 2,4-D at low concentration levels employing a new TiO_2 catalyst is imperative [20].

2.1.2 Chloroacetic Acids

Chloroacetic acids are compounds widespread in the environment, that often occur in industrial waste as pollutants as well in chlorinated drinking water as major chlorination by-products [21-26]. Haloacetic acids are degradation products of halogenated compounds of both, natural and anthropogenic origin. Many of these acids are found to be persistent in water. The likely stability of these acids has led to the search for alternative degradation path ways for this group of compounds to understand their fate and potential accumulation in the environment [27]. Chloroacetic acids are carcinogenic and mutagenic [24] and cannot be completely decomposed by biological techniques [21, 26]. One of these resistant chemicals is **D**i**C**hloro**A**cetic acid (DCA), a widely used industrial pollutant also identified as an intermediate in the biological degradation pathway of many chlorinated hydrocarbons.

2.2 Treatment Techniques Currently Used

Several treatment methods are currently used to treat agrochemical residues. In industrial plants the conventional technologies commonly used, such as biological processes, are not always effective [8] since the contaminants are often not biodegradable. Physical-chemical systems such as incineration, filtration by membranes or adsorption on activated carbon involve high costs [28] or only transfer the pollutants from one phase to another [29].

Due to the inefficiency and high costs of the treatment processes for residues containing agrochemicals, new alternatives have been studied in order to reduce the impact of these substances to the environment.

2.3 New Alternatives for the Effluent Treatment

Among the alternatives proposed and developed, the so-called advanced oxidative processes (AOPs) [30, 31] are being studied with increasing curiosity, since they demonstrate advantages over other systems, especially concerning their capacity to mineralize pollutants within reduced treatment times.

One of the most intensively investigated processes is the heterogeneous photocatalysis using TiO_2. This is of the semiconductors that is very effective for the degradation of organic compounds, due to some advantages, for example its high photo-reactivity, non-toxicity, low cost, chemical and biological inertness, and photo-stability [32]. The application of TiO_2 photocatalysis has been widely reported as a promising alternative technology for the removal of various organic and inorganic pollutants from contaminated water and air [33].

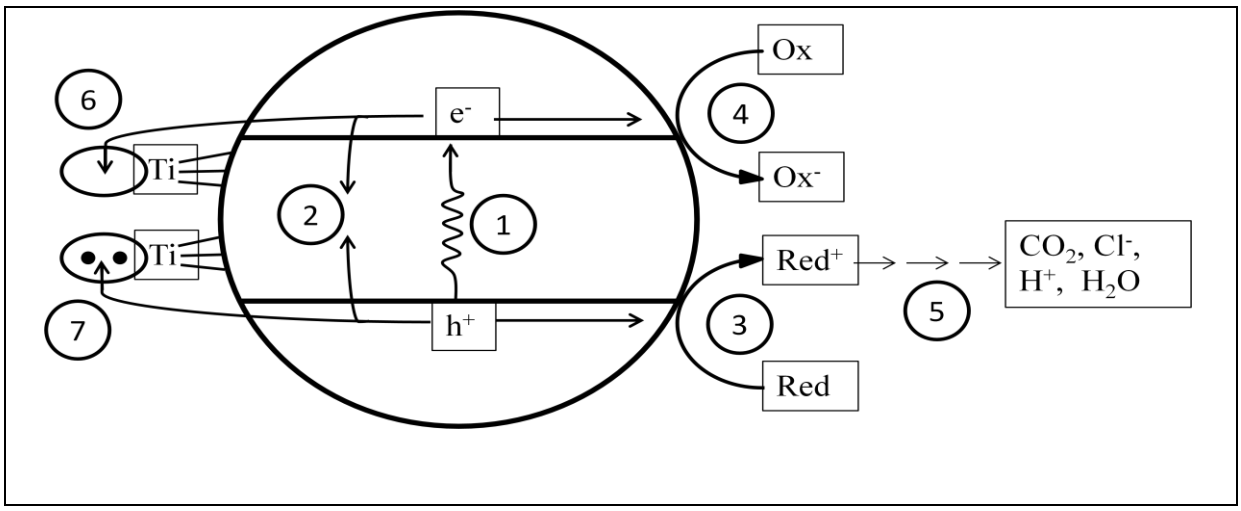

Figure 2: Primary steps in the mechanism of photocatalysis: (1) formation of charge carriers by photon absorption, (2) charge carrier recombination, (3) initiation of an oxidative pathway by a valence-band hole, (4) initiation of a reductive pathway by a conduction-band electron, (5) further thermal (e.g., hydrolysis or reactions with active oxygen species) and photocatalytic reactions to yield mineralization products, (6) trapping of a conduction-band electron at a Ti(IV) site to yield Ti(III), and (7) trapping of a valence-band hole at a surface titanol group (from Mendive *et al.* [2]).

The detailed mechanism of photocatalysis varies for different pollutants, but it is commonly agreed that the primary reactions responsible for the photocatalytic effect are the interfacial redox reactions of electrons and holes (direct photocatalysis) that are photogenerated when the semiconductor catalyst is exposed to light of sufficient energy (see Figure 2) [2]. The mechanism of redox processes induced by light absorption in a photocatalytic system is usually presented in diagrams showing one single semiconductor nanoparticle in which the absorption of a photon with an energy exceeding its band gap energy generates an electron/hole pair (process 1) that either recombines (process 2) or induces two redox processes (processes 3 and 4), which take place in close vicinity on the particle's surface.

Semiconductors, such as TiO_2, have an energy difference between the lower edge of the conduction band and the upper edge of the valence band, defined as their band gap, low enough so that electrons can be excited from the valence band to the conduction by thermal or photonic processes. The following equations illustrate the mechanism of heterogeneous photocatalysis at the TiO_2 surface [34].

The electron hole pair (charge carrier) formation:

$$TiO_2 + h\upsilon \overset{fs}{\rightarrow} e^- + h^+ \qquad \text{Equation 1}$$

Once formed the charge carriers are trapped (equations 2 and 3), illustrated also in Figure 2 (Step 2 and 3):

$$e^- + \equiv Ti^{IV}OH \overset{ps}{\rightarrow} [Ti^{III}OH] \qquad \text{Equation 2}$$

$$h^+ + \equiv Ti^{IV}OH \overset{ps}{\rightarrow} [Ti^{IV}OH^{\cdot}]^+ \qquad \text{Equation 3}$$

After the trapping the charge carriers recombine (equations 4 and 5):

$$e^- + [\equiv Ti^{IV}OH^{\cdot}]^+ \overset{ns}{\rightarrow} Ti^{IV}OH \qquad \text{Equation 4}$$

$$h^+ + [\equiv Ti^{III}OH] \overset{ns}{\rightarrow} Ti^{IV}OH \qquad \text{Equation 5}$$

or react with compounds adsorbed at the semiconductor surface (equations 6 and 7):

$$[\equiv Ti^{IV}OH^{\cdot}]^+ + compound\ (D) \overset{ns}{\rightarrow} Ti^{IV}OH + ox.compound\ (D^+) \qquad \text{Equation 6}$$

$$[\equiv Ti^{III}OH\ ] + O_2 \overset{ms}{\rightarrow} \equiv Ti^{IV}OH + O_2^{-\cdot} \qquad \text{Equation 7}$$

This process has been proven to be effective for the degradation of a variety of environmental pollutants [35-41]. In industrial applications, chlorinated aliphatic and aromatic

hydrocarbons have been reduced to less harmful compounds such as inorganic acids, carbon dioxide and water [42-44]. Despite its dependence on reactions that occur at the interface between the solution and the semiconductor, heterogeneous photocatalysis demonstrates also a certain potential for degradation process occurring in the bulk solution. It is assumed that organic pollutants could be oxidized directly by the holes h^+ as well as by hydroxyl radicals $[\equiv Ti^{IV} OH^{\bullet}]^+$ generated at the TiO_2 surface (indirect photocatalysis).

In the overall photocatalytic degradation the oxidation process is usually the one which is more important. Electrons are frequently trapped by substances such as molecular oxygen, the reduction of which culminates with the formation of different species such as superoxide radicals $O_2^{-\bullet}$, superoxide anions OH_2^-, hydrogen peroxide H_2O_2, and hydroxyl radicals $OH^{\bullet}$, all of which should contribute to the oxidation of the organic pollutants.

There is still a considerable deficit concerning the entire understanding of the basic processes that constitute the overall photocatalytic transformation. However, during the past decade, considerable evidence can be found in the literature that the current mechanistic picture is oversimplified. It is therefore of highest importance to gain further knowledge at the fundamental level concerning the underlying mechanisms taking place on classical photocatalytic materials, such as TiO_2, to advance technological approaches and to improve applications [2].

Titanium dioxide is one of the most important metal oxides for technological applications [45]. It is a n-type semiconductor and by far the most important photocatalyst material. TiO_2 can be found in three different crystalline modifications: Anatase, Rutile and Brookite. Other structures exist as well, for example, contunnite, but currently only rutile and anatase play any role for the applications of TiO_2. Both phases are commonly used for photocatalytic application, however, in the last years some photocatalytic activity has been reported for brookite too. Titanium dioxide is therefore commercially available as anatase and rutile powders, with surface areas ranging from 10 to more than 300 $m^2 \cdot g^{-1}$.

Containing two TiO_2 unit cells rutile is thermodynamically the most stable phase with a density of 4.24 $g \cdot cm^{-3}$. Anatase is a metastable phase with a density of 3.89 $g.cm^{-3}$ and contains four TiO_2 units [46]. Anatase is stable at lower temperatures (below 600 °C) and has a higher specific surface area. There is some evidence that the surface energy densities of anatase are generally lower than those of rutile. Theoretical predictions of the relative stability of perfect rutile and anatase surfaces, however, do not result in a coherent picture [47].

Due to the mixed ionic and covalent bonding in the metal oxide systems, the surface structure has an even stronger influence on local surface chemistry as compared to metals or elemental semiconductors. In both structures, i.e., anatase and rutile, the two bonds between the titanium and the oxygen atoms at the aspices of the octahedron are slightly longer. The anatase and rutile structures show as a common basic building block a titanium atom surrounded by six oxygen atoms in a more or less distorted octahedral configuration (see Figure 3).

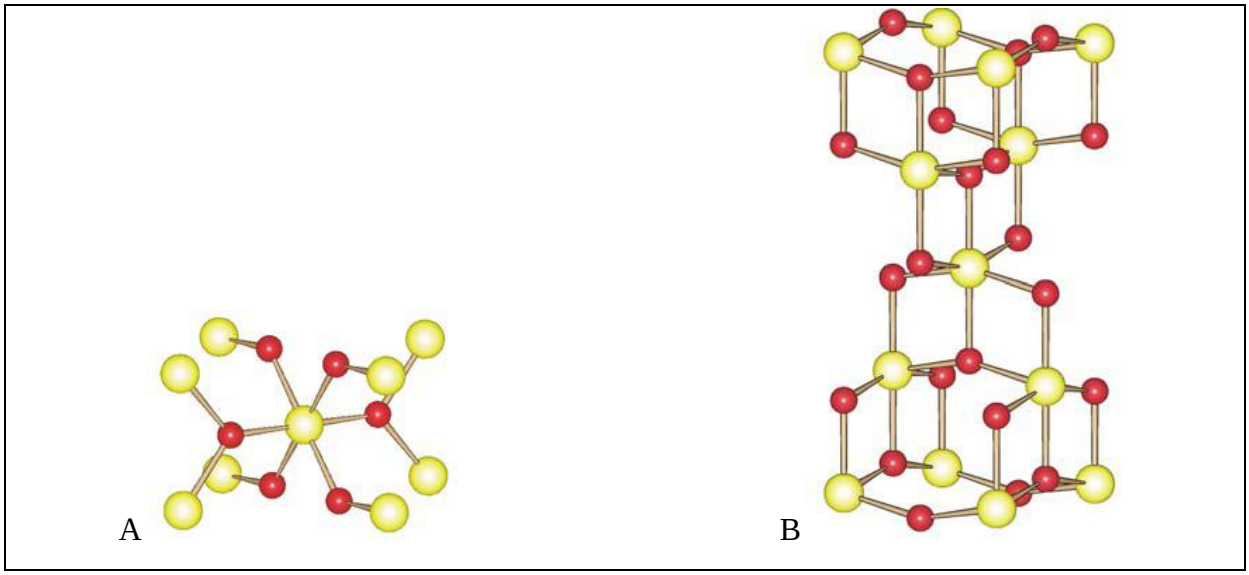

Figure 3: A - Rutile bulk unit cell and B - Anatase bulk unit cell. Ti and O atoms are represented by yellow and red spheres, respectively. (extracted from Mendive [46]).

While both structures have a tetragonal unit cell ($a = b \neq c$), anatase differs from rutile by the space group [47]: Anatase: $D_{4h}^{19} - I4_1/amd$, with a = b = 3.782 Å and c = 9.502 Å; Rutile: $D_{4h}^{14} - I4_2/mnm$ with a = b = 4.584 Å and c = 2.953 Å.

Anatase is the photocatalytically most active polymorph of TiO_2 and plays an essential role in many contemporary environmental and energy-related problems [48]. The band gap energy for anatase is about 3.2 eV and for rutile 3 eV, which corresponds to illumination with wavelengths of 387 nm and 413 nm, respectively [49].

Due to their high surface area nanoscale powders, are frequently used in photocatalysis being mainly composed of anatase. The shape of these nanocrystals is directly influenced by the method of preparation and can thus vary with both, the synthesis process as well as the

synthesis conditions. Hence findings concerning one material do not allow an extrapolation to other materials [50].

The minor knowledge of the real shape of commercial anatase powder particles forces researchers to catch at a straw and to rely on data gained from arbitrary synthesis or even from macroscopic anatase crystals. Moreover, fine powders exhibit high specific surface areas that are desirable for photocatalytic applications. In this connection there is a growing need for precise microstructural investigations on exactly these powders [50].

A better knowledge concerning the relationship between the abundance of specific crystal facets and the photocatalytic efficiency would enable the tailoring of catalysts that show predominantly those surfaces that for specific reactions are catalytically most active.

Named after the greek words “ana” (up or ex) and “tase” (tension) with respect to the peculiarly elongated shape of the tetragonal bipyramid, it has been known for quite some time that even macroscopic anatase occurs in many different shapes, depending on the chemical environment of the mineralogical deposit . Its structure can be different from that of classical macroscopic anatase, which is a tetragonal bipyramid that exhibits more than 95 % of its surface as eight facets of the type (101) and may be truncated by two (001) type facets at the tips, see Figure 4 [47]. Moreover, theoretical calculations predict that the stability of the anatase surfaces follows the increasing order (101) > (100) > (001) > (103) > (110). Those facets are therefore widely assumed to be exposed as the majority on the anatase particle surfaces.

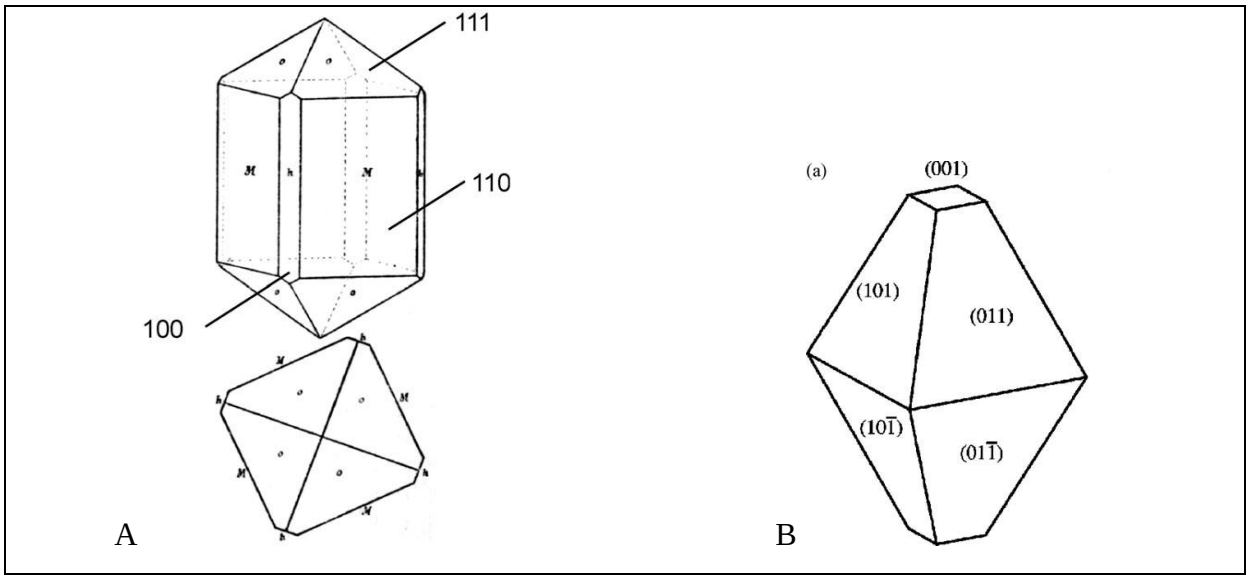

Figure 4: Shape of a macroscopic rutile crystal (A) [51], and of the anatase structure (B) [47].

It is important to note that for anatase nanoparticles the stability of the (100) face by far exceed that of the other faces as in evidence from the experimental results observed by Feldhof et al. [50] for commercial powders provided by the Crystal Global. On the anatase (100) surface five-fold coordinated Ti atoms are exposed as well as three- and two-coordinated O atoms. However, also six-fold Ti atoms and three-fold O atoms are present [52].

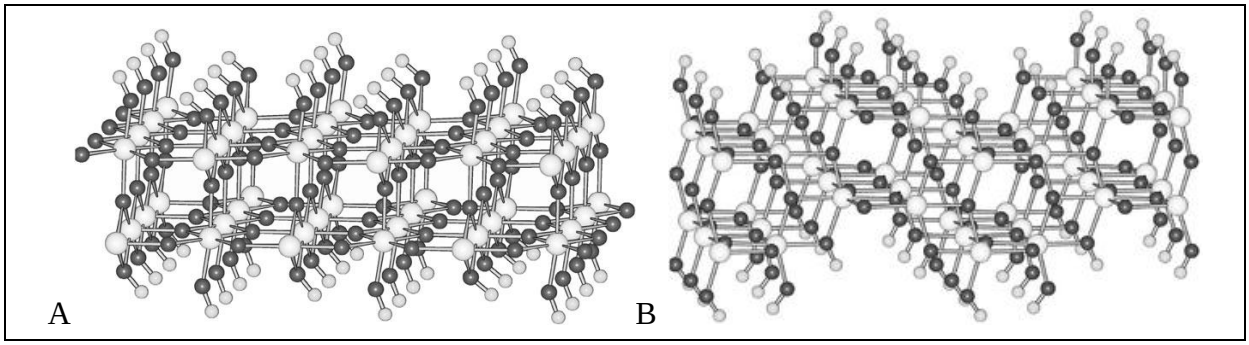

Figure 5: A - Rutile (110) and B - Anatase (100) cyclic clusters with a full coverage of water molecules. Ti, O and H atoms are represented by large light, dark and small light grey spheres respectively. Extracted from Mendive *et al.* [53].

In the case of rutile, which's name derives from the Latin word for red, *rutilus*, the situation is simpler. Because both, experimental observations and theoretical calculations

agree in that either in naturally occurring crystals or nanoparticles the most exposed face is the (110) facet [50, 53]. Other minor exposed surfaces are (100), (001) and (011). Figure 5 shows both, rutile (110) and anatase (100) clusters with a full coverage of water molecules.

Titanium dioxide is like most the metal oxides an amphoteric material and therefore contains positively and negatively charged groups on its surface. The distribution of these charges depends on several factors such as the polarization of water molecules in the electric double layer and charge parameters, for example, the ionic radius of the metal cation. Other factors influencing the character of the metal-oxygen bond are the coordination number, the filling of the d-orbitals and the nature of other ligands [54, 55].

It is expected that the pH of the solution can play a role in the adsorption process in at least two ways. Oxide surfaces are generally covered with surface hydroxyl groups. The nature of the titanium dioxide surface will depend on the pH according to the following equations:

$$-TiOH_2^+ \rightleftarrows -TiOH + H_s^+ \qquad K_{a1} \qquad \text{Equation 8}$$

$$-TiOH \rightleftarrows -TiO^- + H_s^+ \qquad K_{a2} \qquad \text{Equation 9}$$

where K_{a1} and K_{a2} are the dissociations constants for acidic and alkaline OH groups at the titanium dioxide surface and H_s^+ denotes a proton close to the surface. The multivalent hydroxo metal complexes are able to release H^+ ions (deprotonation) from the water molecules absorbed at the surface or to adsorb H^+ ions thus protonating the surface. This behavior enables the surface to act either like a proton acceptor or a proton donor.

Since the equilibrium of the OH groups at the surface is controlled by the equations mentioned above, K_{a1} and K_{a2} can be used to calculate the pH values for each deprotonation. The estimation of the condition at which all OH groups at the surface are neutral, gives the so called **z**ero **p**roton **c**ondition (zpc) of the surface. This point is the average value between both protonation constants, and varies for different TiO_2 samples with values from 3.0 to 8.0. The zpc of PC500 is reported to be approximately 6.0 [56]. To illustrate the distribution of surface species on TiO_2 curves have been calculated from the average constants of dissociation extracted from [57], with $pK_{a1} = 3.6$ and $pK_{a2} = 8.8$, yielding a pH_{zpc} of 6.2.

Figure 6 shows the distribution of the hydroxyl groups at the surface of anatase as a function of the pH condition, obtained from calculations by Rudzinski *et al.* [57].

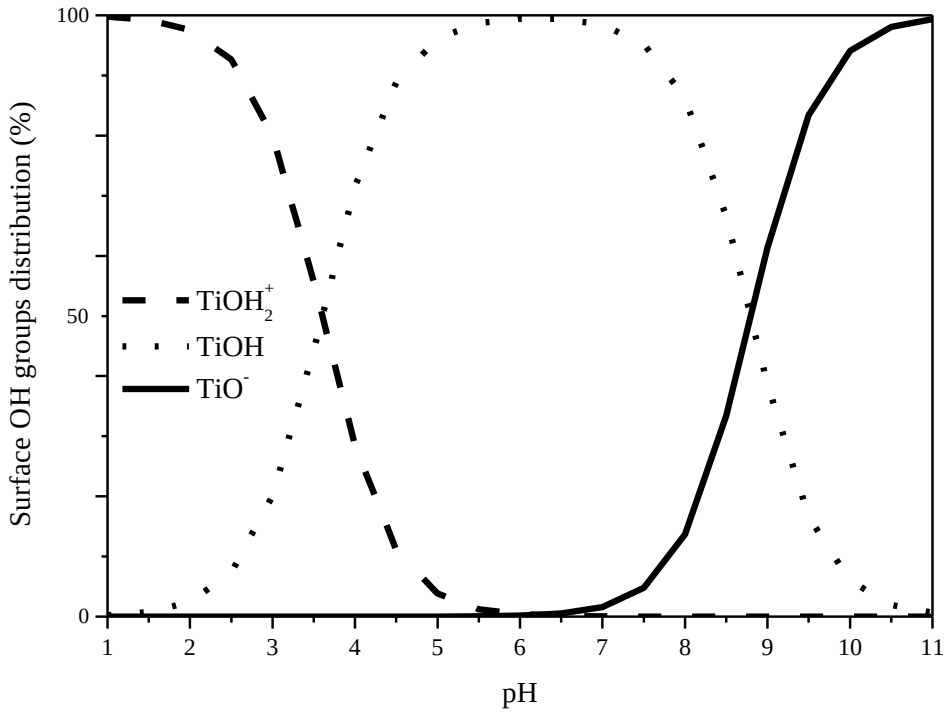

Figure 6: Distribution of the OH groups at a titanium dioxide surface as a function of the pH condition: $TiOH^{2+}$ (– –), TiOH (……) and TiO^- (——) calculated from its dissociation constants reported by Rudzinski *et al.* [57].

An appropriate estimation for the distribution of OH groups at the TiO_2 surface is shown in Figure 7. At pH values below the zpc the OH groups at the TiO_2 surface anatase are mostly positive charged (Figure 7 A). Around the zero point of charge the surface is almost neutral (Figure 7 B), and negatively charged above this pH condition (Figure 7 C).

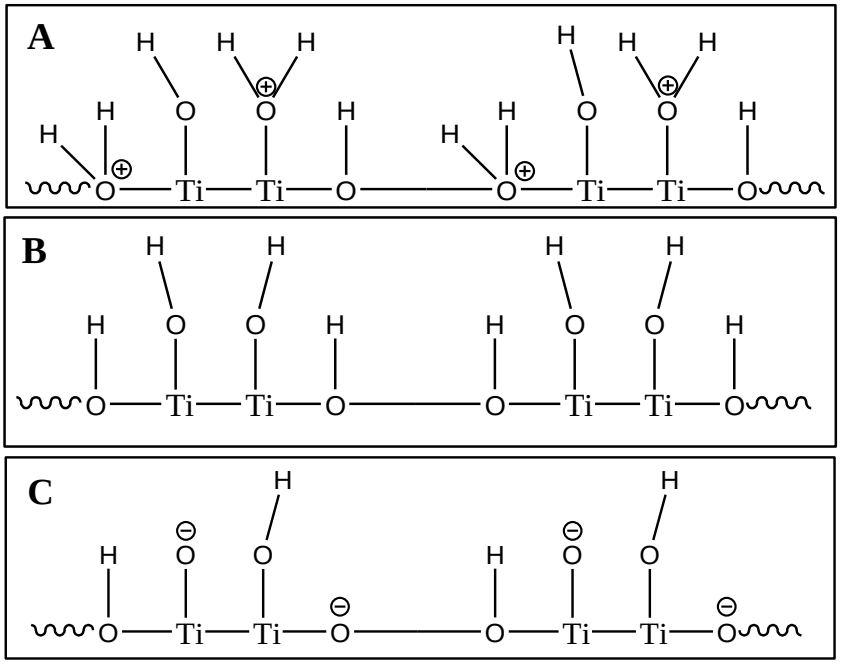

Figure 7: Schematic representation of a TiO_2 surface (anatase (100)) positively charged (A), neutral surface (B) and negatively charged (C).

In aqueous systems adsorption is often described as inner sphere versus outer sphere complexation [55, 58]. Generally, inner-sphere interaction is described as specific adsorption, whereas the outer sphere complex deals with non-specific adsorption [55]. Solvent molecules can, for example, occupy spaces between the surface and the adsorbate.

The specific interfacial conditions, however, apparently are one of the most important determinants for the photocatalytic degradation. Different parameters as, for instance, the charge distribution on the titanium dioxide surface, the affinity of the organic molecules to the semiconductor, the ionic strength, and the pollutant concentration play important roles for the degradation process. The number of active sites for the trapping the holes is determined by the crystalline structure of the TiO_2 particle and by its specific surface area, both of which depend on the size of the particle and on the nature of its surface [33].

DCA has been used as the model pollutant by many research groups for the study of fundamental photocatalytic mechanisms [59], the influence of operating variables on solar photocatalytic processes [60, 61], for kinetic modeling and photo reactor design [62], to compare the activity of new TiO_2 photocatalysts [63, 64], and also to assess the activity of supported TiO_2 [65-68].

Due to its physical properties such as high solubility in water and low volatility, its analysis in aqueous solution systems is facilitated. Additionally, due to its low dissociation constant ($pK_a = 1.48$) DCA is almost exclusive found in the dissociated form at pH values higher than 3.0. This fact enables the investigation of the structures/complexes formed at different pH values, since the pH is known to have a strong influence also on the properties of the titanium dioxide surface.

Decomposition of mono-, di- and trichloroacetic acid in aqueous titania suspensions was extensively studied by several research groups [21, 27, 64, 69, 70]. Based upon different experimental evidence, various proposals have been made concerning the underlying reaction mechanism, particularly regarding the primary steps of the photocatalytic decomposition of chloroacetic acids [33].

It has been concluded that two types of reactions may be responsible for the TiO_2 mediated photodegradation of chloroacetic acids: (1) direct reactions between the photogenerated charge carriers and the organic molecules [62, 69, 71] and (2) reactions of hydroxyl radicals or other oxygen containing radicals with the organic molecules [70, 72].

DCA and **M**ono**C**hloro**A**cetic acid (MCA) are readily decomposed over UV-irradiated TiO_2 catalysts in aqueous media forming CO_2 and HCl [70, 73-75]. On the other hand, using bare TiO_2 **T**ri**C**hloro**A**cetic acid (TCA) is degraded with a very low efficiency [70]. TCA has no C–H bond, and such a molecule has been found to be hardly reactive in TiO_2-based photocatalytic systems [70, 72]. The understanding of its surface behavior is, however, still of enormous importance. Chloroacetic acids are therefore optimal objects for the investigation of applicability of the heterogeneous photocatalysis for the degradation of chloroacetic acids. The study of the mechanism of these photoreactions is considered as an important research topic [33].

For a better understanding of the behavior of adsorbed molecules at the titanium dioxide surfaces, not only in thermally equilibrated systems but also when the semiconductor is illuminated, different analytical methodologies have been proposed to follow the reactions in situ. One of the most promising methods to the study the TiO_2/water interface is the **A**ttenuated **T**otal **R**eflection (**ATR**) technique coupled to a **F**ourier **T**ransform **I**nfra**R**ed (**FTIR**) spectrophotometer.

2.4 Attenuated Total Reflection (ATR) Device Coupled to the Fourier Transformed InfraRed (FTIR) Spectroscopy

Infrared spectroscopy is a powerful method to study adsorbed species on solid surfaces. This method can provide precious information concerning the molecular structure and the orientation as well as about the adsorption strength of surface species.

However, the use of infrared spectroscopy for aqueous systems is not an easy task, especially due to the strong infrared absorption of water itself. This difficulty can be overcome to a large extent by using internal reflection techniques, in which evanescent infrared waves penetrate only into a thin layer of the aqueous solution up to a thickness of a few micrometers from the surface of the **I**nternal **R**eflection **E**lement (IRE), hence the infrared absorption of water can be minimized [76].

During the past several years ATR-FTIR spectroscopy has been used as an "*in situ*" method of examining the chemical nature of interfacial complexes in aqueous suspensions. While this technique provided a great deal of qualitative information concerning the interaction of surfaces with different ligands, however, until now it has been unable to define these systems quantitatively.

In ATR spectroscopy, the probe radiation is an exponentially decaying wave that extends from the IRE into the sample. Because the sampling mechanism arises from reflection phenomena, the profile of the absorption bands in the ATR spectra is influenced by factors other than concentrations and oscillator strengths, such as the thickness and the homogeneity of the sample, the optical constants (absorption index and refractive index) of the sample, and the refractive index of the IRE.

ATR-FTIR spectroscopy of thin particle films immersed in solution is a powerful method for revealing the details of chemical reactions at the solid-solution interface [77, 78]. Metal oxide films on IRE crystals increase the sensitivity of ATR-FTIR measurements due to their large surface area that can concentrate analyte at the interface [79], permitting direct adsorbate/surface interactions to be monitored [80, 81].

Very recently, different studies have been performed concerning the adsorption of different organic acids at photocatalytically active semiconductors [52, 82-85]. In some cases the photocatalytic degradation has also been followed [86-88]. McQuillan *et al.* applied the

single internal reflection technique employing a ZnSe prism as IRE to investigate ionic surfactants, aromatic carboxylic acids, phosphates or bacteria adsorbed on various metal oxides such as TiO_2, ZrO_2 and Al_2O_3 in aqueous media [89].

2.4.1 History and Principles

When radiation enters a medium with a higher refractive index than the surroundings, it will be trapped inside provided that the angle of reflection at the surface of the medium exceeds a particular "critical angle" due to a phenomenon called total internal reflection. A standing wave is established at the reflecting interface, and under the proper conditions all the energy is reflected at this surface and propagated through the medium. This phenomenon has been known for a long time and was first studied by Isaac Newton.

Newton made the important observation that the electromagnetic field extended beyond the reflecting interface. In fact, if the radiation is visible light, an object brought close to the outer surface of the reflecting interface will be illuminated. Since the light is totally reflected inside the medium, the electromagnetic field outside must be non-propagating thus involving no energy loss for the total internal reflection. The electromagnetic field extending beyond the reflecting interface is called evanescent wave. That name derives from the Latin word *evanescere*, which means "vanish or pass away like a vapour".

This non-propagating evanescent wave decays exponentially in amplitude as function of the distance from the reflecting interface. For total internal reflection no energy is withdrawn from this evanescent field, however, energy can be extracted, and this is the basis of the Attenuated Total Reflection technique.

The first reported experiments employing ATR spectroscopy have been performed in the 1930s by Taylor and co-workers [90, 91]. These researchers used prisms as IRE and passed visible light through them in order to measure the refractive index and the absorption spectra of potassium permanganate solutions.

The modern development of ATR spectroscopy, however, started in the late 1950s, initiated by experiments of two independent research groups. N. J. Harrick working at Philips Laboratories in New York found that infrared absorption could be obtained by the use of an IRE made of germanium in contact with a substance exhibiting a lower refractive index [76,

92], while J. Fahrenfort at Shell Laboratories in Amsterdam dealed with the need for recording infrared spectra of weakly or strongly absorbing or intractable materials, and developed the internal reflection technique to ensure that a sample could be brought in contact with an IRE and obtain a spectrum without any tedious sample preparation [93].

This initiation period was followed by a period of relatively slow growth, with the application of the technique being focused on the qualitative and semi-quantitative analysis of a variety of sample types that did not pose serious problems of physical contact to the IRE. In the 1970s new sampling devices were introduced, but it was not until the 1980s that a major upsurge in the application of ATR occurred, including redesign and optimization, further motivated by the widespread implementation of the Fourier Transform analysis for data processing. The development during this time period included the cylindrical IRE and the horizontally mounted IRE. While the first was the central component of newly designed liquid handling systems, the second type was used for solid sampling systems. Thus, devices in the 1990s appeared highly adequate for a rather simple operation, the design permitting rapid emplacement into infrared spectrometers with prealigned optics.

The theory of ATR spectroscopy has been derived in both, a non-rigorous and a rigorous fashion. Some very simple calculations from the non-rigorous theory, already suffice to anticipate or explain the results obtained in the large majority of cases.

A primary parameter is the critical incidence angle Θ, which is the smaller angle formed by the ray and the normal, giving rise to total reflection. Θ is determined only by the ratio of the refractive index of the sample (n_2) and the IRE (n_1).

Calling $n_{21} = \frac{n_2}{n_1}$ Equation 10

$\Theta = arcsin\, n_{21}$ Equation 11

The incident radiation does not enter or exit the sample, as in the case of a reflection. Instead, the radiation penetrates into the sample as an exponentially decaying field or evanescent wave, according to equation 12, where E is the amplitude in the sample at the depth z, γ is a constant, and E_0 is the amplitude at the sample surface ($z = 0$).

$$E = E_0 \cdot e^{-\gamma z}$$ Equation 12

The evanescent wave decays to an intensity of zero ($I = E^2$) only at infinite depth. In practice, the evanescent wave decreases to negligible intensity at rather small distances from the surface of the ATR crystal. The distance from the interface at which the amplitude decays to a value of e^{-1} of its value at the sample surface ($z = 0$) is defined as the depth of penetration d_p (equation 13).

It is a measure of the depth that the radiation penetrates into the sample and defines the thickness the radiation probes.

$$d_p = \frac{\lambda/n_1}{2\pi(sin^2\Theta-(n_{21})^2)^{1/2}}$$ Equation 13

In equation 13, λ is the wavelength of the incident radiation, Θ is the angle of incidence, n_1 and n_2 are the refractive indexes of the IRE and the sample, respectively. Note that $\gamma = 1/d_p$ and that d_p is independent of polarization.

In practical studies d_p is used to estimate the depth that can be probed in the ATR experiments, since it is the depth over which the majority of the spectral information is obtained. The depth of penetration changes linearly with the wavelength of the radiation, as can be noted from equation 13. Therefore, the ATR spectra may differ from the transmission spectra for the same material, showing enhanced signals at longer wavelengths.

It is often of interest to know which thickness of a material is needed to produce a transmission spectrum of equal intensity to the corresponding ATR spectrum. This thickness, d_e, is called the effective thickness. If the radiation of λ_1 is unpolarized, d_e is the average of the parallel and perpendicular components, d_{11} and $d_\perp$:

$$d_e = \frac{d_{11}+d_\perp}{2}$$ Equation 14

The two components are given by equation 15 and equation 16:

$$d_{11} = \frac{n_{21}\cdot\lambda_1\cdot(2\cdot sin^2\Theta - n_{21}^2)\cdot cos\Theta}{\pi\cdot(1-n_{21}^2)\cdot[(1+n_{21}^2)\cdot sin^2\Theta - n_{21}^2]\cdot(sin^2\Theta - n_{21}^2)^{1/2}}$$ Equation 15

$$d_{\perp} = \frac{n_{21}\cdot\lambda_1\cdot cos\Theta}{\pi\cdot(1-n_{21}^2)\cdot(sin^2\Theta - n_{21}^2)^{1/2}}$$ Equation 16

Values for the effective thickness for a variety of IRE can be found in the literature, as well as sample refractive indexes and spectral wavelengths. The effective sample thickness is defined as the thickness of sample that would give the same absorbance value for a transmission at normal incidence as that obtained in a single reflection infrared spectroscopy measurement. The effective sample thickness is important because it provides a relationship between transmission and internal reflection spectroscopy by permitting the direct comparison of spectral contrasts in the transmission and in the internal reflection spectra.

This attenuated-multiple-reflection is the basic idea of the attenuated total reflectance technique. It should also be noticed that the depth of penetration is wavelength-dependent, a fact that should be accounted for if absorbencies at different wavenumber are compared. Therefore, the severity of the "wavelength dependence distortion" of the ATR spectra may be minimized by using a high index of refraction IRE and by employing higher angles of incidence that are as far as possible remote from the critical angle. Computer software may also be employed to "correct" the ATR spectra so that they appear more like the transmission spectra, by applying a simple scaling factor to each point, such as λ_{ref}/λ.

One of the advantages of the ATR spectroscopy is that *in situ* spectra of adsorbed species can be recorded easily at a given metal oxide surface. The experimental procedure consists in the preparation of a thin layer of the oxide, which must cover the upper part of the horizontal IRE material entirely. Ideally, this layer must be stable at least for the duration of the experiment, chemically inert with respect to the IRE material, and its thickness should be appropriate for the evanescent IR wave to reach a small volume of solution above the oxide layer, where the adsorbed species will be formed. The thickness of the layer can be calculated using equations 13 - 16 [46].

Different methods can be used to prepare the adsorbent film, generally three are used: spreading a concentrated suspension or paste or slurry onto the ATR crystal surface [94-96], in-situ synthesizing a sample layer on the crystal surface [97, 98], or coating the IRE with

colloidal particles from a suspension (by spreading, or dip-coating, or spinning) to form a thin film, which is stable if the film is subjected to a flow of solution [83, 99-101]. In this work the last method has been used, with a trapezoidal-shaped ZnSe ATR crystal being coated with a thin film of the particles by spreading the particle suspension. In combination with the flow-cell or the batch-cell technique [46], the interfacial reactions occurring at the film-solution interface could be monitored *in situ*.

2.5 Surface Adsorption

The evaluation of the interactions between organic ligands and oxide minerals is very important for the understanding of environmental chemical processes. Adsorption of organic substances on metal oxides is relevant to oxide dissolution, pollutants removal through adsorption, water remediation through heterogeneous photo-catalysis, etc. For all these processes a rational understanding of the adsorption process is important [102]. Organic molecules usually adsorb onto (hydro)-oxide surfaces through either of two fundamental interactions: inner-sphere adsorption, where the organic molecules or ion directly form a bond with the surface, or outer-sphere adsorption, in which the anion is held at the surface through electrostatic attraction and/or hydrogen bonding.

Outer-sphere surface complexes are normally more susceptible to desorption, being replaced by competitive ligands, and often possess a strong dependence on solution conditions such as ionic strength. Inner-sphere adsorption forms, on the other hand, complexes that are much more stable at the oxide surface.

The **I**nfra**R**ed (IR) spectra of carboxylic acids adsorbed on TiO_2 and in general on metal oxides, differ from their spectra in solution but, in contrast, they closely resemble the spectra of related coordination complexes of the same ligands. This is a clear evidence of chemisorption through the formation of surface complexes [100]. Chemisorption takes place through the coordination of deprotonated carboxylates bound to surface Ti atoms. Various surface complexes have been postulated, differing in the denticity of the ligand and the nuclearity of the surface species (number of surface Ti atoms bond to one ligand).

Several reports have been published regarding equilibrium studies, using basically two different approaches. The traditional one involves conventional batch adsorption studies [103,

104]: a suspension of a certain amount of adsorbent (TiO_2) is equilibrated with a solution of known adsorbate concentration, the supernatant solution is then analyzed to obtain the equilibrium concentrations, and the surface concentration values are derived there from. The data are eventually analyzed in terms of different adsorption models described by the Langmuir isotherm, the BET isotherm, the Freundlich isotherm, *etc*..

The second approach involves the use of ATR-FTIR: a total reflecting crystal (ZnSe or other single crystals) is coated with a film of the adsorbent and allowed to reach equilibrium with a solution of the ligand [100, 105, 106]. This technique senses selectively the adsorbed species, since the penetration depth of the IR beam is not higher than the thickness of the adsorbent film and the species present in the bulk solution do not interfere when they are at a sufficient low concentration (which depends on the investigated compound). This technique allows spectroscopic characterization of the adsorbed species, i.e., different adsorption modes can be solved [102].

Although numerous experimental and theoretical investigations involving titanium dioxide have been performed, the underlying mechanisms of photoreactions at the interface between the oxide nanoparticles and the aqueous solution are still not fully understood. A very promising experimental technique for the identification of intermediate species and therefore the reaction mechanisms is vibrational spectroscopy. This methodology, however, when applied to the study of interfaces and surfaces suffers from a low signal-to-noise ratio. Hug and Sulzberger have contributed significantly to the investigation of surface complexes of several ligands on TiO_2 by means of attenuated total reflection–Fourier transformed infrared spectroscopy [100]. ATR-FTIR is a relatively simple, inexpensive and readily available analytical tool, in particular, since this technique offers the advantage of monitoring reaction kinetics and mechanisms with the possibility of tracing labile intermediates and adsorbed species on photocatalysts nanoparticles [50].

Kinetic studies are normally carried out by withdrawing samples from the reaction medium and following reactant and product concentrations by conventional analytical techniques, i.e., chromatography, mass spectrometry, etc. In this type of studies, labile intermediates cannot be easily detected and adsorbed species cannot be analyzed at all. Regarding the photocatalytic activity of TiO_2, on the one hand, intermediate species have been the focus of interest of many studies concerning the elucidation of reaction pathways for various organic pollutants. On the other hand, the importance of the role of adsorbed species being part of the reactions taking place at the surface of the photocatalyst where some of its

surface atoms are crucially involved throughout the reaction, has not received particular attention in the open literature yet [2].

2.6 Aim of the Work

The aim of the present work is to deepen our knowledge on the adsorption and photodecomposition mechanism of model compounds, e.g. chloroacetic acids especially dichloroacetic acid, and of the pesticide 2,4-D, occurring over TiO_2 nanoparticles.

A strategy based on the (1) investigation and determination of the adsorption properties of the materials, (2) investigation of the adsorption behavior of the organic molecules on the TiO_2 films using the ATR-FTIR methodology, and (3) monitoring of the adsorption kinetic of the chloroacetic acids and 2,4-D by the ATR-FTIR methodology, and photocatalytically degradation of DCA and 2,4-D is proposed. The different affinity of acetic acid, MCA, DCA and TCA to the TiO_2 surface is also explored to confirm the proposed mechanism.

The characterization of the powders involves the determination of some of its characteristics, e.g., the crystallite size and the BET surface. Five different powders have been used in this study. Three anatase samples, i.e., PC500 and PC10 from Crystal Global and the S230 from Finn-Ti Kemira. One powder composed of rutile the R15 also from Crystal Global and the P25 from Evonik Degussa GmbH, which is a mixture of both crystalline phases.

To perform a rigorous investigation of the DCA adsorption at TiO_2an anatase sample has been selected, i.e. PC500. It has been chosen based on some factors: it is composed only of anatase phase; the big amount of powder available, assuring the homogeneity of the powder once only one lot has been used; and fact that it has been already used in previous studies performed in our group, which makes possible the comparison of the investigations.

To include the evaluation of the influence of other particle properties an extension of the investigation has been proposed. Therefore have been employed other TiO_2 powders, i.e., the anatase samples: PC10 with a higher particle size, and the S230, which shows particle size and BET surface area similar to these of the PC500 powder; the rutile sample R15; and the P25, which shows good photocatalytic degradation rates. The photocatalytic behavior of the DCA molecules on these powders has been investigated too.

To aim at obtaining more information about the importance of the molecule structure on the adsorption, the investigation of AA, MCA and TCA on the PC500 sample has been proposed. Moreover, the adsorption from mixtures of the acids on the powder has also been studied.

Finally, the pesticide 2,4-D has been analyzed. The adsorption and photocatalytic degradation has been investigated on the PC500 powder.

3 Experimental Procedures

Initially the different titanium dioxide materials, used in this work, have been characterized. Based on the characterization the working plan for the adsorption studies and photocatalytic degradation has been organized and optimized.

3.1 Chemicals

For the understanding of the adsorption and degradation mechanism of organic compounds at the TiO_2 surface, firstly the different samples used in this work have been characterized. Different materials with different characteristics have been used. The photocatalytically active phase anatase, rutile with lower activity and a mixture of both phases, which presents higher efficiency for DCA degradation [73], i.e., P25 powder [107] have been employed. All TiO_2 powders used in this work are listed in Table 1.

Table 1: Titanium dioxide samples employed. * non-commercial sample provided by Crystal Global, † Now Evonik Degussa GmbH.

Sample Name	Manufacturers/Provider
PC500	Crystal Global
PC10	Crystal Global
R15*	Crystal Global
P25	Degussa AG†
S230	Finn-Ti Kemira

All acids, bases, and reagents used were of analytical grade, and have been used as received without previous treatment.

The aqueous solutions and suspensions have been prepared with deionized water (resistivity = 18.2 $m\Omega \cdot cm^{-1}$) collected from a Sartorius Arium 611 deionizer.

3.2 Titanium Dioxide Characterization

3.2.1 X-ray Diffraction Measurements

Crystallographic characterization has been performed with a Phillips PW1800 diffractometer using a reflection geometry with variable divergence slits, Cu-Kα1,2 radiation and a secondary monochromator, at the Institute of Mineralogy of the Leibniz Universität Hannover. The phase analysis was carried out by the Rietveld method using the TOPAS 2.0 (Bruker AXS) software. During the refinements general parameters such as scale factors, one background parameter, and the zero point error were optimized. Profile shape calculations were carried out on the basis of standard instrumental parameters using the fundamental parameter approach implemented in the program, varying also the average crystal size (integral breadth) of the reflections. Lattice parameters and crystallite size of all phases were refined. Structural data for the known phases were taken from the Inorganic Crystal Structural Database.

3.2.2 Brunauer-Emmett-Teller Surface Area Determination

Surface area estimation of the TiO_2 powders has been performed by the **B**runauer-**E**mmett-**T**eller (BET) method, performed on a Micrometrics AutoMate 23 apparatus. The samples have been previously heated to 125 °C for 30 min to remove possible contaminants and humidity adsorbed on their surfaces. The measurements have been performed using a gas mixture containing 30 % nitrogen and 70 % helium.

3.2.3 Adsorption Isotherm Measurements

Different adsorption isotherm models have been employed to depict the adsorption properties of the materials. Other models have also been tested in order to determine the best description of the adsorption.

Titanium dioxide/fluoride suspensions have been used to measure the adsorption parameters from the adsorption isotherms providing an estimation of the number of available adsorption sites. Moreover, the adsorption constants for each metal oxide powders have been obtained. Therefore, different fluoride concentrations have been added to 20 mL suspensions of 2.5 $g \cdot L^{-1}$ TiO_2 in 0.01 $mol \cdot L^{-1}$ KNO_3. The flasks have been shaken, at 300 rpm, during 24 hours maintaining the pH constant (pH 4.0 ± 0.02) through the addition of KOH or HNO_3 (± 0.5 $mol \cdot L^{-1}$). After 5 min centrifugation (4000 rpm) the samples have been filtrated with a 0.45 µm cellulose nitrate membrane filter (Macherei und Nagel GmbH Co. KG), the supernatant has been analyzed by high performance ion chromatography.

To perform the measurements a Dionex GmbH ICS-1000 equipment with a 35 °C heated conductivity cell DS6 (50 mA), coupled to a suppressor with an electric regenerator (ASRS 300 2 mm for anions) has been used. The samples (25 µL) have been injected by the auto sampler AS-40 (Dionex GmbH). Separation of the anions has been performed with an ionic exchange column Ion Pac AS9-HC 2 x 250 mm and an Ion Pac AG9-HC 2 x 50 mm (Dionex GmbH) pre-column. A solution of 8.0 x 10^{-3} $mol \cdot L^{-1}$ Na_2CO_3 and 1.5 x 10^{-3} $mol \cdot L^{-1}$ $NaHCO_3$ has been used as eluent. Chromatograms have been taken by the Chromeleon program. A similar procedure has been employed to determine the isotherms for the other investigated compounds (**A**cetic **A**cid (AA), MCA, DCA and TCA).

2,4-D concentrations have been determined by **H**igh **P**erformance **L**iquid **C**hromatography (HPLC) in an instrument fitted with an ECOM spol. s.r.o. LCP 4100 pump, a LCD 2084 UV spectrophotometer, and a 200 µl injection loop. A C-18 Inertsil ODS2 150 Å 5 µm 250 x 4.6 mm column was used with a pre-column 10 x 4.0 mm Inertsil ODS2 100 Å 5 µm in the cartridge holder. The flow rate was 1.2 $cm^3 \cdot min^{-1}$ and the detection wavelength was 280 nm. An acetonitrile/water (40/60 %) solution with 0.3 $mol \cdot L^{-1}$ NaOH at pH 2.95 (adjusted with H_3PO_4) was used as eluent.

3.3 Surface Adsorption

3.3.1 ATR-FTIR Spectroscopy

Attenuated Total Reflection Fourier-Transform InfraRed spectroscopy (ATR-FTIR) has been employed to investigate the organic molecules on the metal oxide surface.

The ATR-FTIR spectra have been recorded using a BOMEM MB 122 instrument equipped with Mercury-Tellurium-Cadmium-A detector, cooled with liquid Nitrogen. The horizontal ATR device provided by Pike Technologies consists of a ZnSe monocrystal, which has a thickness of 4 mm and an upper surface of around 490 mm^2. Its light incidence angle of 45° enables 9 internal reflections of the infrared light on the upper face (see Figure 8).

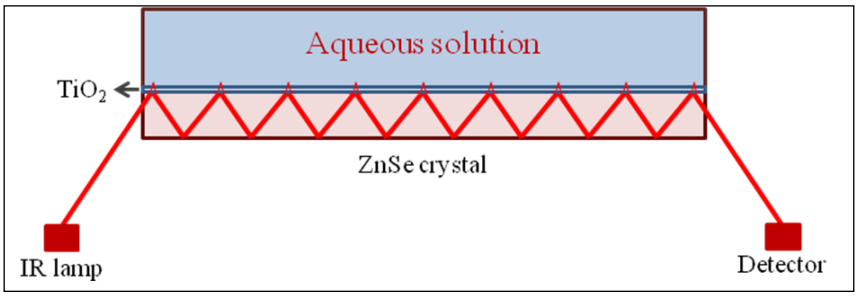

Figure 8: Schematic representation of the Attenuated Total Reflection crystal.

While the ATR-FTIR spectra have been recorded, the ATR device has been constantly purged with argon, avoiding the presence of water vapor and CO_2 in the sample chamber, which show strong interference in important analyzed spectral regions. Other adjustments performed to correct possible interferences have also been done [46].

3.3.2 Photocatalytical Reactor

To perform the adsorption and degradation studies a flow cell reactor has been employed (see Figure 9 a) allowing a better monitoring of the experimental conditions: pH value and temperature. The reactor was built using Plexi-Glass®, a poly-methylmethacrylate

polymer (PMMA), which can be easily coupled and removed from the ZnSe single crystal. The PMMA material permits the visual inspection of the system, controlling the solution level as well as possible instabilities of the TiO_2 layers. Due to its UV-(A) light transparency the study of the metal oxide/aqueous solution under UV-(A) illumination is also possible. The reactor configuration provides the easy disassembly of the reactor in order to remove the TiO_2 layer and to clean the crystal surface after each experiment.

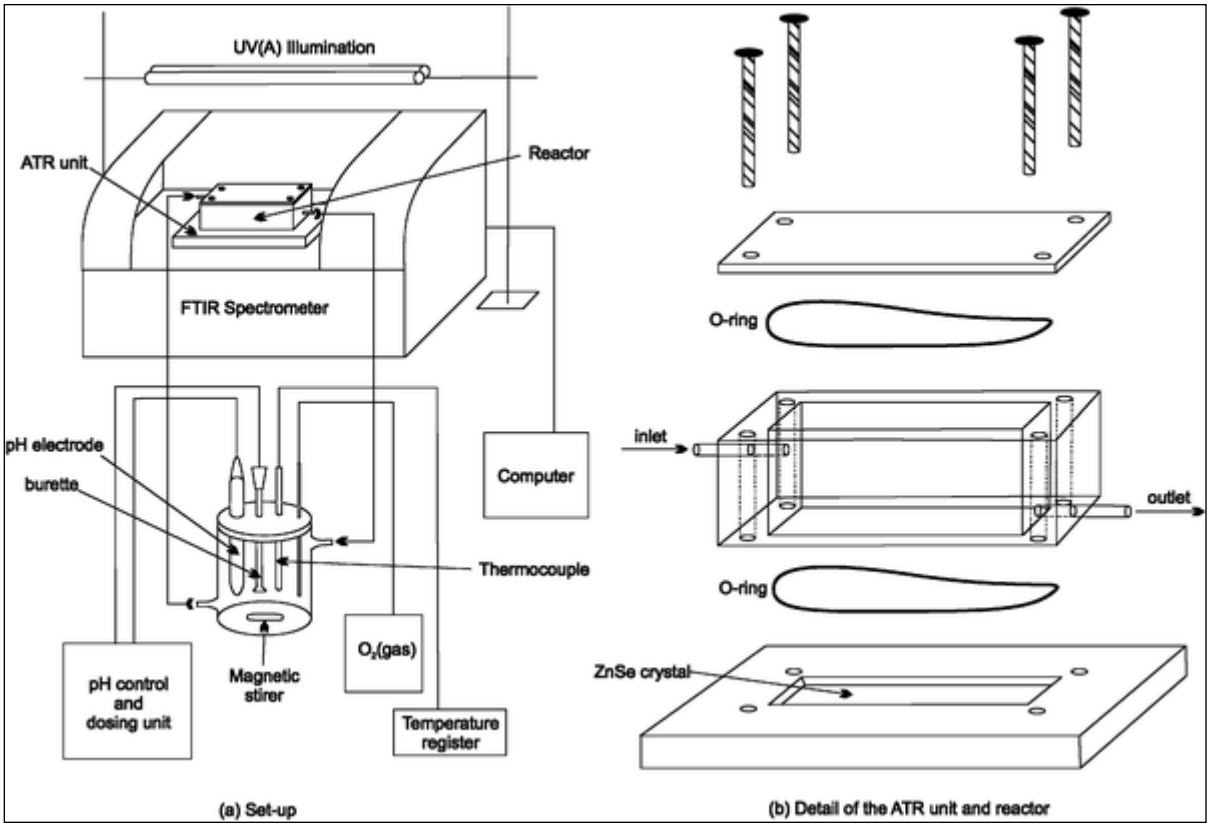

Figure 9: Schematic representation of the *in situ* ATR-FTIR spectroscopy system (extracted from Mendive *et al.* [46]).

Adsorption studies have been performed using batch and flow systems. The batch reactor consists of a reservoir of PMMA coupled to the crystal holder with two small holes at the upper lateral part (see Figure 9 b). The solution has been added or removed through the holes and, when necessary, purged with oxygen or nitrogen.

With a similar configuration the flow reactor has been connected by hoses to an external vessel containing 30 mL of solution (see Figure 9 a) which has been circulated (flow rate 4 $mL \cdot min^{-1}$). The pH of the solutions has been monitored using a semi-micro pH electrode (thermo-Orion Ross 8115) with a reference electrode of Ag/AgCl introduced in the

recipient or a semi-micro electrode (Metrohm 602) with an Ag/AgCl reference electrode. KOH and HNO_3 solutions (± 0.5 mol·L^{-1}) have been employed to adjust and control the pH values by the Dosimat 665 (Metrohm Swiss Made) system using a 5 mL syringe (Metrohm Swiss Made).

Due to the importance of the equilibrium between adsorption and desorption of organic compounds at the TiO_2 surface, the experiments have been performed under constant ionic strength, permitting a better comparison between the different experimental conditions. The electrolyte employed was KNO_3 (0.01 mol·L^{-1}). The temperature of the whole system has been maintained at 20 ± 1 °C.

3.3.3 Titanium Dioxide Layer Preparation

TiO_2 layers have been prepared using suspensions (2.875 g·L^{-1} TiO_2) of PC500, PC10, S230, R15 and P25, previously immersed in an ultrasonic bath for 10 min, to avoid the presence of aggregations already in the suspensions. An aliquot (400 µL) of the suspension has been carefully sprayed on the ZnSe crystal. The device (holder and ZnSe crystal) has been placed overnight in a desiccator to dry. The obtained dry films are, under visual inspection, homogeneous.

Using atomic force microscopy, Hug and Sulzberger have determined that layers with a similar coverage (2.3 g·m^{-2}) exhibit a thickness of 1.7 ± 0.3 mm [100]. This is a very important point since the titanium dioxide films have to be thin enough, to enable the evanescent waves to also excite the adsorbed water and organic molecules and not only the semiconductor particles. Nevertheless the layer has to be thick enough to prevent too much interference by vibrational signals from the molecules in the bulk solution.

The ZnSe single crystal surface has always been cleaned before the preparation of the layers. Occasionally a paste containing micro crystals of diamond with a diameter of 1.0 µm (Metadi II) has been used to carefully polish the surface of the crystal followed by a wash cycle with isopropanol, methanol, and de-ionized water. This cleaning procedure has been performed to remove oxides and or chemical compounds that can be adsorbed at the ATR

crystal, and can be present especially when the TiO_2 layers have been irradiated for longer periods of time.

3.3.4 Interface Adsorption and Photodegradation Experiments

After drying the titanium dioxide layers employed in the batch reactor have been recovered with 0.5 mL 0.01 $mol \cdot L^{-1}$ KNO_3 solution. On average three spectra, each of which being the result of 100 scans, have been taken and used as the blank for the subsequent measurements. The number of spectra collected before the investigation of the acids depends on the stability of the spectral signals in the system. Subsequently five milliliters from the acid solutions have been added to the system and measured. The time intervals necessary for each measurement depend on the necessity of each measurement. Therefore, the number of accumulations taken for each spectrum varied between 30 scans (± 24 s), 100 scans (± 80 s) and 250 scans (± 200 s).

Before the addition into the reactor the acetic acid, MCA, DCA, and TCA solutions (1.0 $mmol \cdot L^{-1}$) have been adjusted to the required pH using KOH and HNO_3 solutions (±0.5 $mol \cdot L^{-1}$).

In the flow reactor the prepared layer has been initially exposed for 35 min to a 0.01 $mol \cdot L^{-1}$ KNO_3 solution, which has been recirculated. Each acquired spectrum has been taken after 200 s employing a re-circulating flow rate of 4 $mL \cdot min^{-1}$ using a peristaltic pump. One spectrum has been used as blank, to subtract the signals of the water vibrational modes as well as those from the KNO_3. The solution was afterwards replaced by 30 mL of dichloroacetic acid solution.

The behavior of the system was analyzed in the dark and under illumination to provide information about the adsorption equilibrium and, the degradation kinetics. Illumination has been performed using two **U**ltra-**V**iolet (UV)-(A) lamps (PHILILPS CLEO 15 W), which have a maximum of emission between 300 and 400 nm. The light intensity was adjusted to 1.0 $mW \cdot cm^{-2}$ and checked with a UV-(A) meter (UV-Technology) before every experiment.

4 Results

4.1 Characterization of the Titanium Dioxide Powders

For the understanding of the adsorption and degradation mechanism of the selected organic compounds at the TiO_2 surface different powders have been used. Samples composed of pure anatase, pure rutile, and a mixture of both phases have been characterized.

4.1.1 XRD Characterization

Table 2 shows the crystalline parameters corresponding to the investigated TiO_2 samples obtained with a Phillips PW1800 diffractometer using reflection geometry with variable divergence slits, Cu-Kα1.2 radiation and a secondary monochromator. The phase analysis by the Rietveld method was carried out using the TOPAS 2.0 (Bruker AXS) software. During the refinements general parameters such as scale factors, one background parameter and the zero point error were optimized. Profile shape calculations were carried out on the basis of standard instrumental parameters using the fundamental parameter approach implemented in the program, varying also the average crystal size (integral breadth) of the reflections. Lattice parameters and crystallite size of all phases were refined. Structural data for the known phases were taken from the Inorganic Crystal Structural Database.

For the estimation of the particle size using the Scherrer's formula (see equation 17) [108] the broadening of the (101) peak of anatase or the (110) peak of rutile were employed (assuming that the crystalline domain is a good approximation):

$$L = \frac{k(180/\pi)}{\beta \cos\theta} \qquad \text{Equation 17}$$

where L is the volume weighted crystalline size, k is equal to 0.92 (the Scherrer constant that normally varies between 0.89 and 0.94) and β is the line broadening at half the

maximum intensity also known as Full Width at Half Maximum in radians and θ is the Bragg angle.

Table 2: XRD characterization of the TiO_2 samples. * Data taken from Mendive [46]

Sample Name	**Crystalline phase**	**Crystalline Domain (nm)**	**Lattice parameters**	
			a (Å)	**c (Å)**
PC500	Anatase (100 %)	8	3.786	9.522
P25	Anatase (84 %)	32	3.787	9.512
	Rutile (16 %)	49	4.597	2.960
R15	Rutile (100%)	20	4.599	2.957
PC10*	Anatase (100 %)	152	3.784	9.520
S230*	Anatase (100 %)	7	3.789	9.499

4.1.2 BET Surface Area Measurements

For estimating the surface area, also called geometric exposed area, the Brunauer-Emmet-Teller (BET) measurements have been applied to three different samples, namely anatase (PC500), rutile (R15) and P25.

The highest exposed area within these samples has been observed for the PC500 sample, i.e., 320 $m^2 \cdot g^{-1}$, in good agreement with the value around 300 $m^2 \cdot g^{-1}$ given in the literature [109], [37] (see Table 3). Pure rutile shows a lower surface area (62 $m^2 \cdot g^{-1}$) in agreement with previous measurements performed by Mendive *et al.* [53] who obtained 65 $m^2 \cdot g^{-1}$. The sample Aeroxide® TiO_2 P25 with an exposed area of 50 $m^2 \cdot g^{-1}$ is in very good agreement with the literature [107]. The measured values as well as those encountered in the literature are listed in Table 3.

Table 3: Brunauer-Emmet-Teller (BET) data for the TiO_2 samples. * Data taken from Mendive [46].

Samples	**BET surface area ($m^2 \cdot g^{-1}$)**	**BET reported in the literature ($m^2 \cdot g^{-1}$)**	**References**
PC500	320	290-335	Gumy *et al.* [109] Liu *et al.* [37]
R15	62	65	Mendive *et al.* [53]
P25	50	50	Degussa Tech. Bull. 56 [107]
PC10*	10	-	-
S230*	230	-	-

4.1.3 Adsorption of Fluoride Anions at Titanium Dioxide Particles in Suspension

The investigation of the adsorption characteristics of the materials is very important, because the resulting parameters are required to model both, the adsorption and the degradation mechanism. The number of available adsorption sites, the formation of mono- or multi-layer adsorbate and the respective adsorption constants all provide, for example important information regarding the adsorption possibilities.

To determine these parameters the adsorption of fluoride ions has been studied here. Due to its small size and similar ionic radius compared to the hydroxyl ions [110], fluoride is an ideal anion to investigate the adsorption properties of metal oxide surfaces. Different fluoride concentrations have been used in the system at pH 5.5. The same value has also been employed in previous investigations reported in the literature for TiO_2 powders [46, 111]. This condition represents the neutral condition of TiO_2 powders, i.e., the pH zpc at which the number of protonated surface hydroxyl groups equals that of deprotonated groups, rather well, not only for the anatase phase but also considering the rutile phase and the P25 powder.

Considering that water molecules are adsorbed on the TiO_2 surface, equilibrium between the protonated and deprotonated form as suggested in equations 8 and 9 has to be

taken into account. Surface complexation involves the coordination of ligands to the surface and is described by the respective surface complexation equilibrium.

If the isoelectric equilibrium is achieved the adsorption of foreign molecules such as F^- commonly occurs just by a replacement of the basic OH group at the surface, as shown in Figure 10. Due to the replacement of the hydroxyl group a change in the pH condition is observed, which under the employed experimental conditions is automatically controlled by the addition of acid solution (HNO_3). The adsorption equilibrium point is reached when the pH of the solution is stable, which for the investigated TiO_2 powders has been achieved after about 24 h.

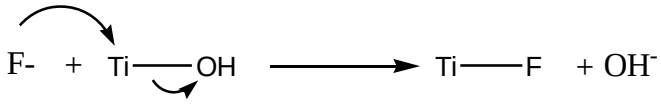

Figure 10: Schematic illustration of the substitution reaction from OH^- by F^-.

Sodium fluoride has been added to the powder suspensions to reach concentrations between 0.02 and 10.0 mmol·L^{-1}. The fluoride concentration was determined using ion chromatography (HPIC).

Developed initially to describe the adsorption of gases on clean solid surfaces the Langmuir isotherm has been adapted to study the adsorption of small molecules or ions by powdered solid adsorbents from aqueous solution [112] just as the **B**runauer **E**mmet and **T**eller (**BET**) isotherm model. Equations 18 and 19 show the mathematical description of the Langmuir and the BET models, respectively.

$$y = \frac{N \cdot K \cdot x}{1 + K \cdot x} \qquad \text{Equation 18}$$

where y is the concentration of fluoride adsorbed at the surface of TiO_2 (mol·g^{-1}), x the concentration of fluoride in solution per employed TiO_2 mass (mol·L^{-1}·g^{-1}), K the Langmuirian adsorption constant in L·mol^{-1} and N the maximal number of adsorption sites at the TiO_2 surface in the first adsorption layer in mol·g^{-1}.

The BET model considers also the occurrence of adsorption in a multilayer fashion, and includes two new parameters:

$$y = \frac{N \cdot K \cdot (x/P)}{1-(x/P)} \cdot \frac{1-(l+1)\cdot(x/P)^{l}+l\cdot(x/P)^{l+1}}{1+(K-1)\cdot(x/P)-K\cdot(x/P)^{l+1}}$$ Equation 19

where y is the concentration of fluoride adsorbed at the surface of TiO_2 ($mol \cdot g^{-1}$), x the concentration of fluoride in solution per employed TiO_2 mass in $mol \cdot L^{-1} \cdot g^{-1}$, K the adsorption constant in $L \cdot mol^{-1}$ and N the maximal number of adsorption sites at the TiO_2 surface in the first adsorption layer in $mol \cdot g^{-1}$, l the number of adsorbed layers and P the saturation concentration ($mol \cdot L^{-1}$).

The adsorption parameters have been calculated from the experimental curves shown in Figure 62 (see Appendix) as F^- adsorption curves for PC500, P25, and R15 respectively, correlating the adsorbed fluoride concentration per gram of semiconductor and the concentration in equilibrium per gram of TiO_2 in suspension after approximately 24 h of equilibration.

The parameters obtained from the adsorption isotherms for the investigated powders are summarized in Table 4. The strength of the interaction and an estimation of the number of molecules in the adsorbed monolayer can be obtained from the adsorption constant (K) and the number of exchangeable adsorption sites (N), respectively. The Langmuir equation seems to be respected by the adsorption of fluoride ions for the anatase sample (PC500) as well as for P25 powder, while pure rutile (R15) shows good fitting using the BET equation. The similarity between PC500 and P25 can be partially attributed to the high content of anatase in the P25 sample.

Table 4: Adsorption parameters obtained from the Langmuir and the BET isotherms.

Sample	**Adsorption constant ($L \cdot mol^{-1}$)**	**Maximum number of adsorption sites ($\mu mol \cdot g^{-1}$ TiO_2)**
PC500 - Langmuir model	41 ± 7	415 ± 17
R15 – BET model	55 ± 20	34 ± 2
P25 – Langmuir model	52 ± 28	140 ± 16

4.2 Dichloroacetic Acid Investigation

For a better understanding of the adsorption behavior of dichloroacetic acid, different investigations can be performed. The utilization of accurate (procedures in controlled and clean atmospheres) and adequate experimental methodologies (sensible and reproducible) are most certainly very useful. Aqueous solutions, however, imply a lot of non controlled parameters. Therefore, studies using different oxides with distinguished surface structures and even the investigation of organic molecules with structural similarities are interesting alternatives for an adequate study of the DCA/TiO_2 adsorption system. For this reason the investigation of adsorption systems with similar characteristics has been conducted here. Furthermore, the comparison of different properties between molecules or particles with similar structures can yield important information concerning the factors that probably influence the adsorption system.

The adsorption of DCA has been investigated for the powders described previously in section 3.1: PC10, PC500, S230, R15, and P25.

DCA degradation has previously been extensively investigated [113-119]. Some characteristics apart from the environmental importance of the dichloroacetic acid molecule motivate its employment in this study. The most important property is its high solubility in water, exhibiting reasonably high polarity and low vapor pressure. Furthermore, due to their low dissociation constant, the DCA molecules are mostly present in the dissociated form over a large range of pH values, enabling in particular the investigation of the interaction of the DCA^- anion with the titanium dioxide surface.

The degree of the DCA^- adsorption should depend on the number of acidic and basic groups at the titanium dioxide surface. Considering that the oxide surface shows high changes of its charges according to the solution pH, the presence of dissociated DCA^- anions simplifies the interpretation of the obtained results.

Moreover, the adsorption of molecules on titanium dioxide photocatalyst particles plays an important role for the direct photocatalytic degradation of pollutants being of fundamental importance to determine how this interaction occurs and whether it is really indispensable for the degradation reaction to occur. The alternative indirect attack from different radicals generated at the TiO_2 surface, on the other hand, can be assumed to play the role of most other important degradation agent alike.

4.2.1 Adsorption of Dichloroacetic Acid at PC500 and P25 Particles in Suspension

Adsorption curves of DCA on TiO_2 powders have been determined following the methodology described in section 3.2.3. Rutile has not been used due to the reduced amount of powder available. The isotherms obtained for the PC500 and the P25 powders have been depicted using the Langmuir isotherm model. In some cases multi-site isotherm models are required to describe the adsorption systems, which, for example, involve several types of sites, different modes of adsorption or a rearrangement (relaxation) of the surface complexes in order to optimize the coverage [120]. Due to the low fitting correlation and taking into account the results that have been obtained by the ATR-FTIR spectroscopic investigation, (as will be explained in more detail in section 4.2), the following model has been suggested to explain the behavior of DCA molecules at the surface of anatase powder. This so-called "modified Langmuir model" combines the traditional Langmuir model with a multi adsorption sites system.

Considering the fact that different adsorption sites are available at the anatase (100) surface, and that DCA can adsorb in different ways at its surface, the following adsorption model is suggested here:

$$2\,S + 2\,DCA \rightleftarrows (2\,S - DCA) \qquad K_1 \qquad \text{Equation 20}$$

$$(2\,S - DCA) + 2\,DCA \rightleftarrows (2\,S - DCA) - (DCA)_2 \qquad K_2 \qquad \text{Equation 21}$$

It is assumed that the respective equilibria can be described by equations 22 and 23, respectively:

$$K_1 = \frac{(S-DCA)^2}{S^2 \cdot (DCA)^2} \qquad \text{Equation 22}$$

$$K_2 = \frac{(S-DCA-DCA)^2}{(S-DCA)^2 \cdot (DCA)^2} \qquad \text{Equation 23}$$

where:

(DCA) is the concentration of DCA in equilibrium in solution, x

(S-DCA) is the concentration of the surface complex 1, N_1

(S-DCA-DCA) is the concentration of the surface complex 2, N_2

(S) is the concentration of surface sites which have not been occupied by (S-DCA) and (S-ACD-DCA), (S) = T - (N_1 + N_2), where T is the total number of available surface sites.

The equations can also be written as:

$$K_1 = \frac{N^2}{(T-(N_1+N_2))^2 \cdot x^2}$$ Equation 24

$$K_2 = \frac{{N_2}^2}{{N_1}^2 \cdot x^2}$$ Equation 25

N_1 + N_2 corresponds to the dependent variable y. Considering that almost all (S-DCA) complexes will be converted to (S-DCA-DCA), the following approximation is valid for N_1 << N_2. Therefore, y ≈ N_2 and the adsorption isotherm can be described by:

$$y = T - \frac{T}{1+x^2(K_1+K_2)^{1/2}}$$ Equation 26

where $K_1 \cdot K_2 = K_3$, and K_3 is the adsorption constant in L·mol^{-1}. The concentration of dichloroacetate adsorbed at the surface of TiO_2 (mol·g^{-1}) is expressed by y, x is the concentration of anions in solution per TiO_2 employed in mol·L^{-1}·g^{-1} and T corresponds to the maximal number of adsorption sites at the TiO_2 surface in the first adsorption layer expressed in mol·g^{-1} TiO_2.

Figure 11 shows the adsorption curve obtained for the pure anatase (PC500) sample. The adsorption parameters have been obtained from the fitting to the Langmuir and to the modified Langmuir equations, respectively. Table 5 summarizes the data obtained from the adsorption curves of DCA/DCA^- for PC500.

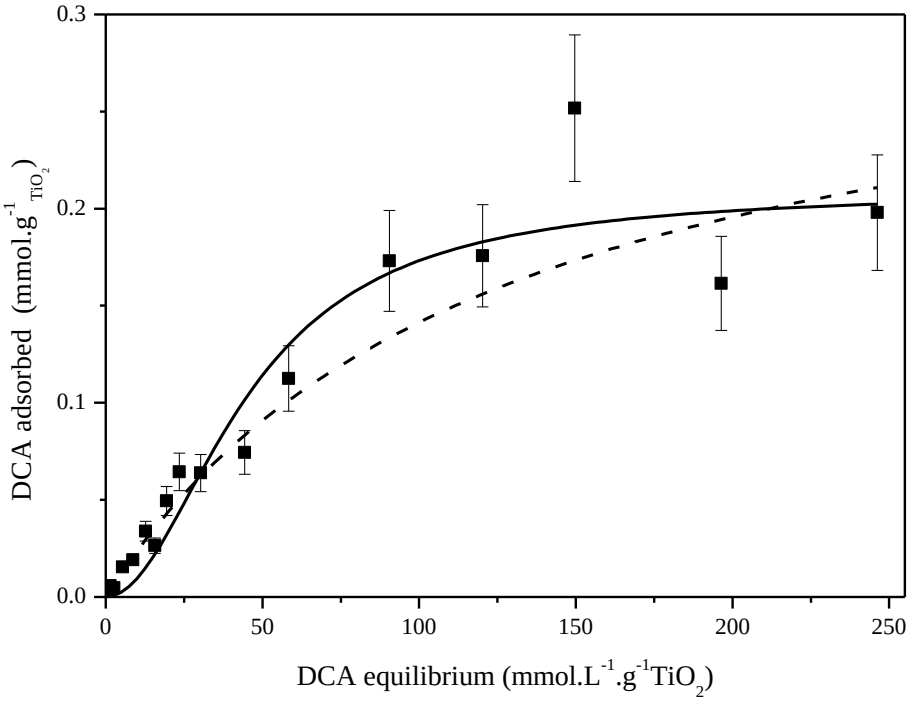

Figure 11: Dichloroacetic acid (pH 3.0) adsorption isotherm on anatase (PC500). The dashed line is the fitting to the Langmuir isotherm equation and, the black line is the fitting to the modified Langmuir isotherm equation.

Table 5: Adsorption parameters extracted from the adsorption isotherms for pure anatase (PC500), using the Langmuir and the modified Langmuir model, respectively.

Isotherm	**K (L·mmol^{-1})**	**N (µmol·g^{-1} TiO_2)**
Langmuir	$8.0x10^{-3} \pm 4.0x10^{-3}$	318 ± 84
Modified Langmuir	$9.7x10^{-4} \pm 2.5x10^{-4}$	201 ± 13

The adsorption curves for DCA on the PC500 powder, exclusively composed of anatase, yield a significantly lower value for the number of available adsorption sites, i.e., 320 and 200 µmol·g^{-1} TiO_2 from the Langmuir and the modified Langmuir models, respectively, than those obtained from the fluoride adsorption measurements presented above (415 µmol·g^{-1} TiO_2). The values of the adsorption constants obtained for both models differ by almost one

order of magnitude, i.e., $8.0x10^{-3}$ L·mol^{-1} for the Langmuir model and about $1.0x10^{-3}$ L·mol^{-1} for the modified Langmuir model.

Table 6: Adsorption parameters extracted from the adsorption isotherms of DCA (pH 3.0) at TiO_2 (P25), using the Langmuir and the modified Langmuir model, respectively.

Isotherm model	**K (L·mmol^{-1})**	**N (µmol·g^{-1} TiO_2)**
Langmuir	$5.0x10^{-3} \pm 2.0x10^{-3}$	278 ± 60
Modified Langmuir	$3.7x10^{-4} \pm 8.5x10^{-5}$	162 ± 10
BET	44 ± 11	13 ± 1.5

The data obtained from the adsorption isotherms of DCA on P25 are summarized in Table 6. Fitting of the adsorption curve using the Langmuir model (see Figure 63 A in the Appendix) a total of 278 µmol of DCA are predicted to be adsorbable per gram of TiO_2, exceeding the value obtained for the fluoride anion (140 µmol·g^{-1} TiO_2) using the same powder. The fitting of the modified Langmuir model, on other hand, yields a similar value, around 160 µmol·g^{-1} TiO_2, as that obtained for fluoride. Considering that the dichloroacetate anion has a larger radius in comparison to fluoride, the structure of the titanium dioxide surface, apparently plays a fundamental role for its adsorption properties.

Table 7: Adsorption parameters extracted from the adsorption isotherms of DCA (pH 9.0) at TiO_2 (PC500), using the Langmuir and the modified Langmuir model, respectively.

Isotherm model	**K (L·mmol^{-1})**	**N (µmol·g^{-1} TiO_2)**
Langmuir	$21.8x10^{-3} \pm 6.0x10^{-3}$	38 ± 6
Modified Langmuir	$9.9x10^{-3} \pm 10.0x10^{-3}$	21 ± 6

It has been observed that the distribution of the charges at the TiO_2 particles does not significantly change the shape of the adsorption curve of DCA in the pH range from 2.0 to

12.0 [121]. The adsorption isotherm of DCA on PC500 at pH 9.0 (see Figure 63 B in the Appendix) has been determined with the purpose to prove this approach. The parameters obtained from this isotherm have been further used to investigate the behavior of the acids at the TiO_2 layer. With 37 and 21 $\mu mol \cdot g^{-1}$ TiO_2 for the Langmuir and the modified Langmuir models, respectively, the alkaline system shows lower number of molecules adsorbed than those observed at pH 3.0.

4.2.2 Dichloroacetic Acid Adsorption at PC500 Films

In studies involving the adsorption of DCA at TiO_2 surfaces M. Hilgendorff [121] concluded that the formation of interfacial complexes mainly depends on three parameters: the pH condition, the electrolyte concentration, and the pollutant concentration.

The interaction of electron donors and acceptors with metal oxide semiconductors is determined, in part, by their surface chemistry [122]. In the case of TiO_2, the principal amphoteric surface functionality is the ‘‘titanol’’ moiety, >TiOH. Due to this amphoteric character the charging process of the surface is controlled by the uptake and release of protons [123]. The resulting surface charge derives from the acid-basic interactions of the solution components with the hydroxyl groups on the TiO_2 surface, as already expressed in equations 8 and 9.

The distribution of the various species ($-TiOH_2^+$, -TiOH and TiO^-) and their dependence on pH is, e.g., described by the site-binding model [124], with hydroxyl ions being considered as charge determining. Consequently, the pH and the electrolyte concentration are the variables that determine the sign and magnitude of the protonic surface charge [123].

The pH value also has a direct influence on the character of the organic acid. For instance, the DCA molecule has been found to exhibit two adsorption possibilities with different adsorption equilibria [64] depending on the pH employed. At low pH values, the titanium dioxide surface is positively charged. While DCA is mostly present in its dissociated form. Therefore, according to Hilgendorff [121] a bidentate complex is formed (Figure 12 A). At pH values higher than 9.0 the TiO_2 surface is negatively charged, DCA is completely

dissociated and it has been suggested the formation of a monodentate complex (see Figure 12 B). The interaction between DCA and the TiO_2 surface is supposed to occur via binding of the COO^- group directly to a Ti atom. After a surficial OH group is released from the surface, the Ti atom and the COO^- group form an inner sphere complex. Additionally, an interaction between the carbonyl group and the OH from the crystalline structure is expected at low pH values.

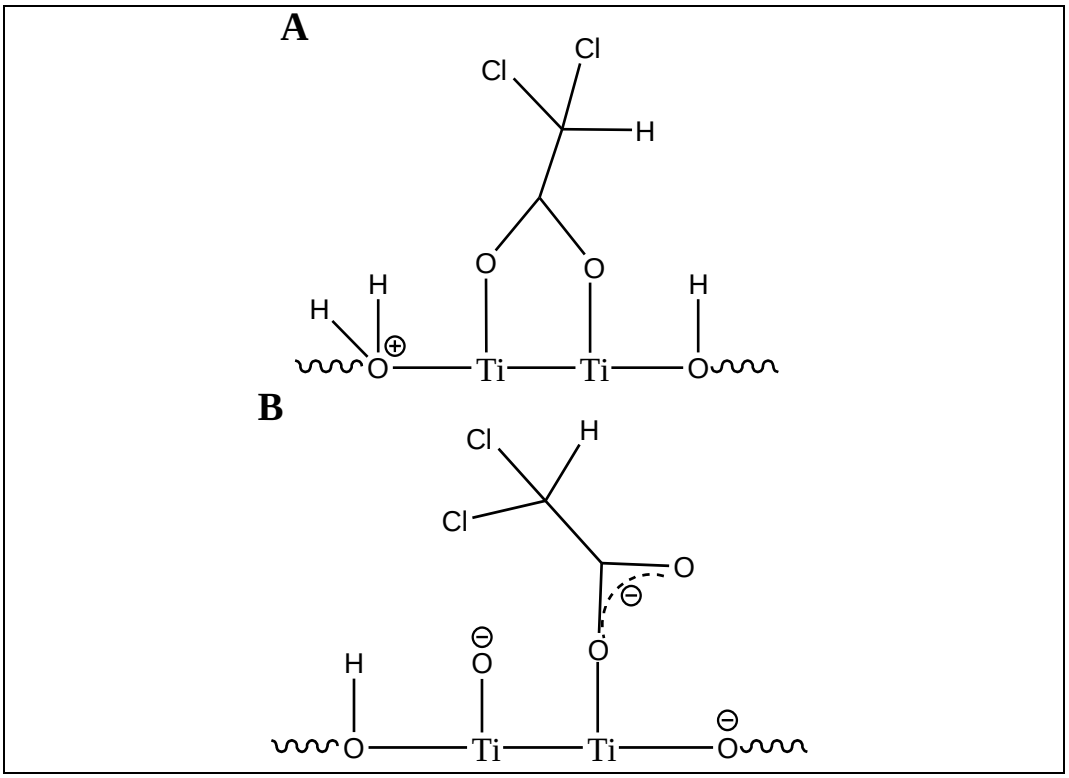

Figure 12: Suggested adsorption structures for DCA^- on the TiO_2 surface positively (A) and negatively charged (B), according to a model proposed by Hilgendorff [121].

A remarkable advantage of the ATR-FTIR methodology is the possibility to investigate systems *in situ*. However, the systems have to be located in a region where the evanescent waves cross the limit of the ZnSe crystal. The exact placement of the systems is the key factor for defining the experimental conditions of the adsorptive behavior of molecules and anions at the adsorbent material. Another important parameter is the concentration of the employed acid to avoid vibrational interferences from the molecules in the bulk solution.

Therefore, different solutions containing DCA have been investigated directly on the ZnSe crystal as well as in the presence of titanium dioxide. These studies have been

performed in a flow system, with the recirculation through the reactor enabling the control of the pH. Furthermore, homogenization of the solution without removing it completely from the IRE surface is facilitated under those experimental conditions.

Solutions containing DCA concentrations between $1.0x10^{-8}$ mol·L^{-1} and 1.0 mol·L^{-1} have been investigated in direct contact with the ZnSe crystal. In this case bands related to vibrational modes of the DCA molecules have only been observed for concentrations above $5.0x10^{-4}$ mol·L^{-1}, as presented in Figure 64 (see Appendix).

As PC500 consists of only one crystalline phase (anatase), it makes this material highly suitable for the optimization of the experimental conditions. Even though it differs in the crystalline structure compared to P25, it shows the same IR band intensities and shape when treated with different DCA concentrations.

IR spectra measured for different concentrations of DCA on PC500 are shown in Figure 64 (see Appendix), proving the appearance of bands at concentrations of 0.5 mmol·L^{-1}. Thus, the optimal range of concentration for investigations should be between 0.5 and 5.0 mmol·L^{-1}. Figure 13 shows the difference between the spectra determined directly on the internal reflectance element and in the presence of the TiO_2 film.

Most investigations have been carried out using concentrations between 1.0 and 5.0 mmol·L^{-1}. Some studies have been conducted using DCA concentrations of 10.0 and 20.0 mmol·L^{-1}.

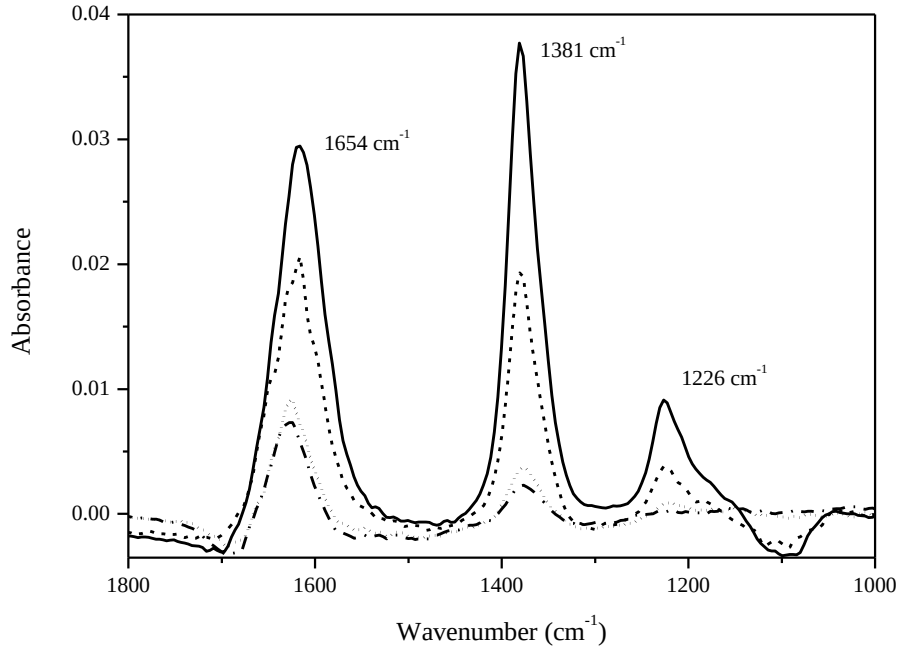

Figure 13: ATR-FTIR spectra for DCA solutions (pH 4.0 in 10.0 mmol·L^{-1} KNO_3): 1.0 mmol·L^{-1} (– –) and 2.0 mmol· L^{-1} (——) in the presence and for 1.0 mmol·L^{-1} (–…–) and 2.0 mmol·L^{-1} (……) in the absence of the TiO_2 film (PC500), taken after 15 min of equilibration.

According to Bellamy et al. [125, 126] the band at 1226 cm^{-1} shown in Figure 13 is assigned to the C-O valence vibration, which is also formed for other chlorinated acetic acids. Near to 1400 cm^{-1} the C-O vibration coupled with an OH in plane deformation vibration (1381 cm^{-1}) is observable. Finally, the COO group also shows a vibrational mode at 1650 cm^{-1}. The band observed at 1381 cm^{-1} is alternatively assigned to the COO symmetric stretching vibration, according to Joung *et al.* [127] and Hilgendorff [121],. Moreover, these authors assumed the band at 1226 cm^{-1} to be caused by the $CHCl_2$ stretching. However, these differences in results might be due to different methodologies. Joung [127] used DRIFT (Diffuse Reflectance Infrared Fourier Transform spectroscopy) for analyzing purposes. Hilgendorff employed higher concentrations of DCA than those used in this study.

The new assignment of these bands is moreover supported by theoretical calculations of the vibrational modes of the DCA molecule, performed in collaboration with Segarra [128]. The observed bands can be assigned as follows: 1620 cm^{-1}: carbonyl asymmetric stretching mode coupled with O-H bending from the carbonyl group; 1381 cm^{-1}: COO symmetric stretching mode with contributions of the C-C symmetric bending (scissoring) mode as well as the OH bending mode; 1226 cm^{-1}: different bending modes from CH. Spinner and co-

workers also employed IR spectroscopy. They reported the same bands for DCA, which they assigned as follows: signals between 1640 and 1660 cm^{-1} and at 1399 cm^{-1}: stretching mode of COO; 1228 to 1218 cm^{-1}: bending mode of the CH bond [129].

The signals above 1600 cm^{-1} have also been analyzed here even though they suffer from a strong spectral interference by bulk water.

The experimental parameters applied in this study, such as the pH condition (pH 4.0) and the number of accumulations taken for each spectrum (250 accumulations), have been initially based on the conditions used by Mendive *et al.* [52, 86, 121] and have therefore been optimized after establishing the adequate DCA concentration.

The choice of the appropriate electrolytes to maintain the experimental conditions, i.e., the electrical double layer formed on the surface of the TiO_2 film, constant is very important, since the main interest of this study is to investigate the behavior of molecules and anions adsorbed on its surface. Therefore, different salts have been tested (data not shown), and it has been observed that none of the tested salts, i.e., KNO_3, KCl, $KClO_4$, K_2SO_4 (10.0 $mmol \cdot L^{-1}$), show IR bands in the investigated spectral region. Due to the necessity to perform measurements of the adsorption and the degradation kinetics of the DCA system by ion chromatography the use of ClO_4^- has been discarded, since under the optimized conditions for the DCA system its retention time for the chromatographic column is extremely high.

Previous studies [130, 131] concerning the adsorption of inorganic anions at the TiO_2 surface have shown that Cl^-, ClO_4^-, NO_3^-, SO_4^{2-} exhibit a retarding effect on the photocatalytic oxidation rates of organic compounds. This can be explained by the competition of radicals and by blocking the active sites of the TiO_2 catalyst. The affinity of these anions to the semiconductor surface is as follows: $Cl^- > SO_4^{2-} > NO_3^-$. Even though some interference with the mechanism of the degradation reaction has been reported for NO_3^- [132], it has been chosen as electrolyte for all adsorption investigations performed here, i.e., the main purpose of this study. The concentration of 10.0 $mmol \cdot L^{-1}$ has been selected based on previous studies performed by Menendes-Flores *et al.* and Lindner *et al.* [73, 75].

The pH value has been previously shown to be one of the most important parameters for adsorption systems. Therefore, an investigation of the pH influence has been performed. Figure 14 shows the FTIR spectra of DCA (1.0 $mmol \cdot L^{-1}$) at pH 3.0, 6.0, and 9.0, respectively. Each spectrum results from 250 accumulations, considering that every accumulation takes approximately 0.8 s. The first spectrum has been collected after 3.5 min so

that changes in its intensity are observed already after a few minutes of investigation. Hence, processes associated to the time necessary to reach the equilibrium between the surface and the solution can be studied conveniently. As explained before changes in the pH can lead to strong changes in the interfacial behavior of metal oxides.

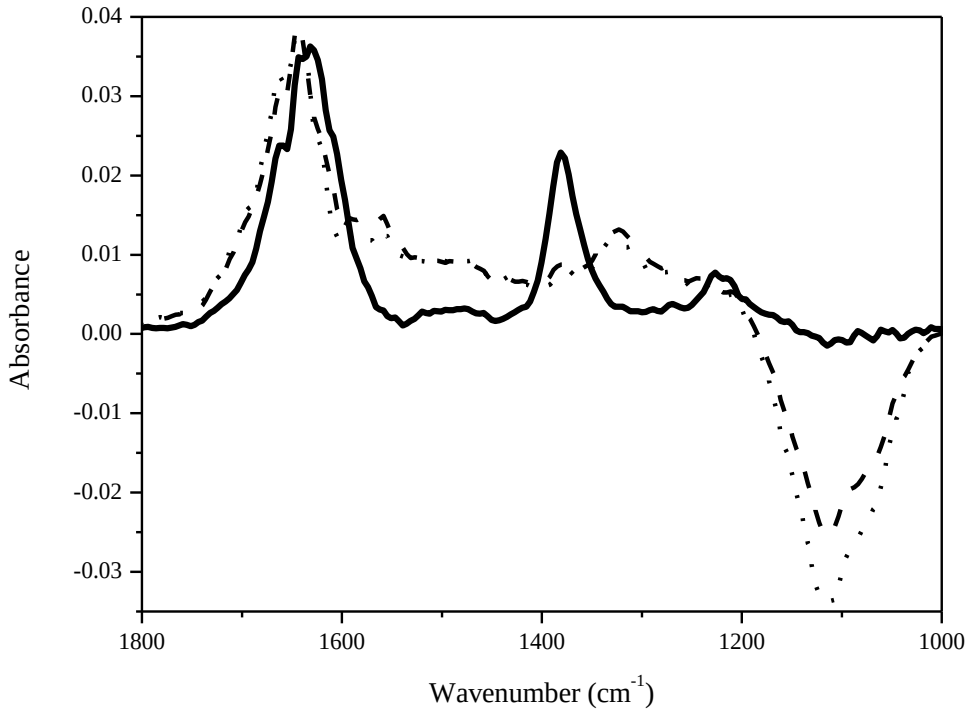

Figure 14: ATR-FTIR spectra of TiO_2 films (PC500) in the presence of 1.0 mmol·L^{-1} DCA at distinct pH conditions in 10.0 mmol·L^{-1} KNO_3. pH value in the solution bulk: 3.0 (——), 6.0 (– –) and 9.0 (·····), taken after 20 min of equilibration.

The vibrational spectra of the molecules in the bulk solution (without the TiO_2 film) have been obtained using higher DCA concentrations (10.0 mmol·L^{-1}). No significant changes have been observed for the investigated pH conditions, i.e., between pH 3.0 and 10.0 (data not shown). In this pH range no significant structural changes are expected, because the DCA molecules are already mostly dissociated at pH 3.0 (more than 95%, see Figure 15).

In the presence of the TiO_2 films, however, strong differences are observed between the pH conditions tested. This confirms the expected influence of this parameter on the adsorption system. The rutile sample and the mixed anatase/rutile sample (P25) have shown similar results (data not shown). Signals related to the DCA^- molecule are observed at low pH values disappearing with increased pH conditions.

For pH values of 6.0 and 9.0 bands typically assigned to the vibrational modes of DCA (1380 and 1226 cm^{-1}) are showing drastically decreased intensities, whereas new bands at 1323 cm^{-1} and 1545 - 1580 cm^{-1} appear. These signals disappear once the pH is changed back to 3.0, indicating that the adsorption of DCA^- does not depend on the pH adjustment sequence. Even when increasing or decreasing the pH value several times, similar signals are observed for the same pH conditions.

At pH 3.0 DCA is mostly (> 95%) present in the deprotonated form (see Figure 15). At this pH the surface interacts more intensively with DCA anions, according to the distribution of the protonated and the deprotonated form of the OH groups at the TiO_2 surface (see Figure 6). Therefore, the most acidic condition used in this study is expected to show the best interaction between surface and organic acid.

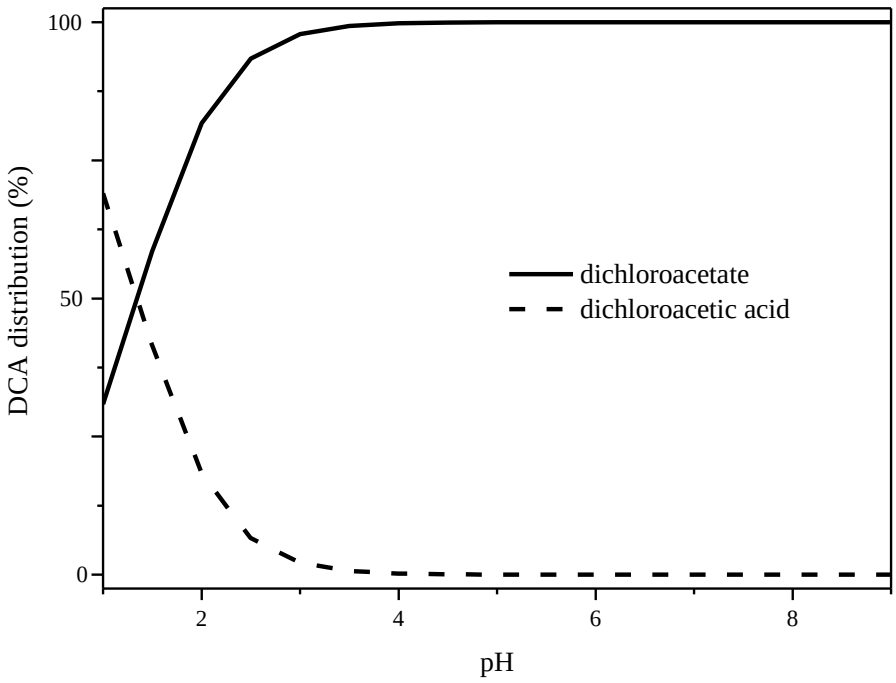

Figure 15: Distribution of DCA (– –) / DCA^- (——) as a function of the pH value, calculated based upon its dissociation constant, pKa = 1.48.

From the data shown in Figure 14 it is obvious that at pH 6.0 and 9.0 signals centered around 1381 cm^{-1} are present, however, the highest intensity of this band is achieved at pH 3.0. Since the signal/noise ratio for the DCA/TiO_2 system is too small, at high pH values an investigation of its adsorption behavior can hardly be conducted here. Hence, the investigations concerning the adsorption have to be performed at pH conditions lower than the

pH_{zpc} of TiO_2. One disadvantage of using such a low pH values is the limited stability of the ZnSe crystal. Any exposure of its surface to extreme pH conditions should be avoided, because H^+ cations can damage the crystal surface (see equation 27) [46, 133].

$$ZnSe + 2\,H^+ \rightarrow Zn^+ + H_2Se_{(gas)}$$ Equation 27

Therefore, two relatively mild pH conditions have been selected and used for the adsorption and degradation experiments. The experiments with 10.0 - 20.0 mmol·L^{-1} DCA have been performed at a pH of 4.0, whereas experiments with low DCA concentrations, i.e., 1.0 - 5.0 mmol·L^{-1}, have been performed at pH 3.0.

The number of accumulations used for each spectrum actually has been defined not purely based on the quality of the recorded spectra, but choosing a compromise between the signal quality and the time to perform an appropriate kinetic study. Different numbers of accumulations per spectra (3, 30, 100 and 250) have been used.

4.2.3 Dichloroacetic Acid Adsorption - Kinetic Studies

Initially, the kinetic investigation of the DCA adsorption process has been performed using a 10 mmol·L^{-1} dichloroacetic acid solution, following the evolution of its vibrational signals in time at pH 4.0. Figure 16 shows the spectra recorded for the system in the presence of a PC500 film. The bands at 1226 and 1381 cm^{-1}, as already seen in Figure 13, confirm the presence of DCA. Even the band in the region above 1600 cm^{-1} can be observed. A small decrease in the signal intensities (1226 and 1381 cm^{-1}) with increasing adsorption time is noticeable.

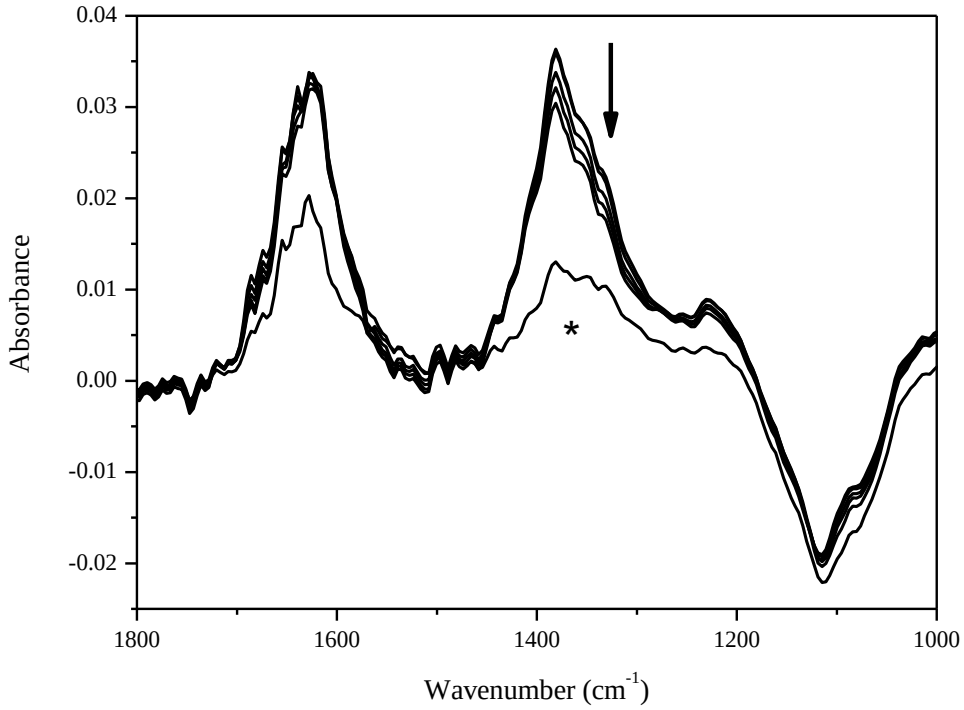

Figure 16: Evolution of ATR-FTIR spectra for a TiO_2 film (PC500) in contact with a DCA (10.0 mmol·L^{-1}) solution at pH 4.0 in 10.0 mmol·L^{-1} KNO_3. The spectrum marked with * has been taken after 3 min, the following spectra were recorded in times of 17, 30, 50, 70, and 90 min. The arrow in the figure indicates the direction of the spectral change with time, after 17 min of equilibration.

Measurements performed using layers prepared with rutile (R15) suspensions also show the presence of adsorbed dichloroacetic acid molecules on the TiO_2 surface. This is confirmed by the presence of bands at 1226 cm^{-1} and 1381 cm^{-1} (see Figure 17), even though DCA molecules from the bulk contribute considerably to these signals.

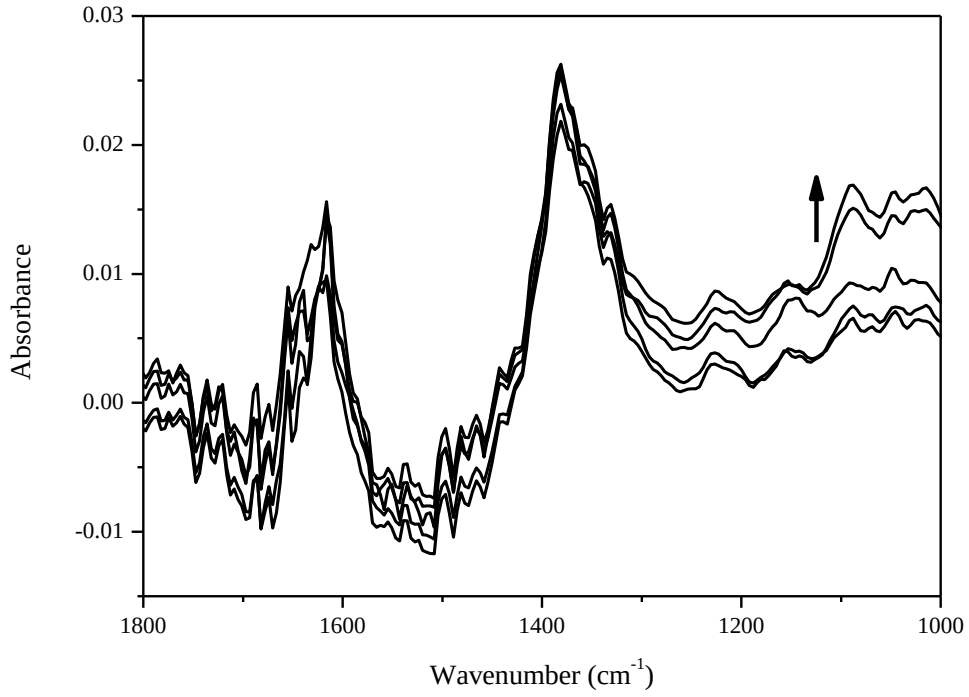

Figure 17: Evolution of ATR-FTIR spectra for a rutile TiO_2 (R15) film in 20.0 mmol·L^{-1} DCA solution at pH 4.0 in 10.0 mmol·L^{-1} KNO_3. Spectra have been taken in times of 3, 17, 35, 50, and 70 min of equilibration. The arrow indicates the direction of the spectral change with time.

Two further anatase samples have been investigated: S230 exhibiting remarkable similarity to the properties of the PC500 powder, and PC10, a quite distinct powder. Although produced by the same company (Crystal Global), the anatase particles present in this material are larger than these of PC500, which is reflected in its low BET-surface area, i.e., about 10 $m^2 \cdot g^{-1}$ [46]. Figure 18 presents the spectra collected for the adsorption of DCA (10 mmol·L^{-1}) on the PC10 film. An important difference in comparison to the spectra taken for the PC500 samples is the low intensity of the CH bending mode at 1226 cm^{-1}, which is almost inexistent.

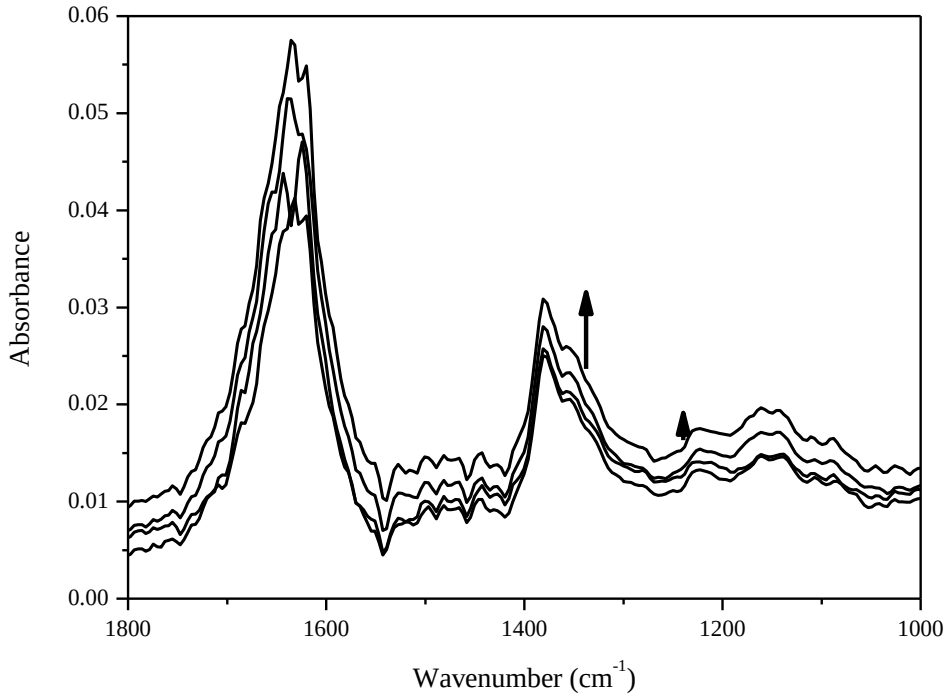

Figure 18: Evolution of ATR-FTIR spectra for an anatase TiO_2 (PC10) film in contact with a DCA (10.0 mmol·L^{-1}) solution at pH 4.0 in 10.0 mmol·L^{-1} KNO_3. The spectra have been taken after equilibration times of 3, 35, 70, and 105 min. The arrows in the figure indicate the direction of the spectral change with time.

An appropriate comparison of the affinity between the organic acid molecules and the anatase surface is only possible when comparing materials with similar properties. Figure 19 shows the spectra collected for the DCA solution (10.0 mmol·L^{-1}) on a S230 layer. The presence of intense bands at equivalent wavenumbers and intensities observed for the other TiO_2 materials also confirms the DCA adsorption at the semiconductor surface. However, a new band centered at 1273 cm^{-1} can be observed as well as a shoulder at around 1412 cm^{-1}, both of which have not been seen for the other tested powders.

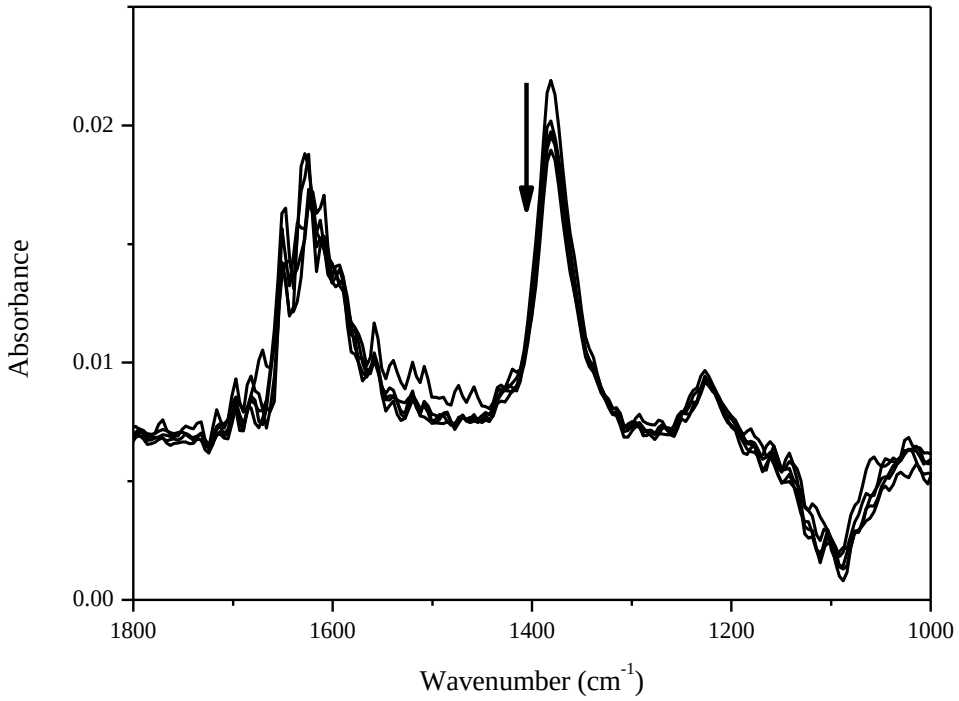

Figure 19: Evolution of ATR-FTIR spectra for an anatase TiO_2 (S230) film in 10.0 mmol·L^{-1} DCA solution at pH 4.0 in 10.0 mmol·L^{-1} KNO_3. Spectra have been taken in times of 3, 20, 35, 50 and 80 min. The absorbance changed nearly parallel to the time. Arrow in the figure indicates the direction of spectral change with time.

The use of high DCA concentrations allows a suitable parallel analysis of the vibrational signals from the molecules in solution and from those adsorbed onto the oxide surface. Apparently, no differences between the signals are observed, i.e., there is a conservation of the DCA spectral bands even when linked to the oxide surface. For a better understanding of the adsorptive process, lower acid concentrations must be employed. This enables an evaluation of the system separately, once the spectral interferences of the bulk system are virtually nonexistent.

According to this approach the following investigations have been performed employing 1.0 mmol·L^{-1} DCA and maintaining the other experimental conditions unchanged (pH and ionic strength).

As will be explained in more detail below, the formation of inner or outer sphere complexes results in very different characteristics and adsorption energies, which influence the adsorption strength. In addition, the way in which the molecule is linked to the oxide

surface also plays a very important role for the distance between the molecules and the ZnSe crystal which in turn have direct impact on the spectral signal intensity.

An investigation considering the first seconds of adsorption was necessary to obtain more detailed information concerning the kinetic aspects of the DCA/TiO_2 interaction. Data for the initial seconds of contact between the solution, 1.0 mmol·L^{-1} DCA, and the TiO_2 film (PC500) have been successfully recorded. Averages of only three scans (although loosing spectral resolution) have been taken for each spectrum. For these experiments a batch system has been employed. 5 mL of solution were added with a syringe through a hole at the side of the reactor, at an initial pH of 4.0. The collected spectra focusing on the first seconds of interactions are shown in Figure 20.

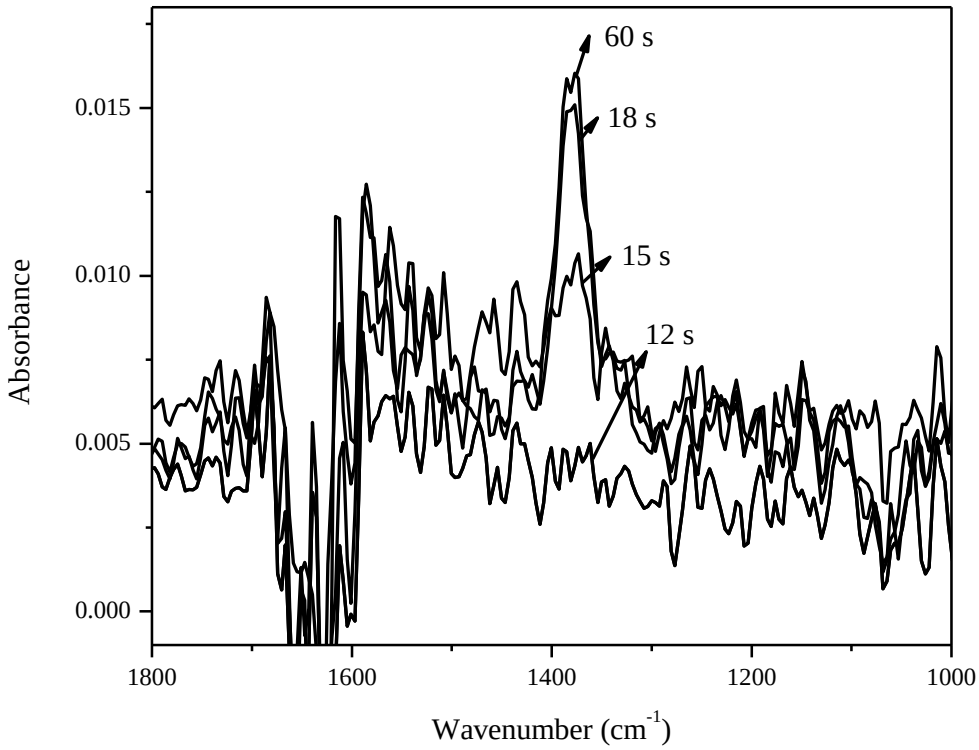

Figure 20: Evolution of ATR-FTIR spectra in time for a TiO_2 film (PC500) in 1.0 mmol·L^{-1} DCA solution at pH 4.0 in 10.0 mmol·L^{-1} KNO_3, during the first seconds of contact.

The spectral sequence shown in Figure 20 presents the evolution of the spectral intensity from the adsorbed DCA molecules at the TiO_2 film during the first 60 s of contact. To observe the first relevant signals around 15 s are necessary. Nevertheless, monitoring of the adsorption process for 10 min has shown a gradual increase of the signal intensity (see Figure 21).

After the initial phase, in which the spectral signals increase, the evolution of the signal intensity changes its tendency. Figure 21 shows the evolution of the height of the spectral band assigned to the COO stretching mode at 1381 cm^{-1}. This band has been selected because it is the strongest spectral signal without interferences of the water vibrational modes, i.e., the H-O-H scissoring bending. A decay of the band intensity is observed after approximately 20 min. The decay is constant and after 6 hours of equilibration, the signal intensity cannot be distinguished from the spectral noise. Even measurements performed with 20.0 $mmol \cdot L^{-1}$ of DCA show a steady decrease of the peak intensity (see Figure 65 in the appendix) after the initial period necessary to reach the highest spectral intensity.

The decay of the signals intensity could be associated with problems in the preparation of the TiO_2 films. The adsorption of water molecules at the TiO_2 surface particles results in an expansion of the semiconductor film. This expansion results in the increase of the distance between the ZnSe crystal and the powder/solution interface. Therefore, the evanescence waves cannot reach the organic molecules. To prove this approach different TiO_2 layers have been prepared, i.e., using 1.4 $g \cdot L^{-1}$ and 5.75 $g \cdot L^{-1}$ TiO_2 suspensions, respectively.

Figure 22 shows the evolution of the peak height at 1381 cm^{-1} in time for the systems prepared with different titanium dioxide suspensions. Unfortunately, the obtained results did not provide clear evidences regarding the adsorption kinetics and the expansion phenomena. However, the intensity of the bands changes according to the film thickness. The decay observed after 120 min reaches similar values for all investigated conditions.

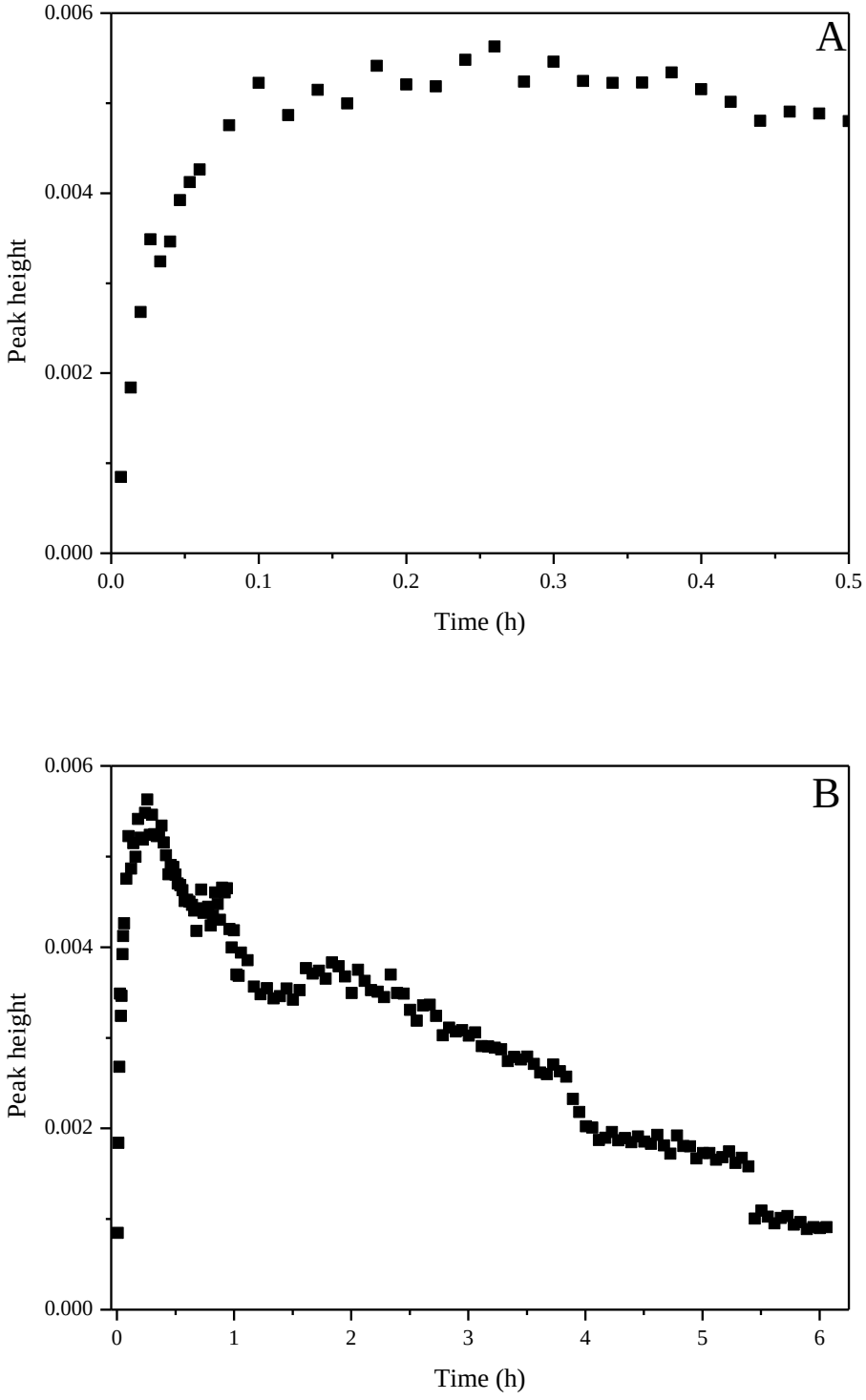

Figure 21: Time evolution of the peak height of the band centered at 1381 cm^{-1}. Obtained from the ATR-FTIR spectra for an anatase TiO_2 (PC500) film in 1.0 $mmol \cdot L^{-1}$ DCA solution at pH 4.0 in 10.0 $mmol \cdot L^{-1}$ KNO_3. A - First minutes of dark-equilibration. B - Dark-equilibration during 6 hours.

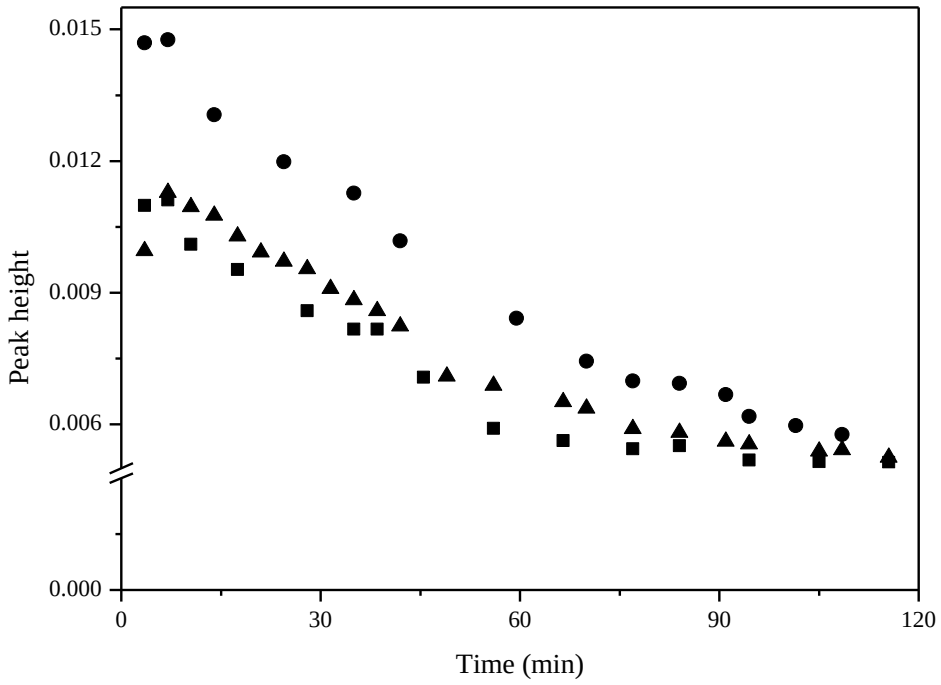

Figure 22: Evolution of the peak height (for the band centered at 1381cm^{-1}) assigned to DCA. Extracted from the ATR-FTIR spectra for an anatase TiO_2 (PC500) film in 1.0 mmol·L^{-1} DCA solution at pH 4.0 in 10.0 mmol·L^{-1} KNO_3. Using different TiO_2 (PC500) films prepared with oxide suspensions of: ■ - 1.4 g·L^{-1} TiO_2, ▲ - 2.8 g·L^{-1} TiO_2, ● - 5.7 g·L^{-1} TiO_2.

Since the change of film thickness does not result in a significant improvement of the DCA spectral signals, further alternatives have been proposed for the investigation of the adsorption behavior. Therefore, experiments employing different conditions have been performed.

The experiments involving DCA solutions at different pH conditions (see Figure 14), show that lower pH values, i.e., pH 3.0 results in higher signal intensities compared to alkaline values. At this pH a stronger electrostatic interaction between the TiO_2 film and the organic acid, due to the higher amount of H^+ at the surface, is expected. Therefore, experiments using 1.0 mmol·L^{-1} DCA at pH 3.0 have been performed. According to Hilgendorff [121], the adsorption of DCA at the surface of P25 powders takes ideally place at pH conditions below pH 3.0, even with the knowledge that these conditions could damage the ZnSe crystal. However, showing more intense vibrational signals than for the system at pH 4.0, the decay of the spectral bands is still observable (data not shown).

An investigation of the behavior of acids with similar molecular structure has been chosen among the possible approaches for the investigation of the TiO_2/DCA interface (the use of other investigation techniques or methodologies, the employment of other oxides, etc). In this assumption, the affinity trends could describe and contribute to the interpretation of a series of similar coupled ligands to a given sample of metal oxide, e.g., PC500. This type of study was shown to be feasible for a sequence of adsorbates onto the same adsorbent. Comparisons within a series of related adsorbents and one ligand is more difficult, because of many uncertainties involved in the surface structure of different solid samples [134]. This approach allows the proposal of adsorption and kinetic models concerning the interaction of the organic substances. Therefore, a systematic investigation of the acetic acid family with its chlorinated derivates has been carried out here. These studies are presented in chapter 4.3.

4.2.4 Dichloroacetic Acid Adsorption - Illuminated system

According to the photocatalytic degradation process the organic molecules can be directly attacked by the photoexcited electron/hole pair or via radicals formed at the TiO_2 surface, which can also react with molecules in the bulk solution. With the photocatalytic degradation, formation of new surface complexes are expected, which should show different vibrational modes.

To aim at obtaining more information about the photodegradation mechanism involving the DCA/TiO_2 interface, investigations with DCA solutions previously purged with O_2 and N_2 have been performed. The purpose of this purge was to assure constant conditions for the trapping of the excited electron (equations 2 and 7). Even knowing that the collected spectra will present a strong interference of the molecules from the bulk solution, higher DCA concentrations (10.0 $mmol \cdot L^{-1}$) have been employed. Because of the longer exposure times of the ZnSe crystal to the DCA solutions, mild pH conditions have been used (4.0), for the photocatalytic experiments.

The adsorption of DCA at the TiO_2 surface in an oxygen saturated system (data not shown) shows many similarities to the unsaturated systems (see Figure 16). The presence of the bands assigned to the DCA molecule is observable, which can be observed for the spectrum acquired after 60 min of adsorption in Figure 23. Based on the fact that the spectral

bands have already reached their maximum intensities this period of time has been selected for the investigations. However, even though their intensities are decaying, the bands are still noticeable, as previously reported.

Therefore, the photocatalytic process has been started following an equilibration in the dark (60 min). Figure 23 shows the evolution of the spectral bands during the illumination. The shift of the spectral band at 1381 cm^{-1}, which remains as a shoulder of the new band centered at 1412 cm^{-1}, is remarkable. Another shoulder is observed at 1354 cm^{-1} and the band at 1226 cm^{-1} is red-shifted to 1230 cm^{-1}. However, the growth of a peak at 1273 cm^{-1} is the most interesting change. Moreover, the stability of these signals, even after 4 hours of irradiation, is also notable, as well as the astonishing increase of the band above 1600 cm^{-1}.

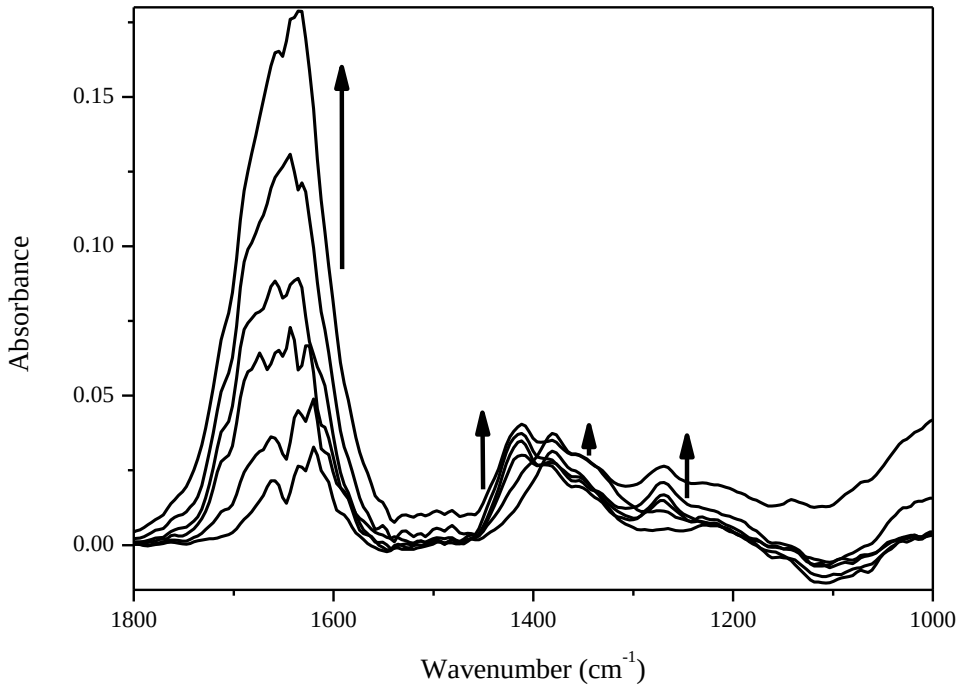

Figure 23: Evolution of ATR-FTIR spectra for an anatase TiO_2 film (PC500) in O_2 saturated 10.0 mmol·L^{-1} DCA solution at pH 4.0 in 10.0 mmol·L^{-1} KNO_3. The first spectrum has been taken after 50 min dark-equilibration, and the following spectra were recorded in times of 3, 30, 60, 120, and 210 min of UV irradiation (with a light intensity of 1.0 mW·cm^{-2}). The absorbance changed nearly parallel to the illumination time. The arrows in the figure indicate the direction of the spectral changes with time.

The shape of the spectra taken for the N_2 saturated DCA solution in the adsorption equilibrium study, is almost identical to these observed for the other two investigated solutions (with O_2 purge and without purge). The typical bands assigned to DCA at 1381 and 1226 cm^{-1} can be clearly observed (see Figure 24). However, under illumination there are

important differences between the different adsorption systems. The most import spectral changes are the increment of vibrational bands intensity at 1520 cm^{-1} and at 1273 cm^{-1}. An increase of the band centered at 1381 cm^{-1} is also noticeable, with the clear evolution of shoulders at 1416 cm^{-1} and 1342 cm^{-1}.

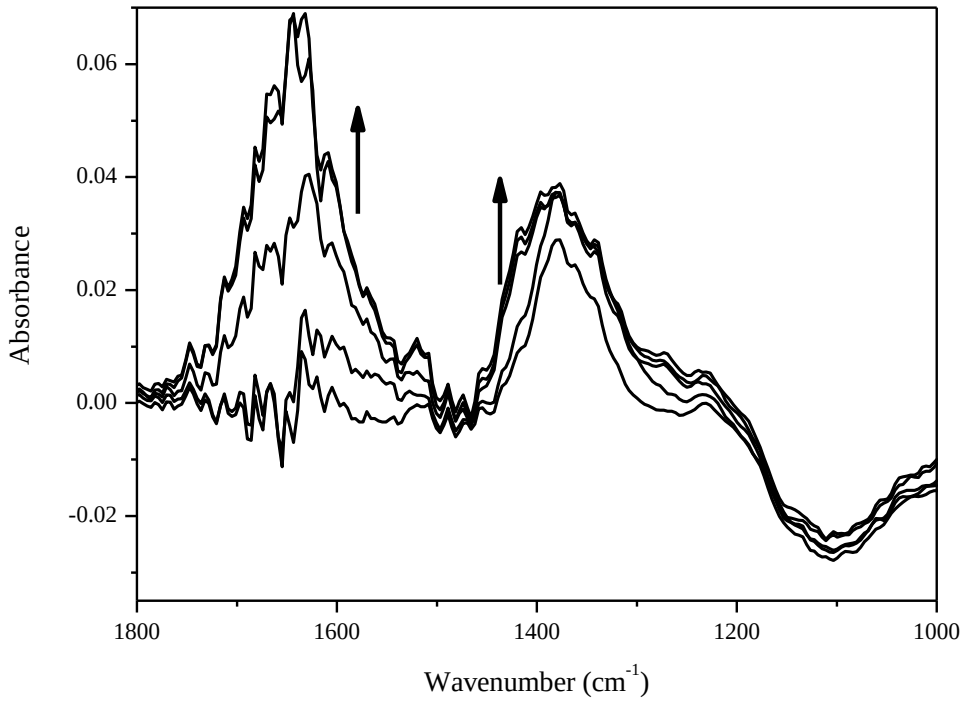

Figure 24: Evolution of ATR-FTIR spectra for an anatase TiO_2 film (PC500) in N_2 saturated 10.0 mmol·L^{-1} DCA solution at pH 4.0 in 10.0 mmol·L^{-1} KNO_3. The first spectrum has been taken after 50 min dark-equilibration, and the following spectra have been recorded in times of 3, 30, 60, 120, and 210 min of UV irradiation (with a light intensity of 1.0 mW·cm^{-2}). The arrows in the figure indicate the direction of the spectral changes with time.

Since the important steps of the photocatalytic degradation could be related to the interaction of the molecules with the TiO_2 surface, an investigation of the intercalating periods of adsorption and illumination has been carried out. The aim of this experiment is to enable the organic molecules to rearrange and/or readsorb at the oxide surface after the photodegradation period.

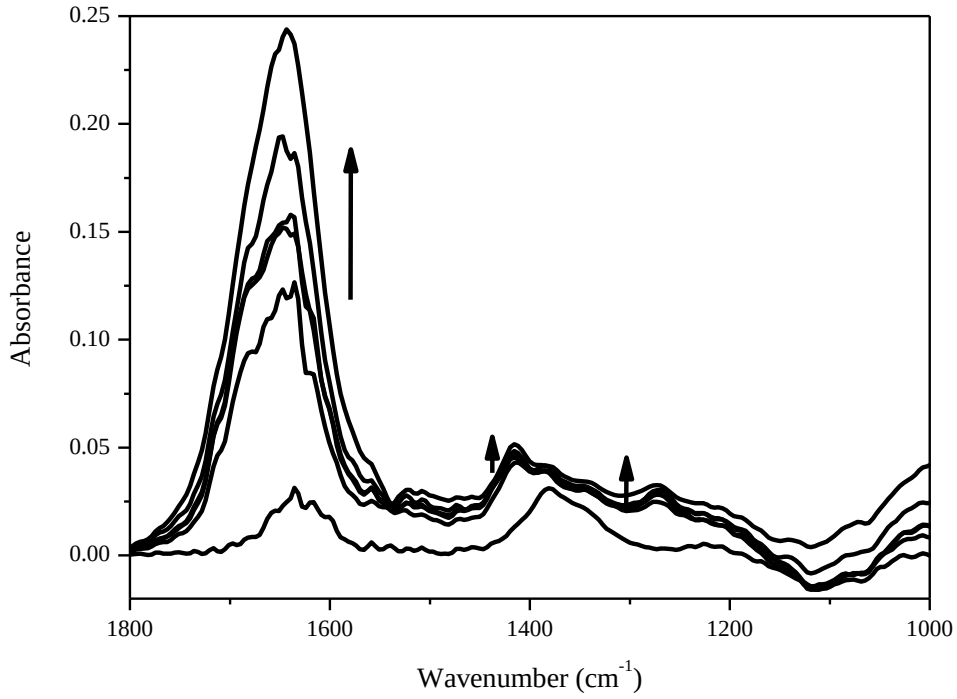

Figure 25: Evolution of ATR-FTIR spectra for an anatase TiO_2 film (PC500) in O_2 saturated 10.0 mmol·L^{-1} DCA solution at pH 4.0 in 10.0 mmol·L^{-1} KNO_3. The first spectrum has been taken after 60 min of equilibration, the following spectra were recorded in times of 30 min after the start of UV irradiation (with a light intensity of 1.0 mW·cm^{-2}), 60 min of dark-equilibration again, 30 min after UV irradiation, 60 min of dark-equilibration and 60 min after the start of UV irradiation. The absorbance changed nearly parallel to the time. The arrows in the figure indicate the direction of the spectral changes with time.

Using a 10.0 mmoL^{-1} DCA solution, the experiment has been performed in an O_2 saturated solution. Figure 25 shows the spectra obtained during this investigation. The spectral shape is similar to that for the photodegradation of DCA in the O_2 saturated solution. The spectral bands, 1381 cm^{-1}, 1412 cm^{-1}, 1354 cm^{-1}, and 1273 cm^{-1} do not show changes with the adsorption intervals. This observation indicates that the time necessary for an adequate rearrangement/re-adsorption of the molecules at the surface, is higher than the dark time provided in this study. Another possibility is that the inner sphere complexes formed at the surface are very strong and cannot be easily substituted. To prove the first possibility different periods of dark equilibration have been tested, i.e., 30, 60, and 120 min. The spectral bands observed in this study (data not shown) show the same evolution already observed for the investigation using 60 min of dark-equilibration. It is important to observe the huge increase in the intensity of the band above 1600 cm^{-1}.

The investigation of other titanium dioxide materials could contribute to a better understanding of the adsorption/photodegradation behavior. The differences in the crystalline structure and the surface shape are expected to have a strong impact on its interaction with organic molecules. Therefore, the photocatalytic degradation, as well as the intercalating periods of the dark-equilibration, has also been investigated for the anatase powders PC10 and S230.

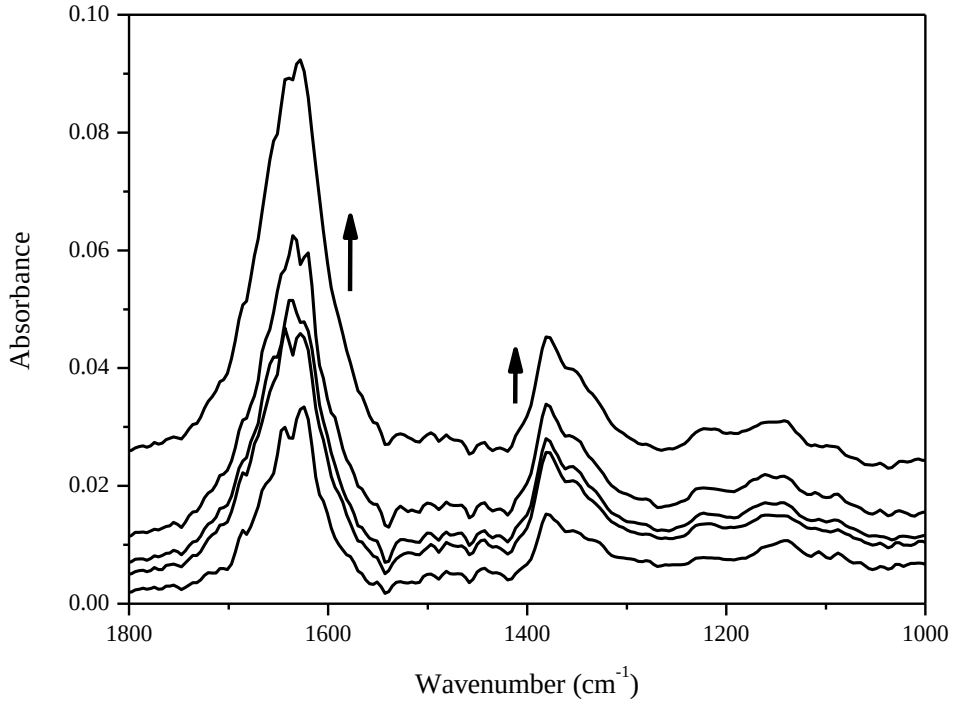

Figure 26: Evolution of ATR-FTIR spectra for an anatase TiO_2 film (PC10) in O_2 saturated 10.0 mmol·L^1 DCA solution at pH 4.0 in 10.0 mmol·L^{-1} KNO_3. The first spectrum has been taken after 60 min dark-equilibration, and the following spectra were recorded in times of 30 min after the start of UV irradiation (with a light intensity of 1.0 mW·cm^{-2}), 60 min of dark-equilibration again, 60 and 120 min after the start of UV irradiation. The arrows in the figure indicate the direction of the spectral changes with time.

Figure 26 and Figure 27 show the spectral evolution of an O_2 saturated 10 mmol·L^{-1} DCA solution at pH 4.0 in contact with a PC10 and a S230 film, respectively. Different from the results observed using the PC500 powder for the molecules adsorbed on the PC10 sample, the spectral bands do not change with irradiation. The bands at 1381, 1226, and around 1152 cm^{-1} as well as the shoulder at 1354 cm^{-1}, almost show the same intensity initially observed, even after long periods of contact. The only changes are the shift observed for the baseline level and the slightly increase of the band intensities.

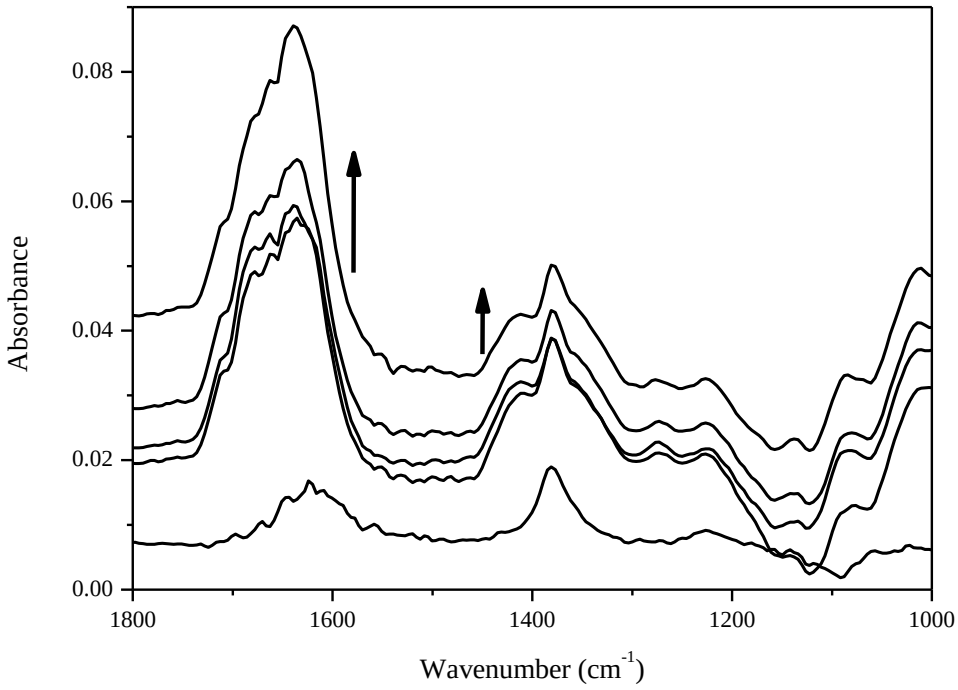

Figure 27: Evolution of ATR-FTIR spectra for an anatase TiO_2 film (S230) in O_2 saturated 10.0 mmol·L^{-1} DCA solution at pH 4.0 in 10.0 mmol·L^{-1} KNO_3. The first spectrum has been taken after 120 min dark-equilibration, and the following spectra were recorded in times of 30 min after the start of UV irradiation (with a light intensity of 1.0 mW·cm^{-2}), 30 min of dark-equilibration again, 30 and 60 min after the start of UV irradiation. The arrows in the figure indicate the direction of the spectral changes with time.

On the other hand, the S230 powder presented spectral changes which are similar to these observed for the PC500 material (see Figure 27). The presence of two new bands at 1416 and 1277 cm^{-1}, as well as the immense increase of the signal above 1600 cm^{-1} again indicates the formation of new surface structures, which are stable during the re-equilibration periods. The appearance of bands at 1138, 1088 and 1014 cm^{-1} already after the first illumination period is also noticeable.

4.3 Investigation of the Adsorption of Chlorinated Acetic Acids at PC500

4.3.1 Monochloroacetic Acid (MCA)

With one chloride atom less than dichloroacetic acid MCA has different physical and chemical properties, which have been shown to directly influence its photocatalytically degradation process. Studies performed by Czili *et al.* [33] suggest that MCA is more easily degraded photocatalytically in the presence of TiO_2 than the other chloroacetic acids. This higher degradation rate is related to its better adsorption at the metal oxide surface, which enables the direct attack of the photogenerated electron/hole pair. Lifongo *et al.* argue, however, that MCA has a stable structure and is therefore less susceptible to degradation than other organic molecules with similar structure, e.g., AA and DCA [27]. A better understanding of its interaction with the TiO_2 surface can obviously clarify the degradation differences compared to the other acetic acids. Therefore, a more accurate investigation involving monochloroacetic acid and the TiO_2 surface has been performed here.

4.3.1.1 Adsorption of Monochloroacetic Acid at PC500 Particles in Suspension

The adsorption of MCA at TiO_2 powders have been investigated on the PC500 sample. This material has been selected due to its good photocatalytic efficiency in comparison to rutile [19, 135], and the simplicity of the data interpretation given that it is composed of only anatase.

Figure 28 shows the adsorption isotherm measured for MCA ($0.5\ mmol \cdot L^{-1}$ - $120\ mmol \cdot L^{-1}$) on the PC500 powder. The dashed and black lines indicate the fitting according to the Langmuir and modified Langmuir model, respectively.

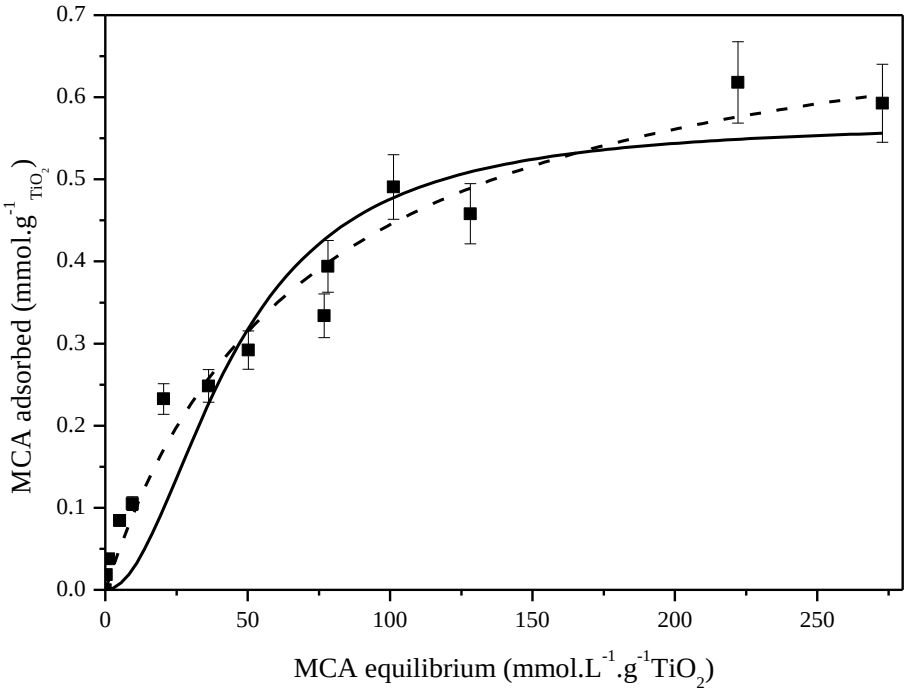

Figure 28: Monochloroacetic acid (pH 3.0) adsorption isotherm on anatase (PC500). The dashed line is the fitting to the Langmuir isotherm equation and the black line is the fitting to the modified Langmuir isotherm equation.

From the fitting it has been observed that both models show a good correlation to the experimental data. The Langmuir model shows an adsorption constant of 14×10^{-3} L·mmol^{-1} (see Table 8), whereas the number of exchangeable hydroxyl sites is 760 µmol·g^{-1} TiO_2. For the modified Langmuir model the number of exchangeable OH groups is 571 µmol·g^{-1} TiO_2. The difference calculated for the adsorption constant is approximately of one order of magnitude.

Table 8: Adsorption parameters extracted from the adsorption isotherms of MCA at pure anatase (PC500), using the Langmuir and the modified Langmuir model, respectively.

Isotherm	**K (L·mmol^{-1})**	**N (µmol·g^{-1} TiO_2)**
Langmuir	$14.0 \times 10^{-3} \pm 3.0 \times 10^{-3}$	760 ± 58
Modified Langmuir	$1.0 \times 10^{-3} \pm 0.3 \times 10^{-3}$	571 ± 43

4.3.1.2 Monochloroacetic Acid Adsorption at PC500 Films

All experiments using MCA have been carried out employing the batch system using 5.5 mL of solution. To allow a better comparison between the MCA and the DCA adsorption, the same experimental conditions previously optimized for DCA have been used (see chapter 4.2). The optimal concentration of MCA, which permits the observation of the spectral signals only from the adsorbed molecules without any interference of the solution phase has been determined to be between 0.5 and 5.0 mmol·L^{-1}. Figure 29 shows the spectra taken for 1.0 and 5.0 mmol·L^{-1} MCA solution in direct contact with the ZnSe crystal, and for 1.0 mmol·L^{-1} MCA solution in contact with the PC500 film. Spectral signals assigned to the MCA molecule have been observed only for the solution measured in the presence of the TiO_2 layer.

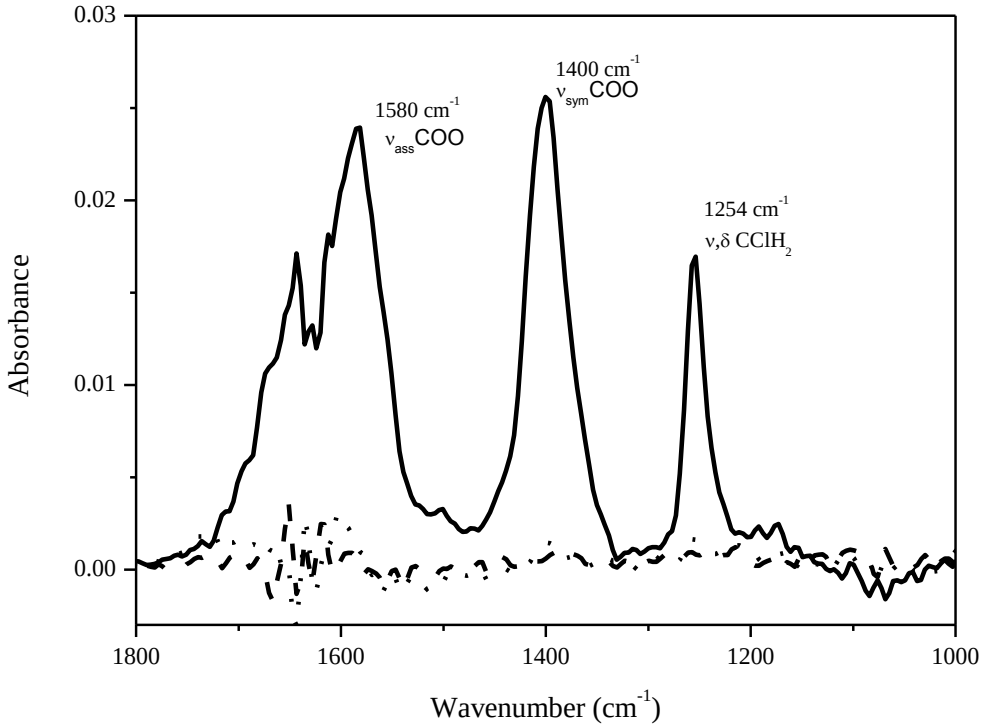

Figure 29: ATR-FTIR spectra for MCA solution (pH 3.0 in 10.0 mmol·L^{-1} KNO_3): 1.0 mmol·L^{-1} (– –) and 5.0 mmol·L^{-1} (·····) in the absence and for 1.0 mmol·L^{-1} (——) in the presence of TiO_2 film (PC500), taken after 15 min of equilibration.

The vibrational signals observed in Figure 29 have also been indicated and identified. The band observed in the region above 1580 cm^{-1} is assigned to the carbonyl asymmetric stretching mode, most likely with contributions from the O-H bending mode of the carbonyl group. In this spectral region signals of the vibrational bending mode from the water molecule

[136] are also observed. The band at 1400 cm^{-1} corresponds to the symmetric COO stretching mode and the OH bending mode is attributed to non-dissociated MCA molecules. Due to its pK_a value, i.e., 2.87 [137], MCA is only partially dissociated in solution at pH 3.0, as shown in Figure 66A (see Appendix). Contributions from the C-C symmetric bending (scissoring) mode are also expected around 1400 cm^{-1}. Finally, the band at 1254 cm^{-1} is assigned to different bending and stretching modes of the CHHCl group [138].

An investigation of MCA solutions (1.0 $mmol \cdot L^{-1}$) on the PC500 layer at 3 different pH conditions has also been performed. This study permits a better comprehension of the system at different electrostatic conditions. At pH 3.0, where approximately half of the molecules are dissociated, the TiO_2 surface exhibits a high protonation level. At pH 6.0 with a titanium dioxide surface presenting almost the same number of positive and negative OH groups all MCA molecules are already dissociated. At the alkaline pH condition, i.e., at pH 9.0, the most adverse condition for the adsorption exists, since both the TiO_2 surface and MCA^- carries mostly negative charges.

Figure 30 shows the spectra recorded for the different pH conditions. Intense spectral changes are observed, suggesting considerable changes in the surface interaction with changing pH. At pH 3.0 the same spectral signals previously shown in Figure 29 are observed, with bands at 1580, 1400 and 1254 cm^{-1}. Increasing the pH to 6.0 alters mostly the intensity of the spectral bands, with the simultaneous appearance of a new band centered at 1323 cm^{-1}. This band is assigned to the symmetric bending modes of the CH_2Cl group. Another band around 1580 cm^{-1} shifts to a high wavenumber region, nevertheless, leaving a shoulder at its original value. At pH 9.0 the signals assigned to the MCA molecule adsorbed at the surface almost disappear. Small bands at 1381 and 1251 cm^{-1} as well as a new signal at 1497 cm^{-1} are the only observable spectral signals. Once the pH is adjusted back to 3.0 the signals initially observed can be observed again (data not shown) indicating a reversible adsorption process. The only exception is the negative band localized between 1200 and 1000 cm^{-1}, which is not reestablished to its initial level.

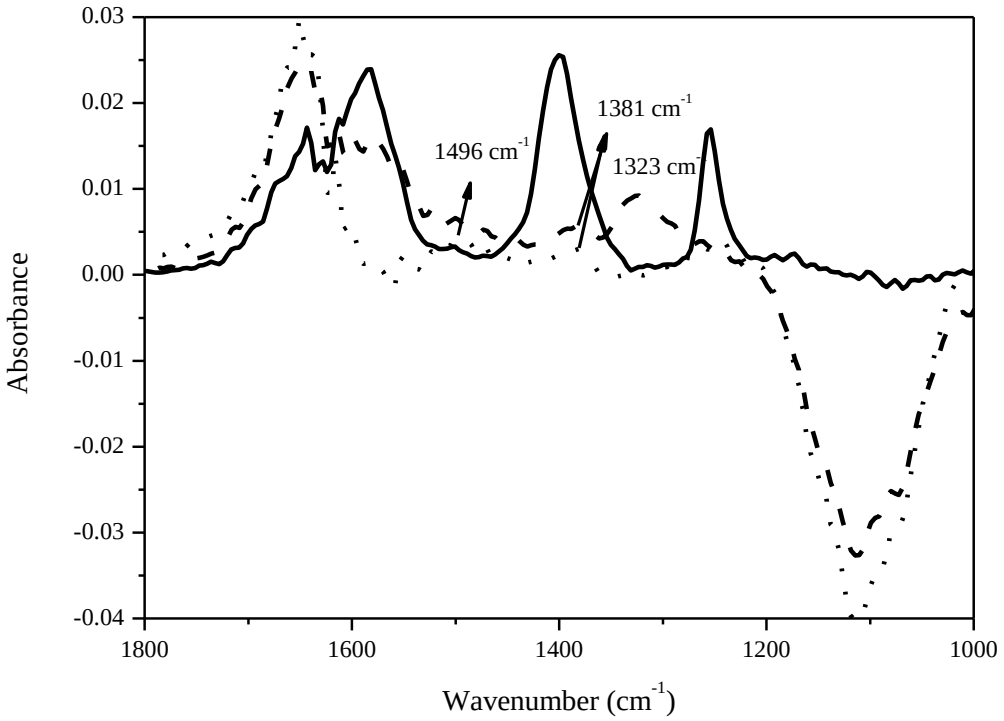

Figure 30: ATR-FTIR spectra for an anatase TiO_2 film (PC500) in 1.0 mmol·L^{-1} MCA at distinct pH conditions in 10.0 mmol·L^{-1} KNO_3. pH condition of the solution: 3.0 (— –), 6.0 (– –) and, 9.0 (·····), taken after 10 min of equilibration.

Kinetic investigations have been performed at pH 3.0, where the most intense spectral signals are observed. The evolution of the spectral signal, shown in Figure 31, has been followed by the time-dependent change of the spectral band centered at 1400 cm^{-1}. It can be seen that at the beginning the signal shows a very fast and intense increase. After about 5 min the maximum intensity is achieved and a slow decay begins. However, different from the DCA measurements, the signals reach an equilibrium after some time, i.e., around 150 min of equilibration.

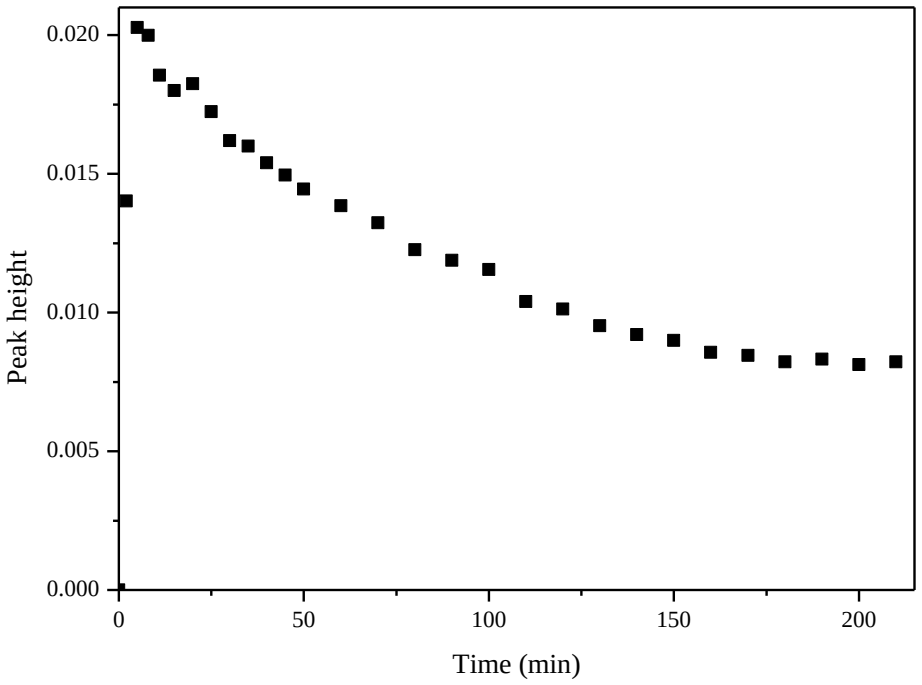

Figure 31: Evolution of the peak height from the ATR-FTIR spectral band centered at 1400 cm^{-1} for MCA (1.0 $mmol \cdot L^{-1}$) solution at pH 3.0 on a TiO_2 film (PC500) in 10 $mmol \cdot L^{-1}$ KNO_3, as a function of the equilibration time.

4.3.2 Acetic Acid (AA)

In contrast to homologues used in this study, AA is the only molecule does not contain chloride in its structure. Therefore, it is expected to show a different interaction with the TiO_2 surface. Investigations involving the adsorption of AA on TiO_2 using Raman and FTIR spectroscopy published recently, suggest a stronger interaction of AA and AA^- with rutile than with anatase [139]. However, its photocatalytic degradation is reported to take place at both titania phases [139].

The adsorption of acetic acid at the TiO_2 surface has been investigated here using the same experimental conditions previously employed for the investigation of the MCA and DCA adsorption.

4.3.2.1 Adsorption of Acetic Acid at PC500 Particles in Suspension

The adsorption isotherms have been measured using anatase (PC500 powder) according to the experimental procedure described in chapter 3.2.3. AA solutions with concentrations between 0.5 - 120 mmol·L^{-1} have been used. Both the Langmuir and the modified Langmuir model have been employed for fitting of the experimental points; see Figure 69 in the Appendix.

The data obtained from the fitting curves are summarized in Table 9. The number of substituted adsorption sites obtained from the Langmuir fitting is 183 µmol·g^{-1} with an adsorption constant of 47 x 10^{-3} L·$mmol^{-1}$. For the modified Langmuir model 162 µmol·g^{-1} OH surface groups are calculated to be exchangeable with the adsorption constant corresponding to 6.5 x 10^{-3} L·$mmol^{-1}$.

Table 9: Adsorption parameters extracted from the adsorption isotherms of AA at pure anatase (PC500), using the Langmuir and the modified Langmuir model, respectively.

Isotherm	**K (L·$mmol^{-1}$)**	**N (µmol·g^{-1} TiO_2)**
Langmuir	47 x 10^{-3} ± 14 x 10^{-3}	183 ± 11
Modified Langmuir	6.5 x 10^{-3} ± 1 x 10^{-4}	162 ± 5

4.3.2.2 Acetic Acid Adsorption at PC500 Films

All experiments using AA have been carried out in the batch system using a reaction volume of 5.5 mL. To allow a comparison to data obtained using (DCA and MCA) the same experimental conditions previously optimized for DCA have been used, i.e.: pH 3.0, 10 mmol·L^{-1} KNO_3, and 250 spectral accumulations. AA concentrations between 0.5 and 5.0 mmol·L^{-1} have been measured both, in the presence and in the absence of the TiO_2 film, to obtain an ideal concentration to perform the adsorption investigations. Figure 32 shows the

spectra taken for a 5.0 mmol·L^{-1} AA solution on the IRE as well as the spectra for 1.0 mmol·L^{-1} AA on the ZnSe crystal and on the TiO_2 layer. The absence of significant bands in the spectra recorded without the TiO_2 film, even using a 5.0 mmol·L^{-1} acid solution permits the use of a 1.0 mmol·L^{-1} solution, which shows bands with good intensities.

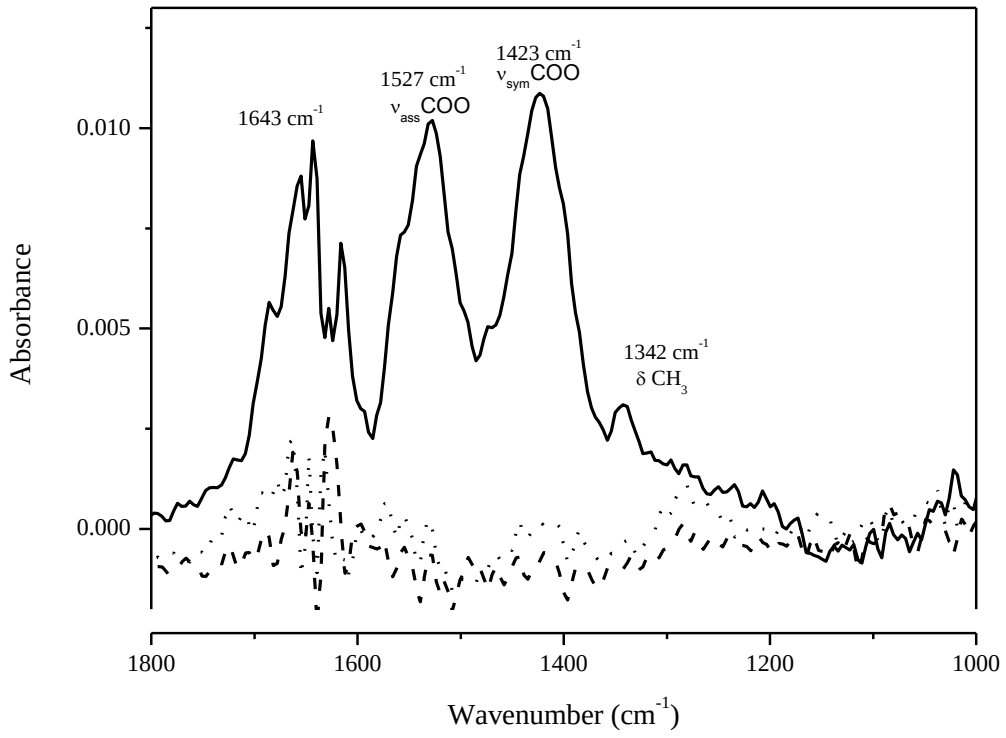

Figure 32: ATR-FTIR spectra for AA solution (pH 3.0 in 10.0 mmol·L^{-1} KNO_3): 1.0 mmol·L^{-1} (– –) and 5.0 mmol·L^{-1} (·····) in the absence and 1.0 mmol·L^{-1} (——) in the presence of an anatase TiO_2 film (PC500), taken after 10 min of equilibration.

Four intense signals are observed in the spectra shown in Figure 32, assigned to adsorbed AA or AA^-. The most intense bands, around 1527 cm^{-1} and 1423 cm^{-1}, are associated to the vibrational modes of the acetate anion, and are assigned to the asymmetric stretching mode of the carbonyl group (ν_aCOO) (surface-coordinated acetate) and the symmetric stretching mode ν_sCOO, respectively. The spectral shoulder observed between 1550 - 1560 cm^{-1} is assigned also to the asymmetric stretching mode of the carbonyl group (ν_aCOO), in this case from aqueous acetate ions. The less intense signal observed at 1342 cm^{-1} is assigned to the symmetric bending mode δ_s CH_3 of acetate [139]. These assignment have been confirmed by theoretical calculations performed by Segarra [128]. According to these calculations other vibrational modes also contribute for the spectral signals. The band at 1527 cm^{-1} carries, for example, contributions from the symmetric bending mode of the C-H groups. The C-C symmetric bending mode shows input for the band centered at 1423 cm^{-1},

whereas the peak at 1342 cm^{-1} has contributions from the stretching mode of the C-O from the COH group. The band above 1600 cm^{-1} is assigned to the carbonyl stretching mode as well as to the O-H bending from the carbonyl group, attributed to molecularly adsorbed AA bound at Lewis acid sites (Ti^{4+}) through the oxygen lone-pair electrons of the carbonyl group [140]. Residual signals from the TiO_2-OH groups are also not totally suppressed.

In agreement with previous work published by Rotzinger *et al.* [141] and Backes *et al.* [140] it has been observed that for acetate the intensity of the $\nu_s(COO)$ vibration is larger than the $\delta_s(CH_3)$ vibration and occurs at a higher frequency. Interestingly a small band appears around 1285 cm^{-1} in the spectrum taken for the 5 $mmol \cdot L^{-1}$ acetic acid solution without a PC500 layer. This signal is probably assigned to the ν (C−O) [139] vibrational mode of molecular acetic acid. In the presence of the TiO_2 film this band cannot be observed.

Figure 33 shows the spectra collected for AA solutions at a TiO_2 layer at different pH values. An increase in the pH from 3.0 to 6.0 results in big changes in the spectral shape, the bands at 1423 and 1527 cm^{-1} almost disappear, and a new peak between 1545 and 1570 cm^{-1} is observable. The band at 1342 cm^{-1} is red shifted to 1330 cm^{-1} showing a strong increase in intensity, while the band above 1600 cm^{-1} increases as well.

The broad band between 1545 and 1570 cm^{-1} has been assigned to $\nu_a COO$ as a combination of surface-coordinated and weakly interacting acetate. The signal between 1346 and 1296 cm^{-1} is assigned to adsorbed $\delta_s CH_3$ vibrations. Since the dissociation constant of AA is 4.75, at pH 6.0 it is almost totally dissociated (see Figure 66 B in the Appendix). Therefore an interaction of AA^- with the neutral surface is still possible, which justifies the presence of the bands.

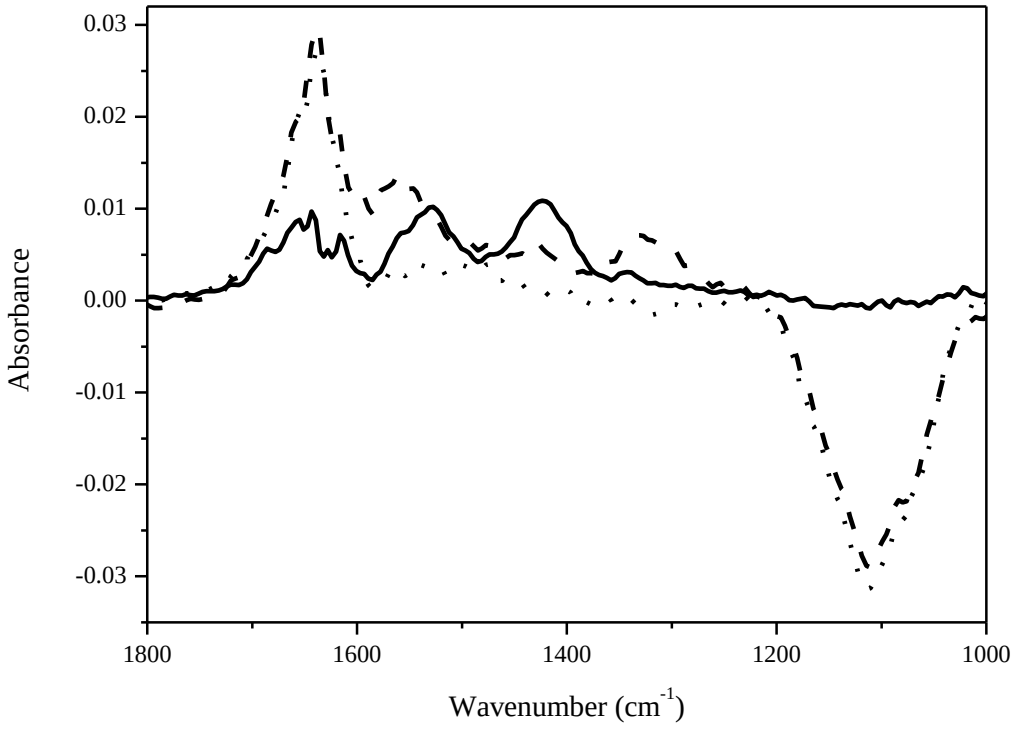

Figure 33: ATR-FTIR spectra for an anatase TiO_2 film (PC500) in 1.0 mmol·L^{-1} AA solution at distinct pH conditions in 10.0 mmol·L^{-1} KNO_3. Solution pH condition: 3.0 (——), 6.0 (– –) and 9.0 (·····), spectra have been taken after 10 min of equilibration.

At pH 9.0 the TiO_2 surface is mostly positively charged. On the spectra small bands are observable (dotted line in Figure 33). Actually, only one appreciable signal is observed above 1600 cm^{-1}, which is assigned to the bending mode (H-O-H) of water [142].

Due to the higher adsorption constant calculated from the adsorption isotherm, it is supposed that the adsorption on the surface is extended for AA^- and AA compared to the chlorinated acetic acids. In Figure 34 the evolution of the peak at 1423 cm^{-1} is shown. The progress of the curve shows an initial increase in the signal intensity, but after around 5-10 min a decay of the signal is observed. After about 80 min the intensity is very low and cannot be distinguished from the spectral noise.

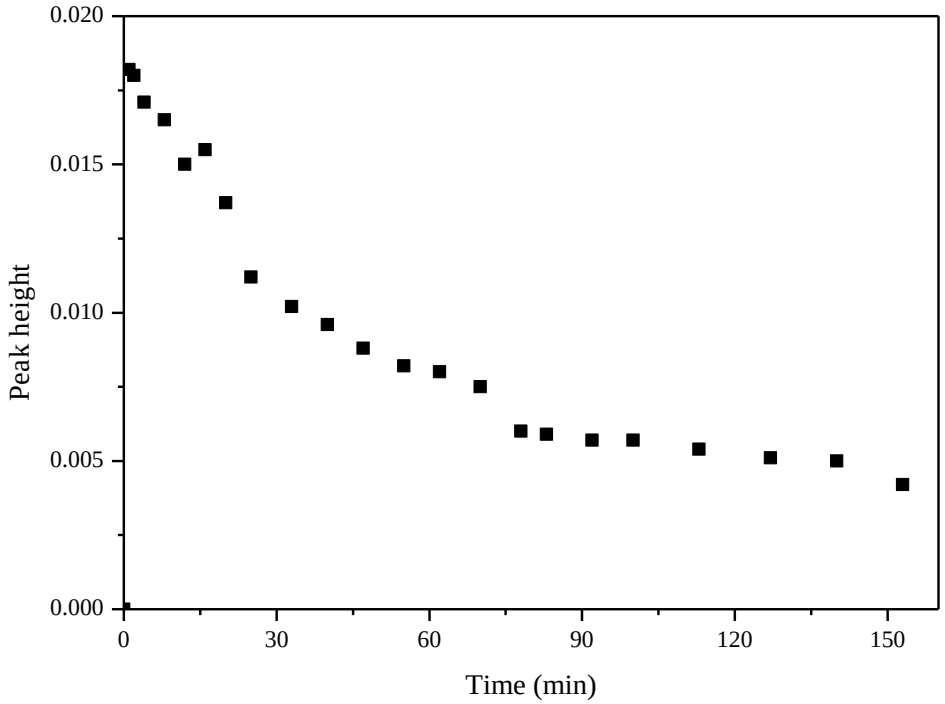

Figure 34: Evolution in time of the peak height from the ATR-FTIR spectral band centered at 1423 cm^{-1} of the AA (1.0 $mmol \cdot L^{-1}$) solution at pH 3.0 on an anatase TiO_2 film (PC500) in 10 $mmol \cdot L^{-1}$ KNO_3.

4.3.3 Trichloroacetic Acid (TCA)

In this part of the investigation the final molecule investigated was TCA. Due to the total substitution of the hydrogen by chlorine atoms TCA is expected to show less interaction with the TiO_2 surface. TCA is known for its good stability against photocatalytic oxidation [33]. Moreover, it is of particular importance to obtain knowledge on details of the degradation mechanism for a better understanding of its interaction with the TiO_2 surface. Therefore, its adsorption on PC500 powder has been studied in detail.

4.3.3.1 Adsorption of Trichloroacetic Acid at PC500 Particles in Suspension

Adsorption isotherms provide important information concerning the oxide surface and its interaction with organic molecules. According to Czili and Horvath [33] TCA shows a weaker adsorption at TiO_2 powders than, e.g., MCA and DCA. Furthermore, knowing that the pK_a of the acids decrease with the increase of the number of chlorides at the acid structures, a higher presence of the anions in solution can be expected. Both observations lead to the assumption that the interaction will not be strongly influenced by electrostatic interactions.

Employing TCA solutions (0.5 - 120.0 $mmol \cdot L^{-1}$) on anatase (PC500), in 10.0 $mmol \cdot L^{-1}$ KNO_3 the adsorption isotherm has been measured at pH 3.0. The fitting of the experimental points has been done using both, the Langmuir and the modified Langmuir model, see Figure 70 in the Appendix. The number of OH sites exchanged on the PC500 powder by TCA anions, obtained from the curve-fitting using the Langmuir model is 147 $\mu mol \cdot g^{-1}$, for the modified Langmuir model it is 130 $\mu mol \cdot g^{-1}$. The adsorption constants are 43.0 x 10^{-3} $L \cdot mmol^{-1}$ and 5 x 10^{-3} $L \cdot mmol^{-1}$ for the Langmuir and the modified Langmuir model, respectively.

Table 10: Adsorption parameters obtained from the adsorption isotherms of TCA on PC500 using the Langmuir and the modified Langmuir model, respectively.

Isotherm	**K ($L \cdot mmol^{-1}$)**	**N ($\mu mol \cdot g^{-1}$ TiO_2)**
Langmuir	$43.0 \times 10^{-3} \pm 35 \times 10^{-3}$	147 ± 28
Modified Langmuir	$5.0 \times 10^{-3} \pm 4 \times 10^{-4}$	130 ± 16

4.3.3.2 Trichloroacetic Acid Adsorption at PC500 Films

For the experiments studying the adsorption of TCA at the TiO_2 surface the same experimental conditions previously employed for the other organic acids have been used. At the beginning it is necessary to establish the TCA concentration, that can be used to perform the adsorption kinetic study, i.e., that does not present strong spectral influence from the bulk molecules. Therefore, it has been performed an investigation involving solutions of TCA (1.0 - 5.0 $mmol \cdot L^{-1}$) in direct contact with the ZnSe crystal and at the PC500 film. Figure 35 shows the spectra recorded for a 1.0 $mmol \cdot L^{-1}$ TCA solution in the absence and in the presence of a TiO_2 layer, and the spectrum of a 5.0 $mmol \cdot L^{-1}$ solution in the absence of the semiconductor layer. The spectrum taken for the 5.0 $mmol \cdot L^{-1}$ TCA without anatase film shows a band centered at 1338 cm^{-1}, the same signal is observed for the 1.0 $mmol \cdot L^{-1}$ solution adsorbed on the PC500 layer. The maintenance of the position of the band is indication of a weak interaction between the TCA and the TiO_2 surface, once the vibrational changes are not obseved. Spectral signals are not observed for low TCA concentrations (1.0 $mmol \cdot L^{-1}$) in the absence of TiO_2,.

The band observed at 1338 cm^{-1} has been assigned to the C-C symetric bending (scisoring) mode, with contributions of the COO symmetric stretching mode and the OH bending. A small band is observed in the region between 1530-1580 cm^{-1}, which can be assigned to the assymmetric carbonyl stretching mode.

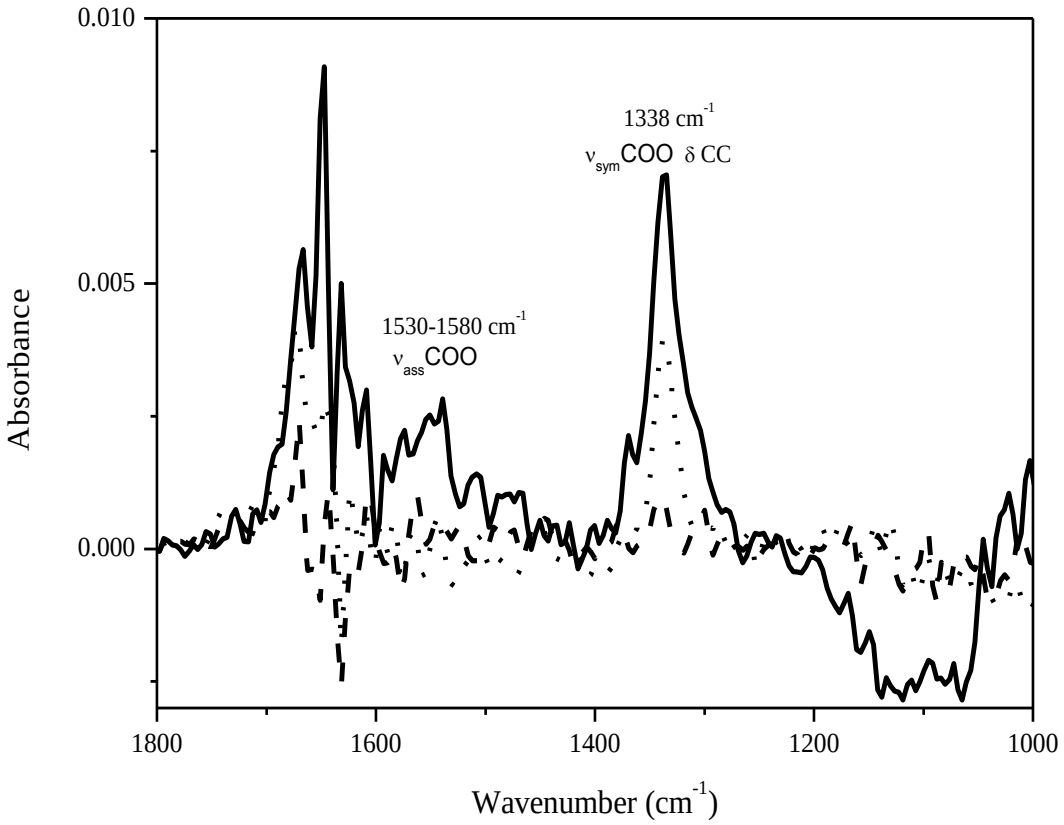

Figure 35: ATR-FTIR spectra for TCA solution (pH 3.0 in 10.0 mmol·L^{-1} KNO_3): 1.0 mmol·L^{-1} (– –) and 5.0 mmol·L^{-1} (·····) in the absence and 1.0 mmol·L^{-1} (——) in the presence of an anatase TiO_2 film (PC500), taken after 10 min of equilibration.

Figure 36 shows the spectra recorded for the TCA solutions on a TiO_2 layer at different pH values is shown. Two spectral behaviors are observed for the recorded data, one for the TCA solution at pH 3.0 and 6.0 and another for the solution at pH 9.0. The presence of spectral bands at acidic pH conditions was expected, once TCA is already completely dissociated at pH 3.0 (Figure 67 in the Appendix) and can interact with the positively charged TiO_2 surface. At pH 9.0 the TiO_2 surface is mostly negative and inhibits the approximations and adsorption of molecules at the surface.

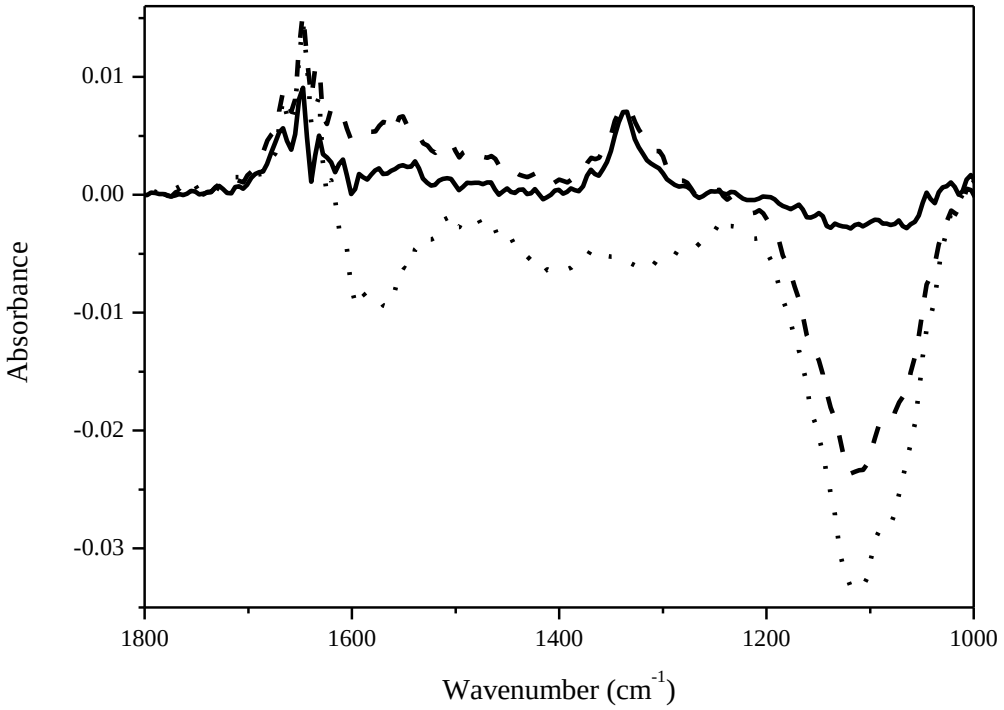

Figure 36: ATR-FTIR spectra for an anatase TiO_2 film (PC500) in 1.0 mmol·L^{-1} TCA at distinct pH conditions in 10.0 mmol·L^{-1} KNO_3. Solution pH condition: 3.0 (——), 6.0 (– –) and 9.0 (·····), taken after 10 min of equilibration.

The negative bands observed at pH 9.0, between 1550 and 1650 cm^{-1} and around 1400 and 1320 cm^{-1}, suggest that compounds previously adsorbed on the surface are released. With the pH re-adjustment of the TCA solution from 9.0 to 3.0 (data not shown), the negative bands are restablished (data not shown). The negative band observed between 1000 and 1200 cm^{-1} does not follow this behavior. The presence of this band has already been observed for the other acids investigated, and has not relation to the molecular structure of the acids.

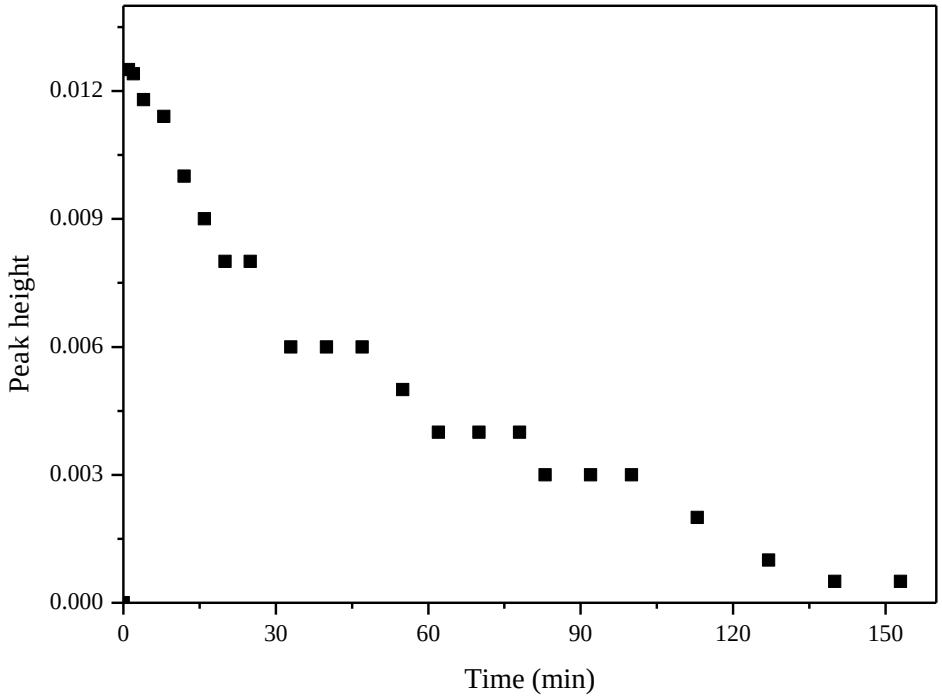

Figure 37: Evolution in time of the peak height from the ATR-FTIR spectral band centered at 1338 cm^{-1} of the TCA (1.0 $mmol \cdot L^{-1}$) solution at pH 3.0 on an anatase TiO_2 film (PC500) in KNO_3 10 $mmol \cdot L^{-1}$.

TCA shows spectral bands with lower intensities than observed for the other acids. e The adsorption kinetic has been investigated using a 1.0 $mmol \cdot L^{-1}$ TCA solution, at pH 3.0. Figure 37 shows the evolution of the height for the spectral band centered at 1338 cm^{-1} in time. The initial increase of the signal is followed by a prompt decay of its intensity, observed already after 4 min of reaction. After around 60 min of equilibration the spectral band cannot be distinguished from the spectral noise.

4.3.4 Chloroacetic and Acetic Acid Mixtures at PC500 Films

The investigation of the adsorption from the acids separately at the oxide surface indicates tendencies and provides evidences of how the adsorption occurs. However, for a better understanding of the affinity trends from acids at the TiO_2 surface the investigation of mixtures from the acids in contact with the film has been proposed. In this sense mixtures of the acid solutions (1.0 mmol·L^{-1}) at pH 3.0 have been prepared. The experiments have been performed in a batch system in similar conditions as previously used for the kinetic investigations of each acid.

Figure 38 shows the mixture of acetic acid and monochloroacetic acid. The most significant signals are observed at 1253 and 1400 cm^{-1}, assigned to the stretching and bending modes of the $CClH_2$ group and the symmetric stretching of COO from the MCA molecule, respectively. A shoulder at around 1346 cm^{-1} from AA (stretching and bending modes of the CH_3) can also be observed. These spectral data demonstrates a high occupation of the adsorption sites by MCA/MCA^-.

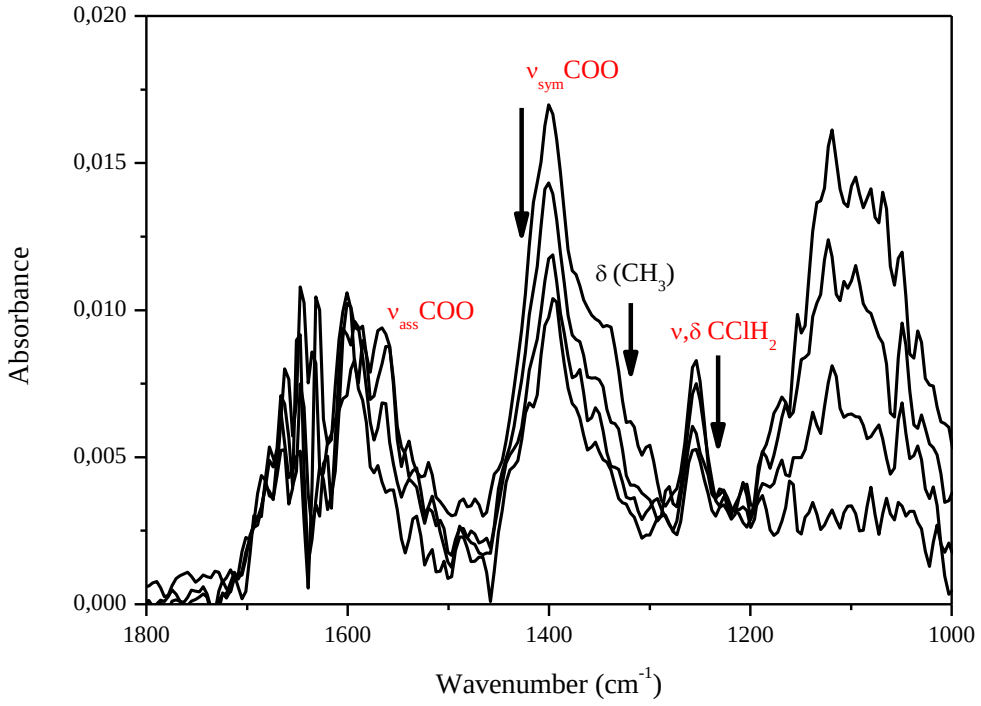

Figure 38: Evolution of ATR-FTIR spectra for an anatase TiO_2 film (PC500) in 1.0 mmol·L^{-1} AA and MCA solution at pH 3.0 in 10.0 mmol·L^{-1} KNO_3. The spectra were recorded in times of 5, 15, 30 and 45 min of dark-equilibration. The arrows in the figure indicate the direction of the spectral change with time. The vibrational signals marked in black are assigned to AA and in red to MCA.

With peaks of lower intensity the AA/DCA solution (see Figure 39), also shows the domination of the chlorinated molecule. DCA adsorbs faster and stronger on the titanium dioxide surface. The presence of a typical peak centered at 1380 cm^{-1} ($\nu_{sym}COO$) and 1226 cm^{-1} ($\nu,\delta\ CCl_2H$) band assigned to DCA can clearly be observed. Only a small shoulder at around 1340 cm^{-1} ($\nu,\delta\ CH_3$) attributed to AA is observable.

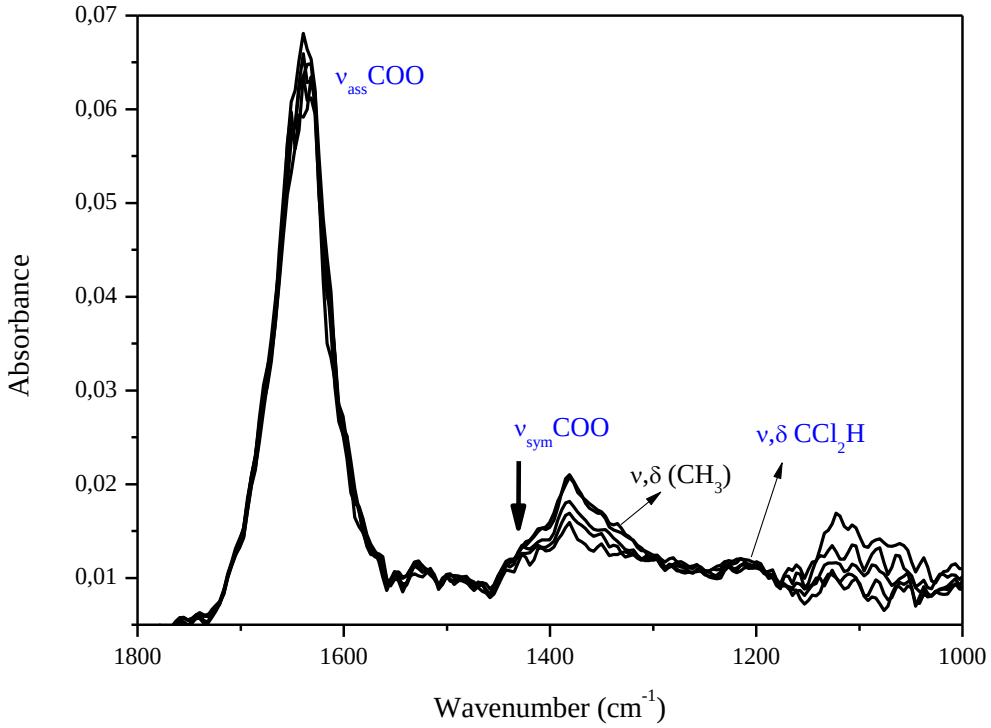

Figure 39: Evolution of ATR-FTIR spectra for an anatase TiO_2 film (PC500) in 1.0 $mmol \cdot L^{-1}$ AA and DCA solution at pH 3.0 in 10.0 $mmol \cdot L^{-1}$ KNO_3. The spectra were recorded in times of 5, 15, 30, 45 and 60 min of dark-equilibration. The arrow in the figure indicates the direction of the spectral change with time. The vibrational signals marked in black are assigned to AA and in blue to DCA.

Even for the mixture involving the TCA molecule, which shows the weakest interaction for the adsorption investigations, AA shows less intense signals (see Figure 40). Assigned to the symmetric stretching mode from COO, the band at 1420 cm^{-1} (slightly shifted) is the only signal related to the AA molecule. The band centered at 1338 cm^{-1} assigned to the symmetric stretching mode of COO and bending mode of C-C is typical for deprotonated TCA molecules.

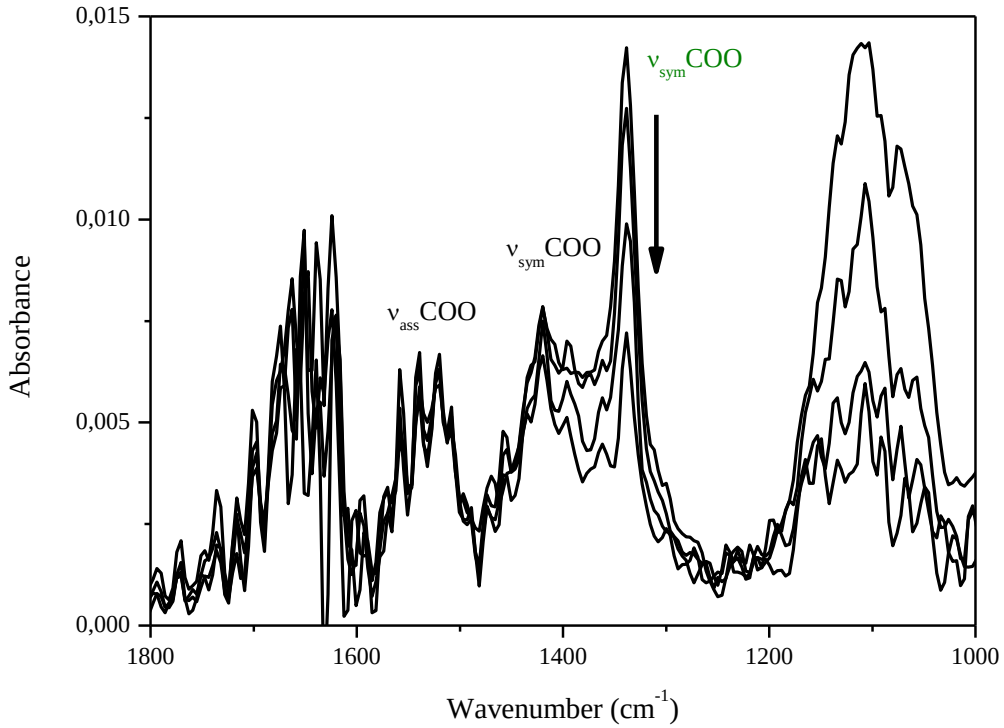

Figure 40: Evolution of ATR-FTIR spectra for an anatase TiO_2 film (PC500) in 1.0 mmol·L^{-1} AA and TCA solution at pH 3.0 in 10.0 mmol·L^{-1} KNO_3. Spectra were recorded in times of 5, 15, 30 and 45 min of dark-equilibration. The arrow in the figure indicates the direction of the spectral change with time. The vibrational signals marked in black are assigned to AA and in green to TCA.

In the competition between the chlorinated molecules, the MCA seems to adsorb faster at the surface, showing stronger signals. But after 15 min of reaction the DCA molecules also show important contribution in the spectra. This contribution is observed by the merged bands at 1380 and 1400 cm^{-1}, assigned to the symmetric stretching mode of COO, from DCA and MCA, respectively.

However, another band at 1254 cm^{-1} assigned to the stretching and bending modes of the $CClH_2$ group from the MCA indicates that the monochlorinated molecule has a more stable interaction with the surface, and can be observed even after 60 min of equilibration. The bands for the symmetric stretching also decay with time and cannot be distinguished anymore after around 30 min of reaction, see Figure 41.

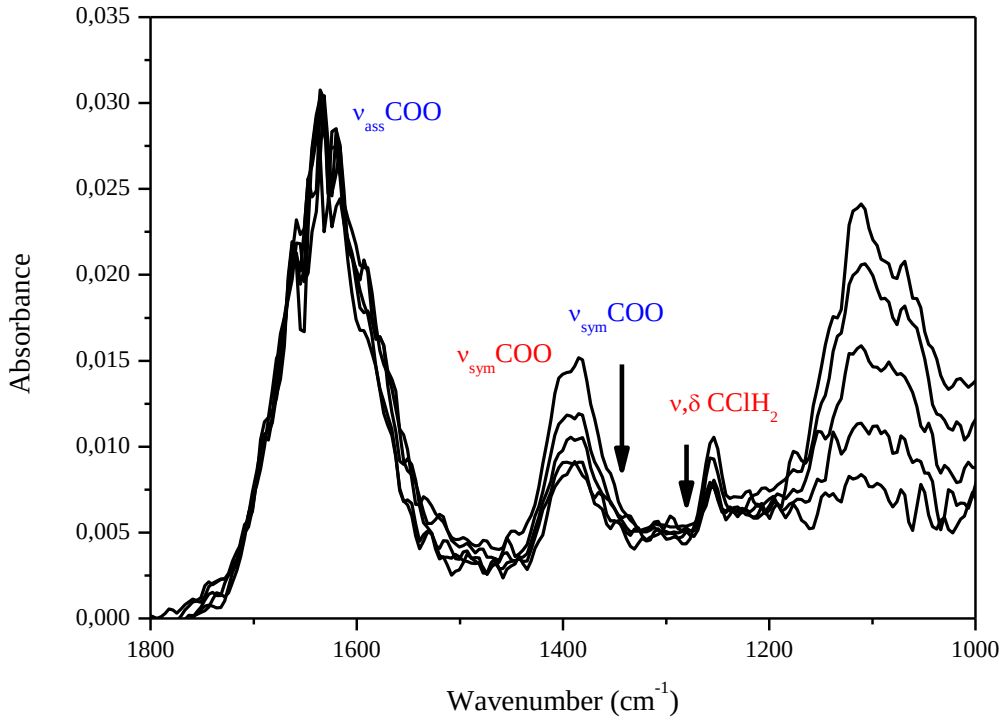

Figure 41: Evolution of ATR-FTIR spectra for an anatase TiO_2 film (PC500) in 1.0 mmol·L^{-1} MCA and DCA solution at pH 3.0 in 10.0 mmol·L^{-1} KNO_3. The spectra were recorded in times of 5, 15, 30 45 and 60 min of dark-equilibration. The arrows in the figure indicate the direction of the spectral change with time. The vibrational signals marked in red are assigned to MCA and in blue to DCA.

Similar behavior has been observed for the MCA/TCA mixture (see Figure 42). The spectral signals at 1253 and 1400 cm^{-1} are assigned to the MCA and the band at 1338 cm^{-1} associated to the TCA. In that case, though, all the bands can clearly be distinguished after 60 min of investigation.

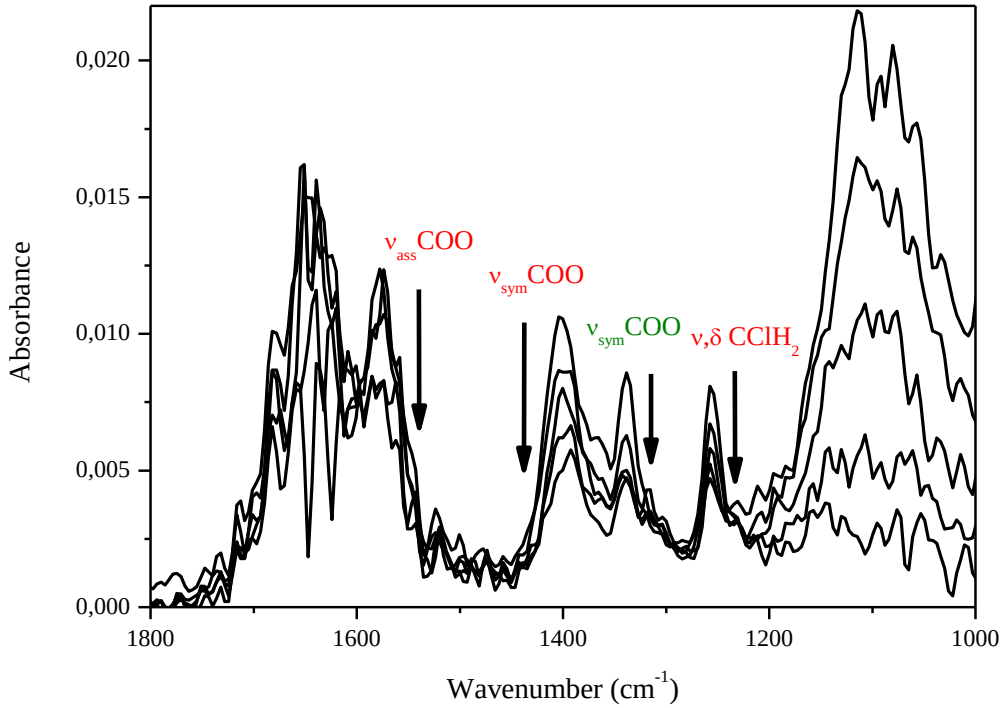

Figure 42: Evolution of ATR-FTIR spectra for an anatase TiO_2 film (PC500) in 1.0 mmol·L^{-1} MCA and TCA solution at pH 3.0 in 10.0 mmol·L^{-1} KNO_3. Spectra were recorded in times of 5, 15, 30, 45 and 60 min of dark-equilibration. The arrows in the figure indicate the direction of the spectral change with time. The vibrational signals marked in red are assigned to MCA and in green to TCA.

The mixture containing DCA and TCA also shows a strong competition for the adsorption sites. With intense signals centered at 1380 and 1226 cm^{-1} assigned to DCA and at 1338 cm^{-1} to the TCA. However, after 45 min of reaction the signals decrease sharply, as can be observed on Figure 43.

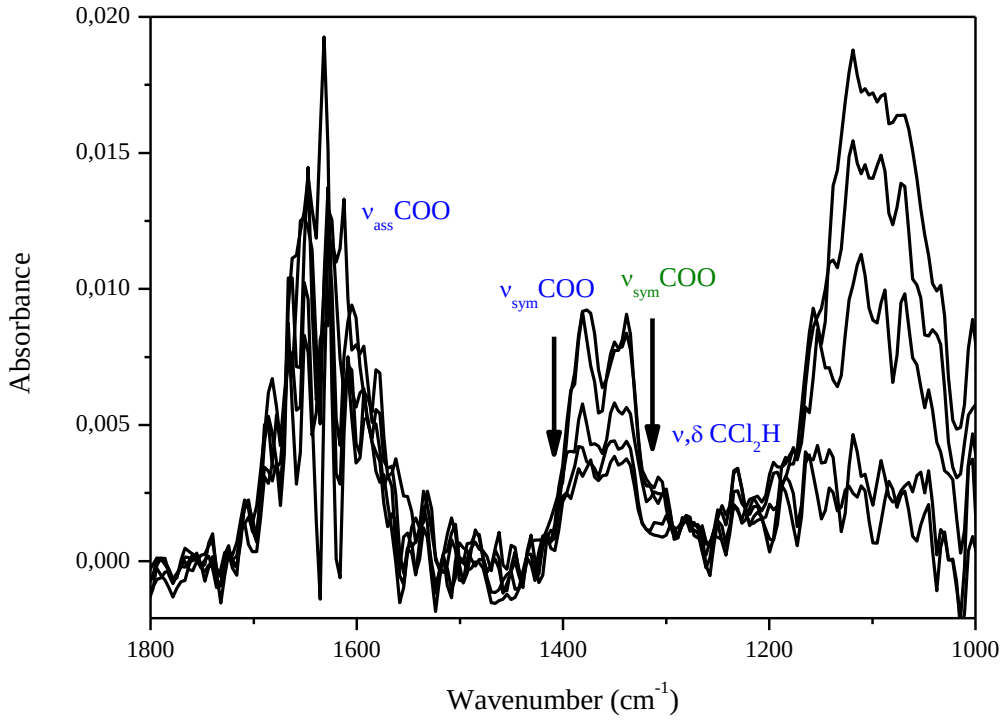

Figure 43: Evolution of ATR-FTIR spectra for an anatase TiO_2 film (PC500) in 1.0 mmol·L^{-1} DCA and TCA solution at pH 3.0 in 10.0 mmol·L^{-1} KNO_3. Spectra were recorded in times of 5, 15, 30, 45 and 55 min of equilibration in the dark. The arrows in the figure indicate the direction of the spectral change with time. The vibrational signals marked in blue are assigned to DCA and in green to TCA.

The presence of a strong absorption signal around 1650 cm^{-1} in almost all experiments involving the DCA molecule and the presence of a broad band around 1100 cm^{-1} in nearly all investigated mixtures, are also remarkable.

4.4 2,4-Dichlorophenoxyacetic Acid Investigation

The adsorption of the pesticide 2,4-D at the anatase (PC500) surface has also been carried out.

4.4.1 Adsorption of 2,4-D at PC500 Particles in Suspension

The solubility of 2,4-D in water is very low, i.e., 2.9 $mmol \cdot L^{-1}$ [143], which has difficult the determination of the pesticide concentrations by the HPLC methodology. This restricts the measurements of the adsorption isotherm, shown in Figure 71, to pesticide concentrations between 0.02 - 1.3 $mmol \cdot L^{-1}$.

The parameters obtained from the fitting of the isotherms are listed in Table 11. According to the adsorption curve data 2,4-D apparently adsorbs on the surface in a multilayer system. The number of adsorption sites occupied by 2,4-D molecules at the TiO_2 surface is 29 and 243 $\mu mol \cdot g^{-1}$ according to the BET and the modified Langmuir model, respectively. The obtained adsorption constants show an enormous error for both models.

Table 11: Adsorption parameters obtained from the adsorption isotherms of pure anatase (PC500) in equilibrium with 2,4-D aqueous solutions, using BET and modified Langmuir model.

Calculated parameter	**BET model**	**Modified Langmuir model**
N ($\mu mol \cdot g^{-1}$ TiO_2)	29 ± 15	243 ± 38
K ($L \cdot mmol^{-1}$)	149 ± 367	$1.4x10^{-3} \pm 4x10^{-4}$
P ($mmol \cdot L^{-1}$)	20 ± 0.2	-
l (layers)	6 ± 3	-

4.4.2 2,4-D Adsorption at PC500 Films

The low solubility of the acid in water has also limited the surface investigations. The highest concentration that could be employed was 2.7 mmol·L^{-1}. The experiments have been performed using 2,4-D concentrations between 0.3 mmol·L^{-1} and 2.7 mmol·L^{-1}. Measurements performed on clean ZnSe crystal show very small signals even for the highest concentration. The spectra taken for the solution on the anatase layer show much higher intensities for the signals of all concentrations investigated. Figure 44 shows the spectra of the 2,4-D solutions taken on the TiO_2 film at different concentrations.

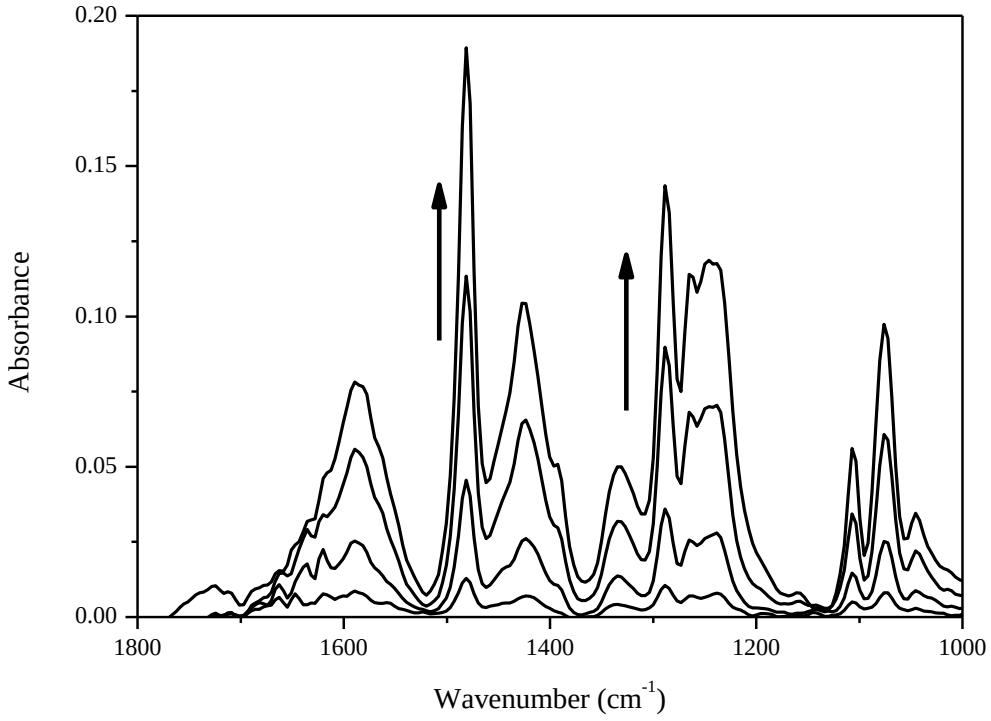

Figure 44: ATR-FTIR spectra for an anatase TiO_2 film (PC500) in 0.3, 0.5, 1.5 and 2.7 mmol·L^{-1} 2,4-D solutions at pH 2.9 in 10.0 mmol·L^{-1} KNO_3. The arrows in the figure indicate the direction of the spectral change with increase of the concentration.

On Figure 45, it is possible to observe the difference of the intensity from the pesticide spectral bands in solution (dashed line) and at the surface of the titanium dioxide film (black line).

The vibrational signals observed in Figure 45 have been assigned to two different parts of the molecule. Vibrational modes attributed to the carbonyl (1420-1280 cm^{-1}) group, to the

aromatic ring as well as to the phenol group (directly attached to the ring) (1590-1480 cm^{-1} and 1265-1070 cm^{-1}) are observed.

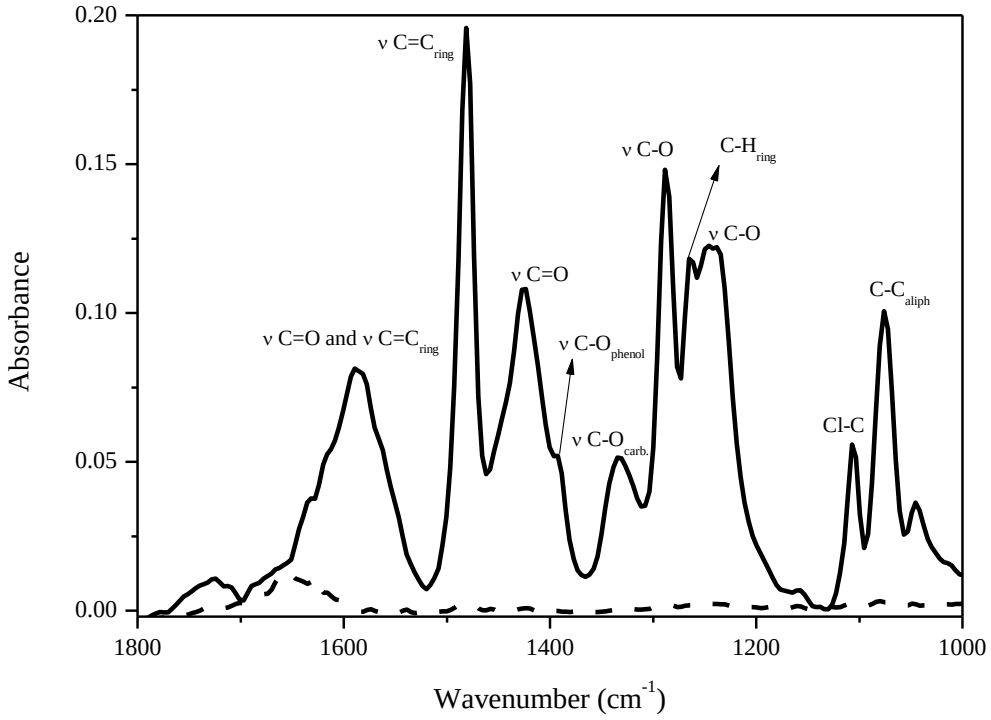

Figure 45: ATR-FTIR spectra for a 2,4-D solution (2.7 $mmol \cdot L^{-1}$) at pH 2.9 in 10.0 $mmol \cdot L^{-1}$ KNO_3 on a TiO_2 film (——) and on the ZnSe crystal (– –). Bands assignment has been done according to: Gines et al., Goyne et al., and Silverstein [144-146].

Due to its pK_a of 1.2 about 65 % of the species are dissociated at the pH (2.9) in the 2.7 $mmol \cdot L^{-1}$ solution.

$$C_8Cl_2H_6O_3 \rightleftarrows C_8Cl_2H_5O_3^- + H^+ \qquad pK_a = 1.2 \qquad \text{Equation 28}$$

Above pH 4.0 the dissociation of 2,4-D is very high. More than 95 % of the species present in solution are dissociated (see Figure 68 in Appendix). To analyze the influence of the pH value on the adsorption of the 2,4-D acid and acetate at the anatase surface, different pH conditions have been investigated. The low and high limitation for the pH condition has been imposed by achievable reactions of solution with the ZnSe crystal, as already pointed out. Thus, the lowest and highest pH for the investigation were 2.9 and 9.0, respectively.

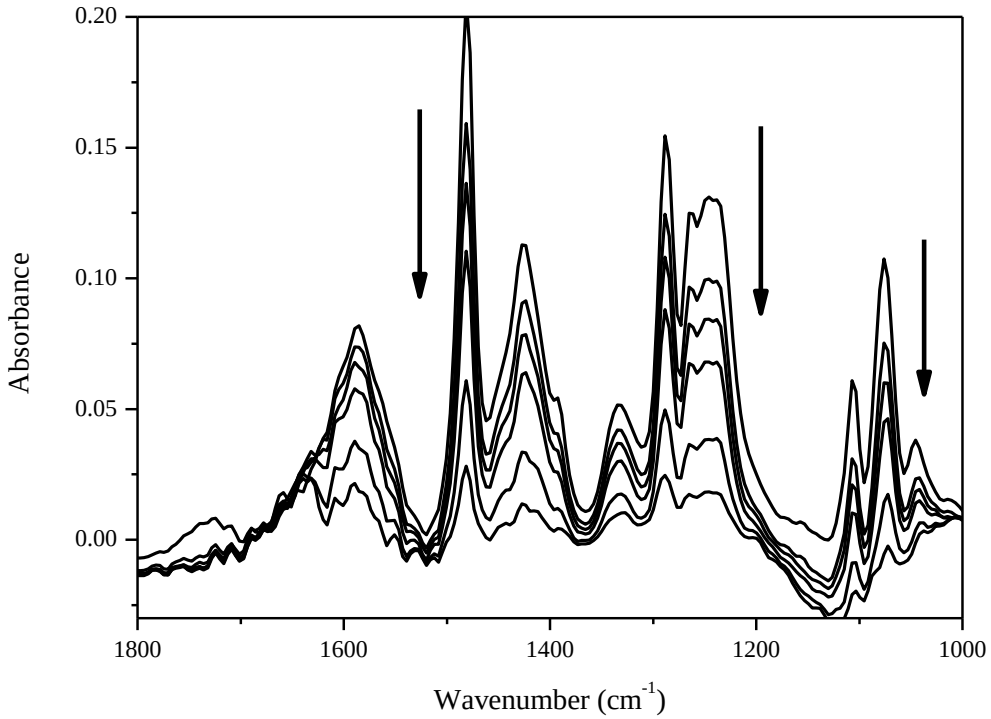

Figure 46: ATR-FTIR spectra for an anatase TiO_2 film (PC500) in 2.7 mmol·L^{-1} 2,4-D solution at distinct pH conditions (2.9; 3.5; 4.0; 5.5; 7.0; and 9.0) in 10.0 mmol·L^{-1} KNO_3. The arrows in the figure indicate the direction of the spectral change with increase of the pH condition.

Figure 46 shows the spectra taken at different pH conditions. Even though the 2,4-D molecule shows vibrational signals in different spectral regions, only the region between 1800 and 900 cm^{-1} has been considered in this study. The interferences of the not completely canceled vibrational modes of water in the other spectral regions are still enormous, in addition to strong hindrance due to the spectral noise. With the increase of the pH condition a decrease of spectral signal intensity has been observed. Changes in the spectra, i.e., shifting or new bands have not been observed though. The pH condition chosen for the investigation was 2.9, which is the pH of the 2.7 mmol·L^{-1} 2,4-D solution. At this pH the intensity of the spectral signals is very high and it is not necessary to make adjusts the pH.

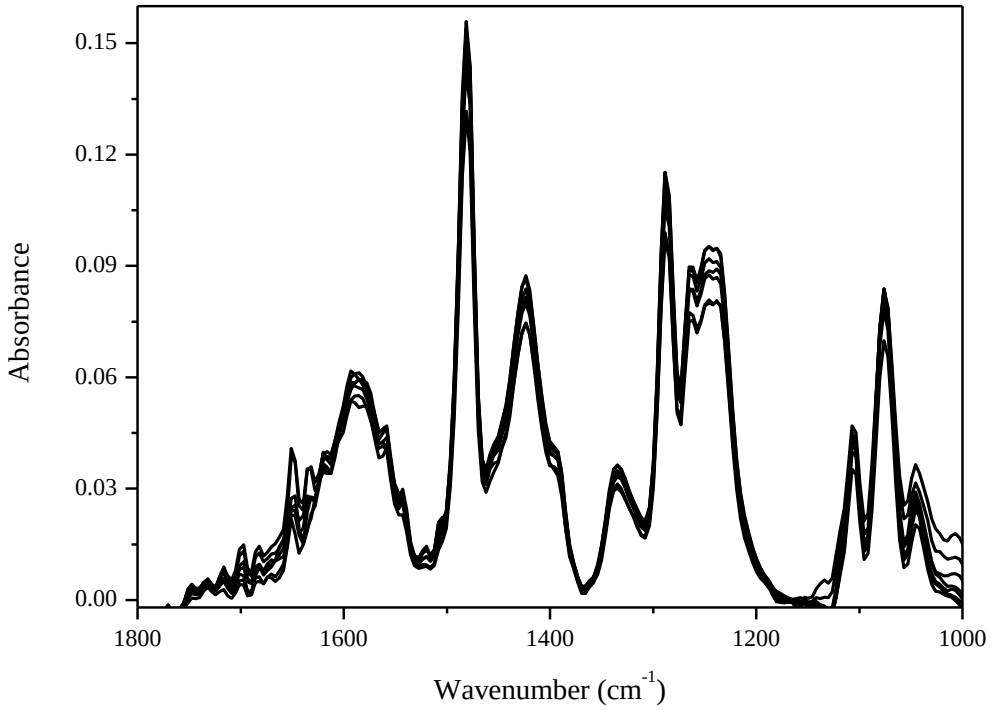

Figure 47: Evolution of the ATR-FTIR spectra for an anatase TiO_2 film (PC500) 2.7 mmol·L^{-1} 2,4-D solution at pH 2.9 in 10.0 mmol·L^{-1} KNO_3. The spectra have been taken after 10, 15, 30, 60, and 120 min of equilibration.

The investigations have been carried out in a batch system, where 5 mL of the pesticide solution have been added to 0.5 mL of the 10.0 mmol·L^{-1} KNO_3 solution, previously used to record the background. The final concentration of the 2,4-D solution was 2.7 mmol·L^{-1}. First signals related to the vibrational modes of the molecule have been observed after 12 s of reaction (data not shown here). Spectra presented in Figure 47 show the evolution of the spectral bands during the first 120 min of adsorption. The system reaches the equilibration after about 10 min, and it is maintained during the next 120 min. The only notable change is a slight decrease of the bands at 1420, 1238, and 1072 cm^{-1}.

The adsorption trend is different when using lower 2,4-D concentration, i.e., 1.4 and 0.5 mmol·L^{-1}. Figure 48 shows the spectral evolution of the anatase film with 0.5 mmol·L^{-1} pesticide solution over 120 min of reaction. The spectral signals after 120 and 60 min for the 1.4 and 0.5 mmol·L^{-1} solution, respectively, fully disappear, with exception of the bands in the 1200-1000 cm^{-1} region.

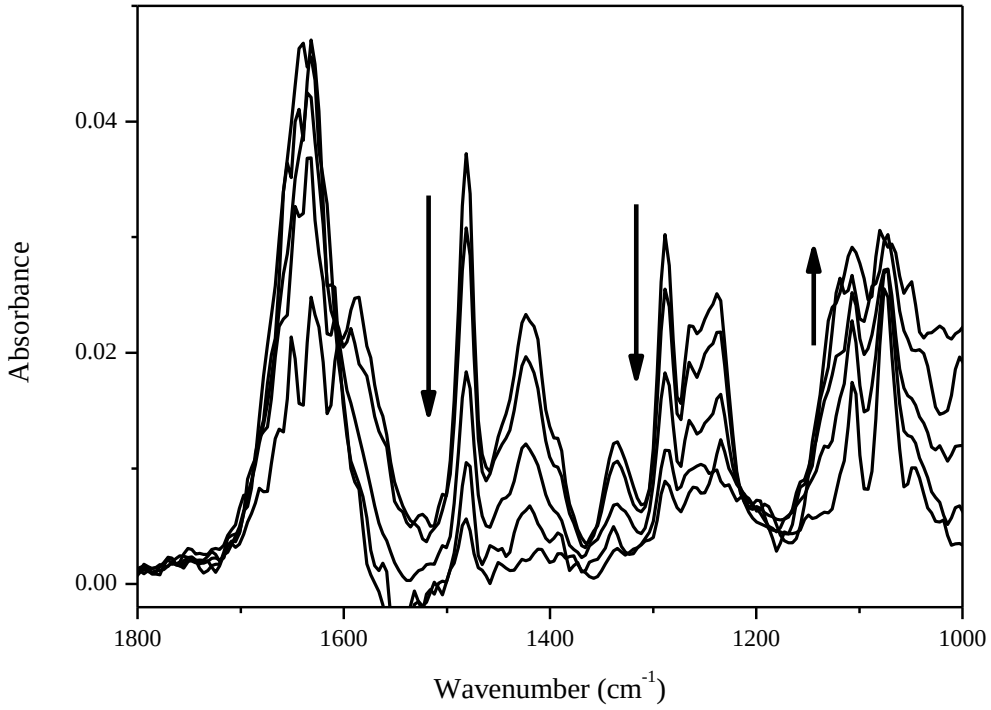

Figure 48: Evolution of the ATR-FTIR spectra for an anatase TiO_2 film (PC500) 0.5 mmol·L^{-1} 2,4-D solution at pH 2.9 in 10.0 mmol·L^{-1} KNO_3. The spectra have been taken after 5, 10, 15, 30, 60, and 120 min of equilibration. The arrows in the figure indicate the direction of the spectral changes with time.

Degradation studies involving the 2,4-D have been performed after 90 min of equilibration, knowing that the spectral signals show lower intensity at this time, especially for low 2,4-D concentrations.

4.4.3 2,4-D Degradation on the PC500 Films

Photocatalytic degradation experiments have been performed for the 2,4-D at the anatase surface for three concentrations (0.5, 1.4, and 2.7 mmol·L^{-1}). In all cases the degradation was not observable by the ATR-FTIR technique. Figure 74 (in the Appendix) shows the spectra recorded for the 0.5 mmol·L^{-1} solution after 90 min equilibration, showing only traces of the spectral bands. Under illumination (even after 90 min of reaction) new signals could not be identified. Similar behavior has been observed for the 1.4 mmol·L^{-1} pesticide solution, using the same experimental conditions.

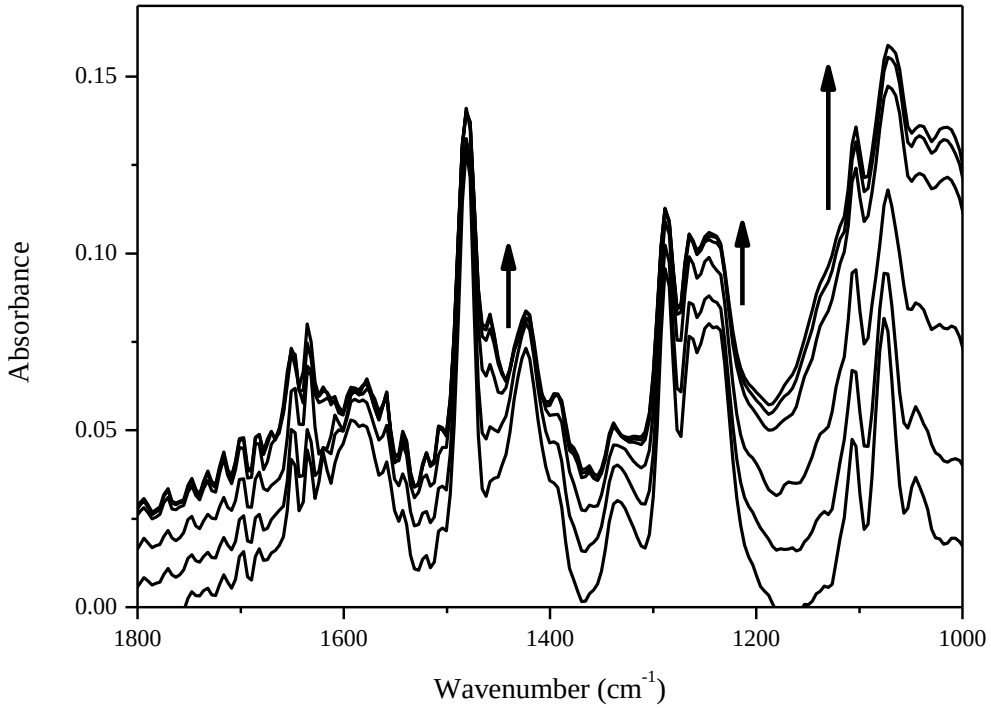

Figure 49: Evolution of the ATR-FTIR spectra for an anatase TiO_2 film (PC500) in 2.7 mmol·L^{-1} 2,4-D solution at pH 2.9 in 10.0 mmol·L^{-1} KNO_3. The first spectrum has been taken after 90 min dark-equilibration, the following spectra were taken 30, 60, 80, 100, and 120 min after starting the UV irradiation (light intensity 1.0 mW·cm^{-2}). The absorbance changed nearly parallel to the time. The arrows in the figure indicate the direction of the spectral change with time.

Figure 49 presents the spectra taken for the degradation of 2.7 mmol·L^{-1} 2,4-D solution after 90 min of reaction in the dark. It can be observed that the spectral signals do not show relevant decrease after 120 min of irradiation and in some cases even an increase. This demonstrates a higher stability of the adsorption/degradation system.

The only considerable spectral change has been observed for the band at 1458 cm^{-1}, which increases with the degradation, whereas for the other bands no shifting has been observed.

5 Discussion

Chlorinated acids are an important group of contaminants. Their interactions with the TiO_2 surface are strongly influenced by the presence of the Cl in the molecular structure. The photocatalytic degradation of these compounds is still unclear. It is important to investigate the adsorption of these acids to identify the importance of this reaction for the photocatalytic degradation. Therefore, the influence on the adsorption behavior of diverse parameters has to be considered.

5.1 Titanium Dioxide Characterization

A broad range of important parameters are known to influence the adsorption of organic molecules/anions on TiO_2 surfaces, such as, the surface area; the degree of particle agglomeration; and the pH condition. Furthermore, the surface shape (i.e., the presence of exposed faces and surface defects) as well as the presence of surface contaminants (adsorption blockers) play an important role.

The number of adsorption sites at the TiO_2 surface provides information about the amount of molecules effectively adsorbed on the surface. The adsorption constant gives an idea about the strength of the interaction between the adsorbate and the adsorbent. Both can be directly obtained from the fitting of the adsorption isotherm models.

To obtain a parameter that easily can be used to compare the adsorption capacity of the different materials the BET surface area has to be considered. Thus, considering the number of OH exchangeable groups per area. In Figure 7 anatase (100) surfaces are represented, and give an idea of the distribution from the hydroxyl groups on TiO_2 at different pH conditions.

The substitution of the adsorption groups at the surface occurs *via* replacement of the basic sites, which represents approximately the half of the OH groups (see Figure 50). These groups are more easily exchanged in acid conditions, i.e., below the zpc condition, which is for TiO_2 around 6.0. Pure anatase samples with a BET surface area similar to PC500 show around 1400 µmol OH groups per gram. The concentration of OH groups is estimated around 300-450 µmol per gram, for P25 [147]. For experiments performed at pH 5.5, slightly acidic than the pH_{zpc}, a total of 415 $\mu mol \cdot g^{-1}$ and 140 $\mu mol \cdot g^{-1}$ TiO_2 have been observed for PC500

and P25, respectively, fitting the Langmuir model, which are below the values reported by Hermann *et al*. [110]. It was expected that the number of replaceable OH groups would be higher, once the lower pH condition employed in this study makes the substitution of the sites easier.

Although, used in diverse degradation studies [37, 135] PC500 powder has scarce information about its surface characteristics in the literature. The P25 mainly composed of anatase shows adsorption properties quite different from those observed for the PC500. This is probably due to its distinct crystallographic characteristics, i.e., presence of rutile. The difference in the number of exchangeable OH groups was expected, because PC500 has higher BET surface area than P25.

R15 shows the lowest value of exchangeable OH groups within the analyzed powders, with only 34 $\mu mol \cdot g^{-1}$ TiO_2. This low number of OH groups exchanged is related to its low BET surface area. Information about its surface properties has not been found in the literature, which makes the interpretation of the data difficult.

An adequate parameter to compare the adsorption efficiency of the different powders is the number of sites/nm^2. Table 12 shows the estimation of the number of sites per area, obtained from the BET surface area (see Table 3) and the number of exchanged OH groups (see Table 4) for the powders.

Table 12: Number of exchangeable OH groups per square nanometer at the surface of different TiO_2 materials.

Sample	Number of exchangeable OH groups per nm^2
PC500	1.1
R15	0.5
P25	1.7

Boehm and Herrmann [111] have observed that P25 shows higher substitution of the surface OH groups than anatase samples. They considered the existence of one monodentate group composed of ≡Ti–OH (see Figure 50 red groups) with basic character and another bidentate group $(Ti)_2$-OH (see Figure 50 blue groups) with acidic character. Based on

adsorption experiments performed employing different materials with different size, the determination of the number of sites available at the powder surface is in average 4.5 basic OH groups per nm^2 [148], [149].

In our measurements the same tendency has been observed. About 1.7 OH groups per nm^2 are exchangeable for the P25 surface and only 1.1 groups for the PC500 sample.

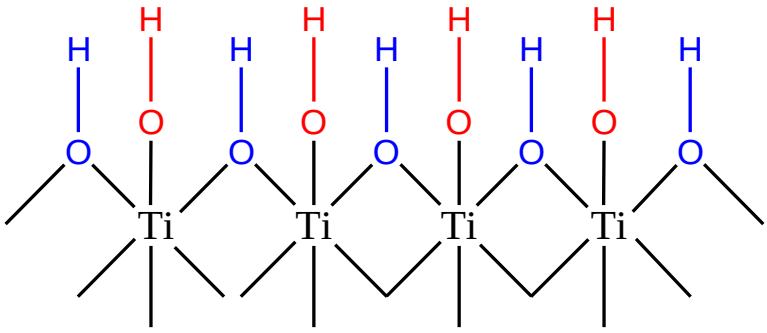

Figure 50: Representation of the OH groups at the titanium dioxide surface. Basic OH groups are red marked and acid OH groups blue marked.

The anatase powder with 400 µmol·g^{-1} TiO_2 has only 1.1 available exchangeable sites per nm^2, in average. It is an indication that even a huge BET surface area, the small particles (about 7 nm) form agglomerates, which can also represent a hindrance for the adsorption process.

According to Mendive [46] six adsorption sites are available at the anatase (100) surface, but the exchange of all groups is not possible. Their distribution in pairs along the surface restricts the adsorption of new anions due to the strong repulsions between the adjacent anions (see Figure 51).

For rutile particles it is commonly assumed that the most exposed faces are (110), and (100) [150]. These surfaces show 6 - 7 OH groups per nm^2 at the surface, in average [150]. Meanwhile, the number of groups replaced by F^- anions is much smaller, with only 0.5 OH groups per nm^2, in this investigation This low number is not surprising. Although, rutile in principle shows a high number of available sites, its crystalline structure is close packed, which has a higher perturbing effect. Besides the formation of agglomerates, which avoids the uniform distribution of the F^- on the TiO_2 surface.

The P25 sample shows a better adsorption of anions at the surface than the other powders; about 2.0 - 2.5 OH groups per nm^2 are exchanged [102, 103, 151]. An explanation

for the better exchange value is the smaller agglomeration degree observed for this sample, besides it shows another crystallographic conformation. However, it is mainly composed of anatase, its fluoride adsorption isotherm curve shows a quite different shape than on PC500.

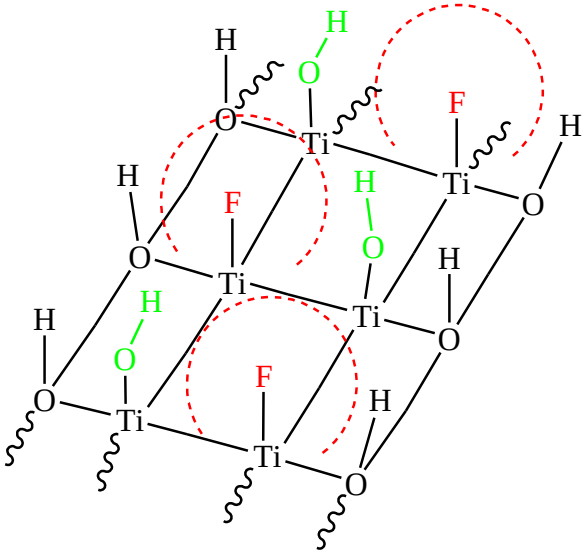

Figure 51: Representation of fluoride adsorbed at the surface of an anatase (100) facet, extracted from Mendive [46].

Due to the larger molecular size DCA shows a low number of adsorbed molecules at the TiO_2 surface. Table 13 summarizes the data obtained for the number of OH groups exchanged by DCA molecules for the PC500 powder, at pH 3.0 and 9.0, and for P25 at pH 3.0. The adsorption of DCA on the rutile particles in suspension has not been investigated owning to the small amount of powder available.

For the pure anatase sample, values obtained from the Langmuir and modified Langmuir model, which were about 320 and 200 $\mu mol \cdot g^{-1}$ of TiO_2, respectively. The larger size of the anions avoids the approximation and consequently the adsorption of new anions at the surface. This fact has been observed for other molecules or anions as well [100, 152-154].

Remarkable differences have been observed between the two adsorption models used to analyze the curves at low pH values. The Langmuir model shows a number of exchangeable sites more alike to the fluoride anions and with a huge standard deviation. In contrast, the modified model only shows the substitution of half of the sites compared with the fluoride. An interesting perspective about the adsorption behavior of DCA will be discussed in more detail in chapter 5.3.

Table 13: Number of surface OH groups exchanged by DCA molecules at the surface of TiO_2 materials per area. N: Number of exchangeable OH groups per nm^2.

Sample	pH	N - Langmuir model	N - Modified Langmuir model	N - BET model
PC500	3.0	0.6	0.4	-
PC500	9.0	0.08	0.04	-
P25	3.0	-	1.9	0.02

The number of DCA molecules adsorbed at the surface is around 0.5 DCA molecules per nm^2, while fluoride anions have exchanged 1.1 OH groups. Taking into account that for the DCA system the used pH value is quite lower than this employed for the F^-, the electrostatic interaction between the positive surface and DCA^- is expected to be higher. The Cl atoms in the molecular structure have a huge electronic cloud, which may hinder the adsorption of other anions in its vicinity. Moreover, the crystalline arrangement at the surface has to be considered. The different facets of the anatase show different adsorption possibilities, which will change the relationship at the oxide/solution interface.

DCA shows appreciable adsorption at the P25 surface according to the modified Langmuir model, about 2 molecules per nm^2. However, for the BET model, which shows the best fitting of the curve, the number of adsorbed molecules at the first monolayer is only 0.02 per nm^2. This difference can be explained by the model suggested in chapter 4.2.3. With the formation of complexes involving various molecules at the TiO_2 surface, which are not considered as multi-layer, a high number of molecules are considered to be adsorbed at the oxide surface. The fitting of the Langmuir isotherm model for DCA on the TiO_2 was not good, resulting in elevated standard deviation and a very high value of molecules adsorbed at the TiO_2 surface.

At pH 9.0 approximately 0.06 nm^{-2} occupy the adsorption sites at the PC500 surface. This value is approximately one order of magnitude lower than this observed at pH 3.0. This behavior is expected, since at alkaline conditions the TiO_2 surface and the DCA molecules are both negatively charged, which obstructs the adsorption.

The differences observed for the strength of the adsorption are irrelevant. PC500 and P25 show adsorption constants between 4×10^{-4} and 1×10^{-3} $L \cdot mmol^{-1}$, respectively, for the

modified Langmuir model; and 5×10^{-3} and 8×10^{-3} $L \cdot mmol^{-1}$ for the Langmuir model, respectively. The estimation of the constant for both models show high standard deviation. These values are two orders of magnitude lower in comparison to the fluoride adsorption. This indicates less intense interaction of the DCA molecules with the surface. The constant observed for the adsorption curve of DCA at PC500 using the Langmuir model is about 22×10^{-3} $L \cdot mmol^{-1}$, while the value obtained from the modified model cannot be considered due to the high standard deviation. This value is higher than that observed at low pH conditions, and contradictory. The presence of only a low amount of adsorbed molecules at the surface probably builds up the interaction between the surface and the DCA molecules.

5.2 Dichloroacetic Acid Adsorption at the PC500 Surface

In contrast to previous studies performed in our group involving oxalic acid [46], the difference of the intensities for the spectral signals of DCA in bulk solution and adsorbed at TiO_2 surface is very low. But, it is large enough to enable the adsorption investigations. Moreover, this difference suggests the formation of adsorption structures at the TiO_2 surface.

As already expected the interactions with anions are favored at $pH < pH_{zpc}$. The organic molecules in solution are strongly affected by the pH condition, which is closely related to their dissociation constants. The correlation of the dissociation constant and their interaction with the catalyst surface is only a rough approximation, because the pH conditions are only valid for the bulk solution. The formation of electrical double layers at the solution-oxide interface can influence the polarizability of the molecules, as well as the dissociation equilibrium at the semiconductor surface.

Low pH conditions facilitate the interaction between TiO_2 and DCA. The low dissociation constant of DCA guarantees that even for the lowest pH condition investigated most of the molecules are dissociated. This condition turns the interaction with the TiO_2 favorable, because the positively charged PC500 surface attracts more efficiently the DCA^-. At this condition the dissociated molecules are able to approach the surface and form a bond between the Ti atom and the carbonyl group (see Figure 52). This linkage has been already observed for DCA solutions at pH < 4.0, by Hilgendorff [121]. He observed the formation of bidentate complexes, i.e., both oxygen atoms of carboxylic group interact with the surface.

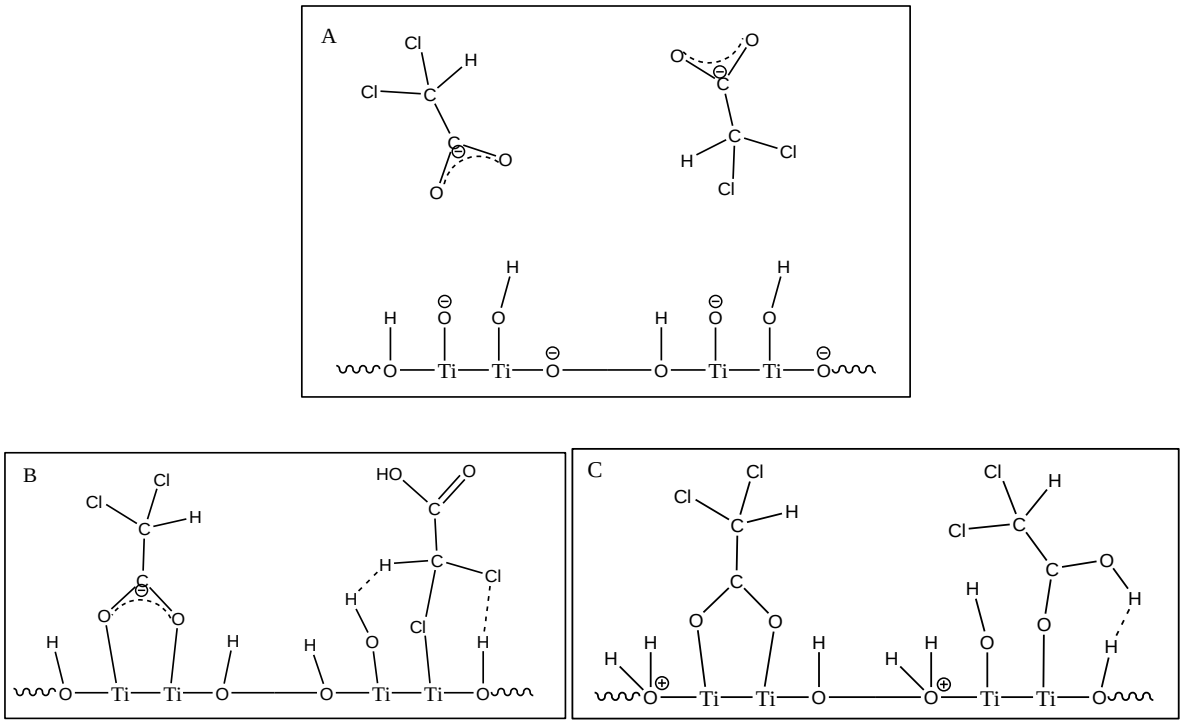

Figure 52: Schematic representation for the adsorption of DCA at the anatase (100) surface pH > pH_{zpc} (A), pH ≈ pH_{zpc} (B) and pH < pH_{zpc} (C).

At pH values next to the pH_{zpc} the interactions are less intense due to the weakly charged surface. The presence of a small amount of molecules in the surrounding of the TiO_2 surface obstructs the exchange of the OH group. In addition, the basic OH groups are almost neutral and cannot be easily exchanged (see Figure 52 B). This condition becomes worse with the increase of the pH condition; the negative charged surface repulse the negative charged DCA anions. In this case the interactions are probably weak bonds, i.e., hydrogen bonds or dipole-dipole interactions (Figure 52 A). According to Hilgendorff [121], at pH conditions higher than 4.0 the formation of monodentate complexes are observed.

Considering the points depicted above, it is expected that the spectral signals at pH conditions 6.0 and 9.0 would lose intensity, provoked by the weak interaction with the surface. This approach is only partially right, since the spectral bands really decay, but the decay is followed by the growth of new signals. A band centered at 1340 cm^{-1} is observed, it is assigned to the C-O vibration coupled with an OH in-plane deformation from DCA. This confirms the change in the adsorption mode on the oxide surface. Another observation supporting the different interaction modes is the recovery of the bands centered at 1381 and 1226 cm^{-1} with the adjustment of the pH condition to 3.0 again. The disappearance of the band at 1340 cm^{-1}, eliminates the possibility that contaminants introduced by the pH adjustment are responsible for the spectral bands observed at high pH values.

Considering that the adsorption at low pH values of DCA at TiO_2 can take place in different ways. The Ti atom can directly bind to the carbonyl group [121] (Figure 53 left), as already explained, or through the acid-base interaction between the DCA^- and the Lewis acid site at the surface, i.e., Ti^{4+}. This interaction occurs *via* one of the lone-pairs of the halogen atoms [155] (Figure 53 right).

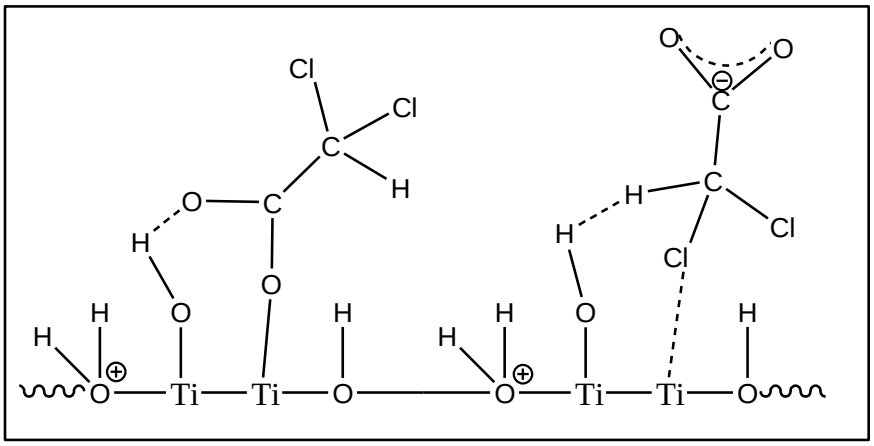

Figure 53: Schematic representation of two adsorption possibilities of DCA at anatase (100) surface at $pH < pH_{zpc}$.

5.3 Kinetic Aspects of the Adsorption

According to the kinetic investigations, the required time to observe the first signals related to the adsorbed DCA structures at TiO_2 is lower than 15 s. In Figure 20 the signal of the stretching vibrational mode of COO undergo an intense increase at this time. This increase indicates that the DCA^- molecules are able to exchange reasonably fast with the OH^- groups at the surface. The peak height observed for the band at 1380 cm^{-1} (see Figure 21) shows a low but constant increase of the signals during approximately 20 min of interaction. From that time and in the following 5 h the intensity of the DCA stretching COO band decreases, and after 6 hours the signals cannot be distinguish from the spectral noise, anymore.

Investigations performed by Mendive [46] and Ivanova [156] involving adsorption of oxalic acid on TiO_2 using different electrolyte concentrations show that, the higher the amount of anions in solution, the lower the adsorption of molecules at the semiconductor surface. Electrolytes may have a strong contribution on the adsorption process, especially due to its importance on the formation of the electrical double layer. Smaller anions such as

fluoride have, due to their size, a relatively easier way to approach the surface. The surface is already populated by small ions, but their high mobility facilitates the approach to the surface and subsequent adsorption. In this sense a larger molecular structure, e.g., with DCA can be considered a hindrance. The molecules have difficulties approaching the surface and interact with it. For this reason it is expected that the adsorbed anions will keep on the surface, since the release of anions will be hindered by the presence of the electrical double layer. This statement is not confirmed by the development of the spectral signals in time.

Parameters such as ionic strength and pH play a very important role in this study, and have therefore to be carefully controlled. The pH condition has not only an influence on the molecules but also shows a significant relation to the changes in the surface charge.

Another interesting aspect observed in the investigation of different pH regimes is the presence of a negative band between 1000 and 1200 cm^{-1}. This indicates that the increase of the pH causes profound changes on the oxide structure, considering that these changes are irreversible. The negative signals are independent of the adsorbate, and are observed for other investigations involving the PC500 powder. This indicates that the signals are related to some contaminant previously adsorbed at the TiO_2 surface, which is released during the experiments. According to studies performed by Mendive [46] one of the major impurities encountered in powders produced by Crystal Global is sulfate. It results from the sulfonated precursor used by the synthesis process [46]. Therefore, an explanation for the negative bands observed at stable pH conditions is the slow, but steady desorption of sulfate anions from the TiO_2 surface. However, at more alkaline pH conditions this process is accelerated. The effect is most pronounced in pure anatase samples with a large surface area (PC500), which shows higher concentrations of SO_4^{2-} in the supernatant solutions than the PC10 or the R15 powders [46].

There are also observable bands at this spectral region assigned to compounds formed from the reaction of the acid solution with the ZnSe crystal (see equation 29), as suggested by Mendive [46]. Under irradiation, the formation of such compounds (H_2Se) is followed by the production of other oxides. These oxides are attributed to the attack of charge carriers from the photocatalytic excitation, as presented in equations 31 - 35 [46, 133]. All those possibilities have to be considered for the adequate analysis of that spectral region.

$$H_2Se \rightarrow Se^{2-} + 2H^+$$ Equation 29

$$Se^{2-} + 2h^+ \rightarrow Se^0$$ Equation 30

$$2H^+ + 2\,e^- \rightarrow H_2$$ Equation 31

$$H_2Se \rightarrow Se^0 + H_2$$ Equation 32

$$ZnSe + 2H^+ \overset{h\nu}{\rightarrow} Zn^{2+} + Se^0 + H_2$$ Equation 33

The spectral differences observed for the adsorption of DCA (10 mmol·L^{-1}) on the different materials are not restricted to the above mentioned region. In fact the most important difference is related to the intensity observed at 1381 and 1226 cm^{-1}. The signals are weaker for larger particles (PC10 and R15) compared to the ones with smaller particle size (PC500 and S230). The only constant fact is the difficulty to keep the spectral signals independent of the experimental conditions. Different decay profiles are observed for the DCA IR bands at the S230, PC10 and R15 films, however, the most comprehensive and clear tendency is observed on the PC500 film (see Figure 16). This behavior has been observed even at high DCA concentrations (20.0 mmol·L^{-1}).

The kinetic process begins after around 15 s for all investigated molecules. This time can also be considered the average period necessary for molecules to reach the titanium dioxide surface. The further increase in the signal intensity extends over approximately 5 to 15 min, depending on the molecule. DCA needs a longer time to reach the maximal intensity of the signals, afterwards the band intensities start to decrease. In contrast TCA signals begin to decay already after 8 min of reaction. The decay of the intensity does not stop, and after some time, depending on the investigated molecule, the signals show intensities in the range of the spectral noise. The only exception to this behavior was MCA. The MCA spectral signals begin to decrease after about 10 min of adsorption. However, this decay discontinues after approximately 150 min of equilibration.

The use of different thicknesses for the oxide film actually does not change that tendency (see Figure 22). However, appreciable difference between the heights of the DCA bands at the different films has been observed. This fact can be explained by the depth of penetration (see chapter 2.4), which depends on the wavelength and the angle of incidence of

the radiation, as well as the refractive indices of the ZnSe. Although independent of the thickness of the TiO_2 film, the bands reach almost the same intensity after 120 min.

Even at pH 3.0, the adsorption systems involving chloroacetate and acetic acid are not guaranteed to be stable. In fact at that pH the most intense signals have been observed. But the decay profile of the signals is maintained over time, with the exception of MCA. Moreover, Hilgendorff [121] suggests pH 2.0 as most favorable condition for the adsorption, but to preserve the ZnSe crystal this pH condition has not been used.

The weak spectral intensity for the bands of the adsorbate, i.e., DCA; AA; MCA; and TCA, indicates a fragile adsorption. Using similar experimental conditions Mendive [83], has observed a strong and stable interaction between oxalic acid and TiO_2. So the decay observed in all DCA concentrations investigated is strong evidence that the molecules do not have a stable interaction with the oxide. Moreover, Ivanova [156] has also observed that DCA adsorption at TiO_2 is clearly weaker than oxalic acid.

According to Figure 52, which shows possible scenario at the different pH conditions investigated, spectral signals are expected only at low pH conditions. The signals observed at pH 4.0 using different DCA concentrations suggest that the adsorption takes place *via* the carbonyl group. This is supported by the strong spectral contributions observed at 1381 cm^{-1} and above the 1600 cm^{-1} region assigned to the COO group. The subsequent decrease of the bands intensity indicates, however, a change in this behavior. This suggests that after the first adsorption step the adsorbed molecules aim the most stable conformation. Taking into account the behavior observed for the adsorption isotherms (see Figure 11), the formation of diverse complexes at the surface is proposed.

Hilgendorff [121] dismissed the possibility of adsorption from acetate anions as bidentate structure on the TiO_2. The incompatible distances between the atoms from the DCA carbonyl group (2.4 Å) and the distance between the Ti-OH groups at the TiO_2 surface (0.5 Å) and the elevated tension of a five-member ring does not enable the maintenance of such a structure. In general, the surface species on TiO_2 is usually adsorbed to hydroxyl groups or water by chemical and physical adsorption, which suggests the possibility of the formation of different adsorbed structures at low and high concentrations [127]. Therefore, monolayers on the TiO_2 can be easier reach at high DCA concentrations.

Considering the experimental evidences from the adsorption isotherms and from the ATR-FTIR spectroscopy, the adsorption behavior of DCA at the anatase (100) surface can be

explained in a two step system. Firstly, the adsorption of DCA molecules occurs *via* interaction of the carboxyl group and the basic Ti-OH sites (Figure 54 A). This results in the formation of mono or bidentate structures at the oxide surface, depending on the dissociation degree of the adsorbate. These structure flips at the surface after some time and interact with the surface through the Cl atoms forming complexes.

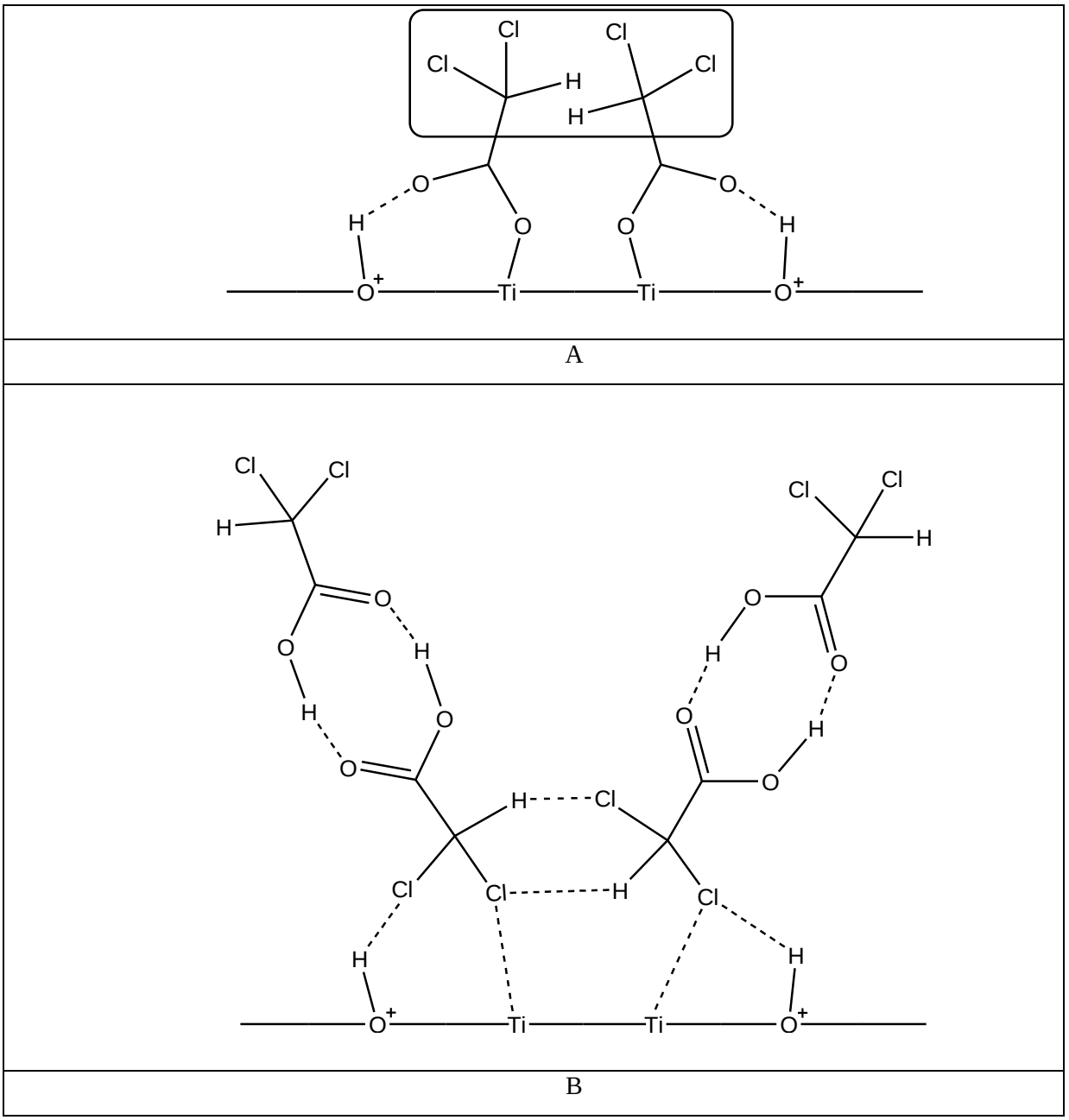

Figure 54: Schematic representation for the formation of the adsorption structures of DCA at the anatase (100) surface. A - Initial adsorption step. B - Adsorption after equilibration.

This change in the adsorption mode is initiated by the repulsion between the CCl_2H moieties of the adjacent molecules (Figure 54 A). The steric obstruction is the driving force to trigger the conversion into two adjacent complexes as shown in Figure 54 B, which are flipped structures binding weakly via the terminal Cl atoms. The complex formed in Figure 54 B has additionally stability from the three 6-member rings built at the surface. The adsorption can bring more stability for the adsorbed complexes, due to the formation of a second monolayer involving additional DCA molecules, via the interaction of the carbonyl groups from the dichloroacetate molecules directly adsorbed at the surface with other DCA molecules from the solution bulk.

This model would explain the behavior of the DCA adsorption isotherms, and corresponds to the Langmuir modified model suggested for its explanation in which two different structures presenting different interaction affinities are present. The suggested model can also explain the change in the DCA/TiO_2 IR spectral behavior. At the beginning of the adsorption kinetic DCA molecules are very close to the TiO_2 surface, with strong contributions of the COO group (especially at 1380 cm^{-1}). However, these signals decrease with the time and finally disappear since the Cl atoms show weaker affinity to the surface. Beyond the observation of spectral signals assigned to the Cl-C vibrational modes are only observable at wavenumbers < 1000 cm^{-1}, which cannot be followed with the employed ATR-FTIR system, due to the limitations of the ZnSe crystal.

5.4 Adsorption and Degradation in Oxygen and Nitrogen Saturated Systems.

The spectral signals are relatively stable during the adsorption investigation of 10 $mmol \cdot L^{-1}$ DCA purged with O_2 or N_2. Spectra taken after 50 min of equilibration show the presence of bands at 1226 cm^{-1} and 1381 cm^{-1} (see Figure 23 and Figure 24). The only remarkable change is the constant decay of the spectral signals. This decay can indicate the formation of complexes at the surface as suggested in Figure 54. The absence of oxygen in the adsorption system does not show influence on the adsorption behavior.

Nevertheless under irradiation the presence/absence of oxygen shows a high influence. In Figure 23, the typical signals assigned to DCA are replaced by two new bands, at 1415 and 1273 cm^{-1}, which increase in time. Those vibrational signals are assigned to CO and COO

stretching modes from small carboxylic acids, e.g., acetic acid or formic acid [157]. Another change observed in the spectra is the presence of the shoulder at 1342 cm^{-1} assigned to the CH_2 deformation of an acetate or monochloroacetate [157].

The shift of the band at 1381 cm^{-1} to higher wavenumbers (1415 cm^{-1}) can also be an indication for a change in the adsorption nature of the organic molecule. Hilgendorff [121] noted that the decrease of the difference between the symmetric and asymmetric stretching bands of the carboxyl group from DCA is related to the formation of a bidentate structure. This occurs due to the higher rigidity of the oxygen and carbon bond, forming a stressed ring at the surface, which hinders the symmetric vibration of the carbonyl group. Thus, it is necessary more energy to enable that vibration. In contrast, the asymmetric vibrational mode apparently likes that formation, and due to a coupling of its vibration needs low energy to vibrate, than the monodentate structure or the free DCA molecule. The coordination of DCA should strongly influence its activation and further photocatalytic degradation. The maintenance of the signal at 1380 cm^{-1} during the photocatalytic degradation is a good indication for the adsorption mechanism. The adsorption sites, which get free due to degradation, can be occupied by new DCA molecules. The maintenance of the spectral signals, i.e., assigned to the COO group, during the photocatalytic degradation indicates that the new molecules adsorbed preferentially through the carbonyl group.

It is expected that more than one reaction mechanism takes place at the interface. The formation of mono- and bi-dentate complexes are more susceptible in irradiated system, once the energy supplied to the system is very high causing enormous alterations in the interface. Changes in the degree of surface hydroxylation, by desorption of adsorbed impurities [158], or by changes in the bulk or surface of the solid, caused by energy released due to the recombination of the electron/hole pairs [159]. This enables the adsorption of molecules at new surface sites, opening new adsorption possibilities.

One of the reasons why dichloroacetic acid has been selected for this study was the fact that it does not present long live degradation sub-products. The absence of intermediates is based on measurements performed commonly for suspensions in the bulk solution, taken during the irradiation period. However, observing the spectra shown in Figure 23 and Figure 24 the presence of intermediates has to be considered.

Under acidic pH conditions, direct oxidation of dichloroacetic acid by the hole forms dichloroacetate radicals, as presented in the follow equation 34.

$$CHCl_2COO^- + h^+ \rightarrow CHCl_2COO^{\cdot}$$ Equation 34

According to Bahnemann *et al*. [64] carbon dioxide and the dichloromethyl radical are formed due to decarboxylation. Adsorbed molecular oxygen can react with the formed radical and produce the dichloromethyl peroxil radical [64]. A simplified scheme of the DCA photocatalytic degradation is described below [62].

$$CHCl_2COO^{\cdot} \rightarrow HCl_2C^{\cdot} + CO_2$$ Equation 35

$$O_2 + HCl_2C^{\cdot} \rightarrow CHCl_2COO^{\cdot}$$ Equation 36

$$2\,CHCl_2COO^{\cdot} \rightarrow 2\,COCl_2 + H_2O_2$$ Equation 37

$$COCl_2 + H_2O \rightarrow CO_2 + HCl$$ Equation 38

Comparing the systems purged with oxygen and nitrogen clearly demonstrates the photocatalytic degradation kinetic takes different ways. The importance of an effective electron acceptor (oxygen) is observable and supported by the changes (shifting, decay and growth) of bands in the O_2 saturated solution. These changes have not been observed in the experiment purged with N_2.

The spectra taken for DCA degradation in the N_2 saturated system (Figure 24) only shows the broadening of the spectral band assigned to the symmetric bending mode of the carboxyl group. This is probably related to the change or distribution in the position of the molecule and anions on the metal oxide surface. The generation of electron/hole pairs, with its consequently recombination, accumulates energy in the particles causing its separation [2]. In the spaces created between the particles, water and organic molecules are now able to absorb. This separation exposes other faces of the anatase particles, enabling the DCA molecules to populate other crystalline planes, which changes the adsorption behavior and causes shifting of the vibrational signal. A similar effect for the investigation of oxalic acid adsorption and photo degradation at TiO_2 surface has been previously observed by Mendive [83]. It was especially noted for particles with larger size. Another explanation for the broadening is the presence of degradation intermediates, which present similar molecular structures. These

intermediates can also adsorb at the surface and overlaps the vibrational signals of the adsorbed DCA. The maintenance of the spectral band intensity (around 1381 cm^{-1}) strongly indicates a continuously formation of new bonds between the titanium dioxide surface and the carbonyl group of the molecules. Anions used as electrolyte like nitrate, or sulfate released from the TiO_2 surface can act as electron acceptor and influence the degradation system.

The presence of dissolved oxygen in solution, as expected, is extremely important for the heterogeneous photocatalysis process. The existence of oxygen sometimes increases the photodecomposition rate for more than 200 times [33]. In the absence of oxygen the spectral changes are restricted to the vibrational mode of the carbonyl group, whereas in the oxygen purged system more bands are involved, even the formation of new bands can be observed.

The trap of photoexcited electrons avoids the recombination step, enabling a more efficient attack of the holes to the adsorbed substances. Furthermore, the reaction of electrons with, i.e., O_2 generates radicals (equation 7). These radicals can also react with the organic molecules increasing the degradation efficiency of the whole system (see equations 39 - 41) [160].

$$O_2^{\cdot -} + 2H^+ \xrightarrow{e^-} H_2O_2 \qquad \text{Equation 39}$$

$$H_2O_2 \xrightarrow{e^-} OH^{\cdot} + OH^- \qquad \text{Equation 40}$$

$$R^{\cdot} + O_2^{\cdot -} \rightarrow R - O_2^- + H^+ \Leftrightarrow R - O_2H \qquad \text{Equation 41}$$

Samples of the supernatant have been collected during the degradation investigations and analyzed by HPIC technique. The results of the quantification were not precise enough to provide some information about the efficiency of the photocatalytic degradation, and the differences between the O_2 and N_2 purged systems. The low consumption of DCA molecules is mainly due to the low surface available for adsorption and degradation. In addition, the use of a flow reactor impedes the measurement of small changes in the concentration of the compounds, since the whole solution volume is constantly mixed.

Very different spectral shapes in the adsorption studies involving the intercalation of adsorption and degradation periods have been observed for the different powders used. The measurements performed at the PC500 show spectral bands, already observed for the

photocatalytic degradation (see Figure 23), with the evolution of bands at 1342 and 1273 cm^{-1}, and the region around 1500 cm^{-1} (see Figure 25). These changes can be associated with the formation of intermediates or to new adsorption bonds between DCA/DCA^- molecules and new exposed faces of the anatase crystals. The band assigned to the COO symmetric stretching keeps its intensity, which again indicates the constant formation of bonds between the carbonyl group and the TiO_2.

The S230 powder shows an analogous spectral behavior in comparison to PC500. The most relevant difference is the lower intensity of the bands at 1412 cm^{-1} and 1273 cm^{-1} (see Figure 27) and the shoulder at 1354 cm^{-1}. These spectral changes are probably also related to new adsorption possibilities arising from the new crystalline faces exposed due to the absorption of energy by the particles.

With larger particle sizes, the PC10 sample shows a slightly different adsorption spectrum. The formation of a small shoulder around 1354 cm^{-1} is observable after 60 min of adsorption. This signal is assigned to the vibrational mode of the COO group, slightly shifted. Observing the evolution of the spectra (Figure 26), it can be affirm that the powder shows some photocatalytic activity. The bands do not show a considerable increase in its intensities, but keep it. This indicates a continuous replacement of the adsorption sites by new dichloroacetate anions. The absence of new signals can be attributed to the high particle size of the powder, which contributes to a lower aggregation and almost all TiO_2 surfaces are already exposed, not suffering significant changes with the irradiation and its consequences.

Differently from anatase, rutile samples show a constant decay of the spectral signals, which has already expected denotes its photocatalytic inactivity [161-164], without formation of new spectral bands. The spectral signals initially observed at 1381 cm^{-1} and 1226 cm^{-1} decay under irradiation. This does not prove its degradation, but can indicate the formation of surface complexes as suggested in Figure 54.

5.5 Adsorption of Acetic and Chlorinated Acetic Acids at the Anatase Surface

5.5.1 Kinetic Aspects of the Adsorption

The absence of Cl atoms in the organic structure can provide interesting information for the understanding of the chlorinated acetates behavior at the semiconductor surface. The electronic cloud shows another distribution in the molecule without the chlorine atom in the structure, with direct influence on the interaction of the molecule with the TiO_2 surface.

Recent studies comparing the adsorption behavior of carboxylic acids, e.g., AA and formic acid, have proposed three possible structures for the adsorption of the carboxylate group at a TiO_2 surface [141]: (1) As a bidentate structure, where both oxygen atoms binding the same Ti atom (Figure 55 A); (2) As a monodentate replacing the basic OH group at the surface (Figure 55 B); (3) as a bidentate structure involving the carboxyl group and two Ti centers from the surface (Figure 55C).

Due to its low dissociation (pK_a = 4.75), the carbonyl group of the acetic acid shows a more complex adsorption behavior than the other investigated molecules. The peaks observed in the spectra at different pH conditions taken for AA (see Figure 32) show the strongly change of the adsorption mode of the molecules with changing the pH condition.

At neutral pH conditions the spectral regions from 1545-1570 cm^{-1} and at 1330 cm^{-1} increase. At this pH the molecules are mostly dissociated (see Figure 66 B). The increase of the intensity may be related to the higher interaction of the acetate anion with the TiO_2 surface. According to Liao *et al*. [165] and Backes *et al*. [140] with the dissociation of the AA molecule, the main change in the interaction with the surface is the formation of a bidentate structure involving two distinct Ti atoms (see Figure 55 A). While non-dissociated AA preferentially adsorbs in the monodentate structure. This is facilitated by the presence of the hydrogen atom, which interacts with the OH group in the vicinity, stabilizing the complex (see Figure 55 B). The displacement of the spectral band from 1545 to 1570 cm^{-1}, and the decay of the intensity for the band centered at 1423 cm^{-1}, see Figure 33, are attributed to the stiffness of the carboxyl group stabilized by formation of the bidentate structure.

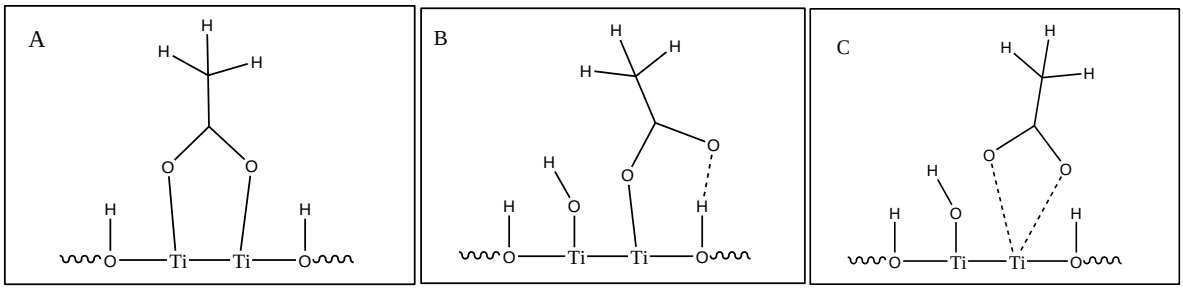

Figure 55: Adsorption structures for AA and AA^- on the positively charged anatase (100) surface: (A) Two metal sites bidentate structure (B) Monodentate structure and (C) One metal site bidentate mode.

According to Nakamoto [166] the shift of the symmetric stretching mode of COO^- of the adsorbed acetic acid/acetate to higher wavenumbers in comparison to free ions combined with the displacement of the asymmetric stretching mode of COO^- to low wavenumbers hold the formation of a bidentate structure. This occurs because both O atoms bind to Ti atoms, hindering a good deflection of the C–O distribution. For the adsorption of acetate at anatase similar correlation has been suggested by Rotzinger *et al*. [141].

Mattsson and Österlund [139] have observed a correlation between the wavenumber difference of the COO values and the particle size. Smaller sized particles normally show larger difference. The difference between the symmetric and asymmetric stretching signals for the PC500 powder, with an average particle size of 7 nm, is 104 cm^{-1}. This value is higher for particles of 25 nm with a difference of 97 cm^{-1} observed by Mattsson and Österlund [139]. Hence, this tendency is also valid for our investigations.

The absence of relevant signals in the spectra taken at alkaline conditions indicates that the negatively charged surface repulse the acetate anions. This inhibits the formation of surface structures. Similar behavior has been observed for the MCA^- and TCA^- in alkaline pH conditions. In both cases spectral signals are virtually not present, indicating low or no interaction with TiO_2.

However, MCA and TCA show different behaviors with respect to the almost neutral pH condition. TCA does not show any significant spectral change (shift or increase) as compared to the acidic condition (see Figure 36). In contrast the spectrum shape of the adsorbed MCA molecules shows a sharp decay of some bands, especially the bands at 1254 and 1400 cm^{-1}, and a slightly change of the band at 1580 cm^{-1}. The appearance of a new band at 1323 cm^{-1} is also observed (see Figure 30). These changes are explained by the modification in the interaction of the molecules with the surface, in similar way than that

previously explain for the AA/AA^- structures. The presence of mono and/or bidentate structures is expected, because MCA has a pK_a of 2.87, which implies that at pH 3.0 around 50 % of the molecules are dissociated. At pH 6.0 the chloroacetate is mostly present, and preferentially forms a bidentate complex. This postulation is also supported by the shift of the symmetric and asymmetric stretching modes of the carbonyl group, to 1381 cm^{-1} and to wavenumbers > 1600 cm^{-1}, respectively. For TCA changes of this nature cannot occur, the pK_a constant is very low and almost all molecules are already dissociated at pH 3.0. In this case the anion always interacts with the semiconductor surface in the same way, at least for pH 3.0 and 6.0. The adsorption behavior is only different for the negatively charged surface.

The shift in the position of the vibrational signals assigned to the carbonyl group, above explained, can also give an idea how the interaction of the organic acids takes place at the positively charged TiO_2 surface.

Displacement of the band assigned to the COO asymmetric stretching mode to higher wavenumbers can be observed with the increase of the Cl substitution in the molecular structure. This indicates that the presence of high electronegative atoms dislocate the electronic cloud to the halogen moiety. Thus, weakening the interaction between the TiO_2 surface and the carboxyl group, and consequently causing a decay of the carboxyl character withdrawing the interaction with the Ti site. This yield to the shift and decay of the vibrational signals assigned to the carbonyl group. A representation of this change is proposed in Figure 56, the interaction is weaker according to the increase of the number of Cl atoms in the molecular structure.

The decrease in the interaction between the carboxyl group and the TiO_2 surface for molecules with high chlorine substitution supports the model proposed in Figure 56. The formation of a bond between the Ti site and the chlorine atom as exposed in Figure 53 is also possible. This structure has also to be considered, for the adsorption of TCA, as can be seen in illustration E (see Figure 56).

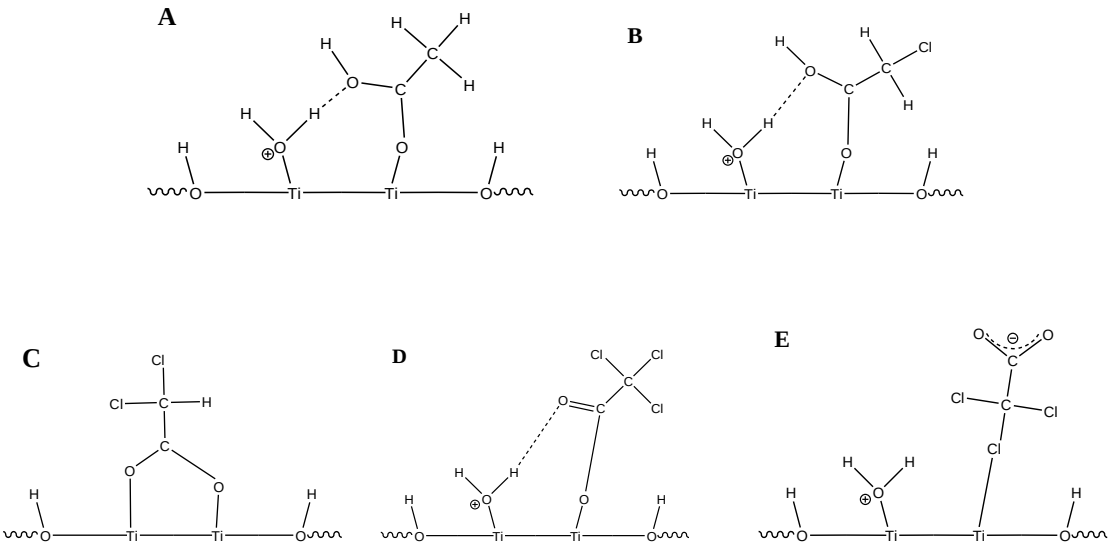

Figure 56: Adsorption structures for acetic acid (A), monochloroacetic acid (B), dichloroacetic acid (C) and trichloroacetic acid (D and E) on the anatase (100) surface positively charged (pH 3.0).

Structures for the complexes formed at the surface at almost neutral surface are proposed in Figure 57. As previously exposed, the low dissociation value of TCA molecule does not show change in its adsorption. Regarding the evidence that dissociated molecules have a propensity to adsorb in the monodentate form. This postulation is also confirmed by the maintenance of the position from the spectral bands, with enhance of the pH.

The DCA/PC500 system shows another behavior. The presence of new spectral bands, with increased pH from 3.0 to 6.0, suggests the change of the surface structures. This behavior does not confirm the preferential adsorption mode proposed for dissociated acids, once the most probably change is the formation of a bidentate complex, as proposed by Hilgendorff [121].

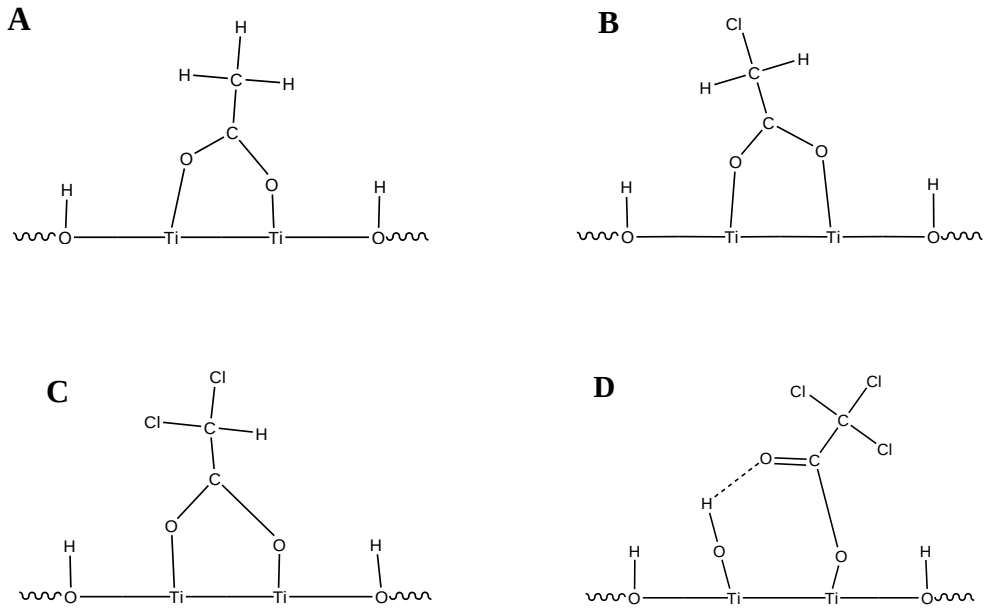

Figure 57: Adsorption structures for acetic acid (A), monochloroacetic acid (B), dichloroacetic acid (C) and trichloroacetic acid (D) on the anatase (100) surface (pH 6.0).

However, the AA and MCA molecules confirm the preferential formation of the couples monodentate structure/non-dissociated molecule and bidentate structure/anion. The spectral changes observed in Figure 30 and Figure 33 confirm the change of the adsorption structure with the formation of a bidentate. It is worthwhile to note that MCA is only partially dissociated at pH 3.0, and that probably both, mono and bidentate structures are presented at this pH conditions.

The only change observed for the adsorption kinetic of AA at TiO_2 was the decrease in the bands intensity. This can indicate that AA reacts at the TiO_2 surface in similar way than observed for the DCA molecule. However, the fitting of the adsorption isotherm shows a typical Langmuir model. Therefore, it is not possible to affirm in which way the AA interacts with the TiO_2 surface based only on the results obtained here.

The number of adsorbed molecules at the surface is for both; Langmuir and modified Langmuir model; around 0.3 AA molecules per nm^2 (see Table 14). These values are lower than the number of adsorbed molecules observed for MCA or DCA, and indicate a low interaction with the TiO_2.

Table 14: Number of surface OH groups exchanged by chloroacetic acids at the surface of PC500, per square nanometer, obtained from the adsorption isotherm. N: Number of exchangeable OH groups per nm^2.

Adsorbate	N - Langmuir model	N - Modified Langmuir model
AA	0.43	0.30
MCA	1.43	1.07
TCA	0.28	0.25

Figure 34 shows the decay of the spectral signals of AA in time. This tendency is evidence for a weak interaction of the AA with the TiO_2 surface, even showing a different interaction profile.

The carbonyl character of the TCA adsorbed complexes, observed in the vibrational spectrum, is low. The signals almost disappear after 60 min of adsorption. The decay in the intensity of the band centered at 1338 cm^{-1} (see Figure 38) indicates the fragile interaction between the acid and the TiO_2 surface. This interaction occurs probably *via* the binding of the Cl atoms at Ti sites. The large size of the Cl atoms obstructs the approach of more molecules in the vicinity, thereby hindering the formation of other bonds. This explains the low number of molecules adsorbed at the surface, i.e., 0.04 and 0.25 molecules per nm^2 in comparison to the other acids (see Table 14) for the Langmuir and modified Langmuir model, respectively.

With the highest coverage, i.e., 1.43 and 1.07 molecules per nm^2 for the Langmuir and modified Langmuir model, respectively, MCA shows the best interaction with the TiO_2 surface. However, these values are masked by the presence of interactions of dissociated molecules and of non-dissociated with the surface. Due to the partial dissociation of the molecules at pH 3.0, the character of the interaction is a mixture between the formation of complexes observed for the DCA and structures formed for the AA.

MCA is the only molecule that still shows spectral bands after more than 60 min of equilibration. This indicates the presence of stable structures at the TiO_2 surface. Especially the maintenance of the band centered at 1400 cm^{-1} is a strong indication for the formation of a bidentate complex. The slow decay of the other bands is evidence that the mixture of structures initially present changes during the equilibration.

A suggestion for the MCA/MCA^- interaction with the TiO_2 surface at pH 3.0 is shown in Figure 58. The high MCA/TiO_2 interaction has already been reported in the literature [33]. Furthermore, another indication for the adsorption model is the bad fitting of the adsorption isotherms using the different models suggested in this work. The presence of two different molecules, i.e., the dissociated and the non-dissociated form of MCA, on the surface cannot be adequately described by these models.

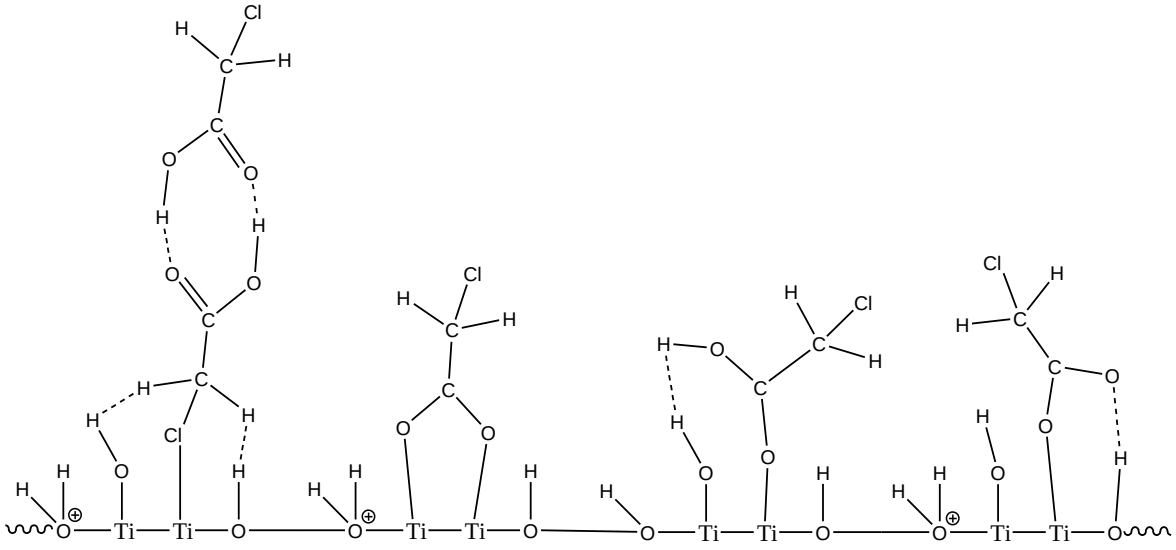

Figure 58: Schematic representation of the different adsorption modes for MCA on the positively charged anatase (100) surface (pH 3.0).

5.6 Adsorption from Solutions Containing Organic Acid Mixtures at the Anatase Surface

ATR-FTIR has also been used to investigate the competitive adsorption of chloroacetic mixtures at the surface of TiO_2. The different dissociation constants and distribution of the electrons on the molecular structure may play an important role on the competition for the adsorption sites at surface. The use of different carboxylic acids, which have different dissociation constants, in solution also changes the electrostatic conditions. Therefore, additional information about the adsorption mechanism can be obtained from the comparison of the behavior from the different acid mixtures.

AA has a disadvantage in competition with the other chlorinated acids. Due to its high dissociation constant ($pK_a = 4.75$), the electrostatic interaction between the positive surface

and the chlorinated anions is stronger (Figure 38, Figure 39 and Figure 40). Vibrational contributions from the AA carbonyl group are only observable in the solution containing TCA. In the presence of the other acids, i.e., MCA and DCA, only peaks assigned to the bending mode of the CH_3 group are observed. This indicates another adsorption mode for the AA. According to the data obtained from the AA kinetic study, the molecule preferentially forms monodentate structures, i.e., a bond between a Ti site and the carbonyl group. However, for the solutions containing MCA and DCA the signals observed for the acetic acid carbonyl, i.e., at 1527 and 1423 cm^{-1}, are not present. The band at 1340 cm^{-1} indicates that AA probably interacts via hydrogen bonds with the OH groups from the TiO_2 surface, or with the already adsorbed MCA and DCA molecules.

That behavior suggests that the interaction between TiO_2 and AA is strongly dependent on the presence of other molecules in solution. All the chlorinated acids show good interaction with the oxide surface, and can even form satisfactory bonds on the TiO_2 when competing for the adsorption sites.

The capacity of TCA to compete for the adsorption sites is astonishing, considering the low number of adsorption site exchanged by TCA molecules (see Table 14). This may be an indication for the importance of the electrostatic attraction of the electronegative Cl atoms for the adsorption.

Nevertheless, the low dissociation constants of TCA and DCA, almost completely dissociated at pH 3.0, are not a guarantee for an effective adsorption. In the presence of MCA the competition for the adsorption sites is immense. In both mixtures, i.e., MCA/DCA and MCA/TCA, spectral contributions from DCA and TCA have been observed (see Figure 41 and Figure 42). However, the signals assigned to the MCA are also very intense. MCA can apparently profit from its broad variety of adsorption possibilities (see Figure 58). Actually, MCA shows the most intense vibrational signals in the mixtures where it is present, which is an indication of a very fast and strong interaction. It is important to note, that the decay of the signals does not mean in the increase of other bands, which suggests the formation of stable structures, e.g., the complexes shown in Figure 54.

The presence of vibrational bands assigned to carbonyl group of DCA and TCA in the DCA/TCA mixture, indicates that the competition for the adsorption sites is more intense in this particular case.

The observation of bands assigned to the symmetric and asymmetric stretching mode of the carbonyl group from the chlorinated acids in all mixtures, again indicates the formation of the Ti-OOC bond as first step of interaction. The mechanism following this step is, however, not so clear. The decay of the bands assigned to the carbonyl group was nearly uniform in almost all experiments. This is evidence that the acids interact with the surface, but this interaction is weak and cannot be maintained for a long period of time.

The exchange of organic molecules, such as oxalate and salicylate (and vice-versa), onto TiO_2 has been shown to follow the predictions of simple equilibrium calculations, based on the stability constants obtained from systems containing each ligand alone [167]. In some cases those tendencies are not confirmed. The affinity sequence obtained for the molecules investigated here is MCA > DCA ≈ TCA > AA, which is based on the number of adsorbed molecules on TiO_2, and the intensity of the vibrational bands observed for the acid mixtures. It is interesting to observe that the trend of the photocatalytic degradation of the same acids in PC500 suspensions is slightly different: DCA > MCA >> AA ≈ TCA [168]. This tendece confirms the results obtained by Czili *et al.* [33], which proposed the direct attack of OH radicals on the chlorinated molecules (MCA and DCA), and a indirect mechanism for the TCA.

The adsorption of the molecules on the surface of the TiO_2 particles is not a pre-requisite for the photodegradation of the molecules. The photocatalytic degradation mechanism involving TiO_2 is much more complex than assumed. Various investigations have compared adsorption isotherms and degradation curves for different compounds, showing different results. Hence, the importance of the adsorption for the photocatalytic degradation is still uncertain [169].

5.7 Adsorption of 2,4-D Molecules at the Anatase Surface

The adsorption of phenolic compounds at TiO_2 follows the Langmuir equation only up to a certain concentration [120], [170]. Above that limit the molecules undergo a transformation from the classical monolayer adsorption equilibrium, which happens at low concentration, to a multilayer regime, and a first plateau of adsorption is observed [120], [170]. With the increase of the surface adsorption the conversion from pure chemisorption to

a mixed chemi- and physi-sorption system has been observed [171]. In this sense, a better description of the experimental data is obtained by fitting with the BET adsorption model.

The number of adsorption sites occupied by the 2,4-D molecules on the first adsorption layer is 30 μmol per gram TiO_2. This value corresponds to a small portion of the available sites at the PC500 anatase surface. The number of molecules per square nanometer is 0.06, while fluoride shows 1.1 exchangeable OH groups. Taking into account the huge size of the 2,4-D molecule compared to the F^-, the capacity to exchange the OH groups is still good.

The pH condition also shows a strong influence on the intensity of the spectral signals recorded for the 2,4-D solutions on the PC500 film. The interaction of the pesticide with the TiO_2 is dependent of the number of protonated sites of the surface and especially the distribution of the dissociated and non-dissociated form of 2,4-D in solution. The distribution of these forms can be calculated from the dissociation constant (see Figure 68). An increase of the pH value, e.g., from 2.9 to 3.5, does not directly imply an increase in the intensity of the spectral signals. Apparently, the distribution of the adsorption sites at the surface plays a more complex role than the protonation molecules in the bulk solution.

The analysis of the ATR-FTIR spectrum of 2,4-D is more complex. The occurrence of different organic groups, i.e., the aromatic ring, the carboxylic group and aliphatic part, implies the presence of more spectral signals. Therefore, the assignment of the bands is more complex than for the carboxylic acids previously investigated. The assignment of the bands considers different investigations [144-146]. The presence of signals assigned to the carbonyl group (1420-1280 cm^{-1}) can be observed, as well as signals of the aromatic ring and phenol, i.e., at 1590-1480 cm^{-1} and 1265-1070 cm^{-1}, respectively.

The 2,4-D is mostly deprotonated at pH conditions below 2.9. However, the presence of protonated or deprotonated species in solution do not influence the vibrational modes observed for the adsorbed structures. The only change that occurs with the increase of the pH condition is the decrease in the intensity of the vibrational signals.

With the identification of the bands from the pesticide, some points regarding its interaction with the anatase surface can be proposed. The spectral signals observed for the investigation performed with a 2.7 $mmol \cdot L^{-1}$ 2,4-D solution show a good stability (see Figure 47), which denotes a longer and stronger interaction between the molecules and the TiO_2. On the other hand, experiments performed with low pesticide concentrations, see Figure 48, show

the decay of some signals. At the same time, other spectral bands almost maintain their intensity, which indicates that some interactions at the interface keep constant while other contact points become weaker. This behavior suggests changes in the molecule arrangement at the TiO_2 surface.

At low concentrations not all sites are occupied by 2,4-D molecules, leaving empty spaces which enable the rings to rotate, for instance, around the Cl-O axis (see Figure 59 A). These rotations alter the stability of the structure to some extent observed in the remarkable decrease in the intensity of the bands, except from those involving Cl atoms which upon rotations can more efficiently contribute to the IR signal, having a lower decrease of its signals. This behavior is supported by the maintenance of the spectral region between 950 and 1200 cm^{-1}, assigned mostly to vibrational modes of the aromatic ring. It is especially observed for investigations employing low pesticide concentrations, i.e., 0.5 and 1.4 $mmol \cdot L^{-1}$. In contrast, the intensity of the bands in the region commonly assigned to the carboxyl group decreases.

With increasing adsorbate coverage, i.e., using 2.7 $mmol \cdot L^{-1}$, the adsorption sites at the (100) anatase surface are occupied by 2,4-D molecules, which is closed packed and likely stabilized by ring-ring interactions [120]. The surface complex is laterally adsorbed to guarantee these interactions. Free rotations of the rings are therefore sterically hindered, and almost unchanged spectral signal are obtained (see Figure 59 B).

Investigations performed by Zhou *et al*. [172] involving theoretical simulations of adsorption studies for polar molecules, e.g., benzene, at the TiO_2 surface indicate a very weak adsorption on TiO_2. The molecule is positioned in the gap between the O atoms on the surface, this interaction is oriented parallel to the surface. Even with the formation of a monolayer at the surface, the molecules keep the position that gives more stability. This distribution is always parallel to the surface and between the bridging oxygen [172]. However, studies performed by Orlov *et al*. [173] for 4-chlorophenol have suggested that the molecule adsorbs at different angles on the TiO_2 surface depending on the degree of molecular coverage on the oxide. For a monolayer an angle of 70 degrees has been observed, while for an one fifth covered layer the angle decays to 60 degrees.

The behavior observed in this study corresponds to the investigation performed by Orlov *et al*. [173] . Additionally, some factors also have a strong influence on the formation of the adsorption structures. For example, the interaction between carboxyl groups of adjacent

molecules, in a similar way as suggested for the DCA molecule (see chapter 5.2.1), can explain the low intensity of the signals observed at low 2,4-D concentrations. At high concentrations the surface complexes are already stabilized by the ring-ring interaction.

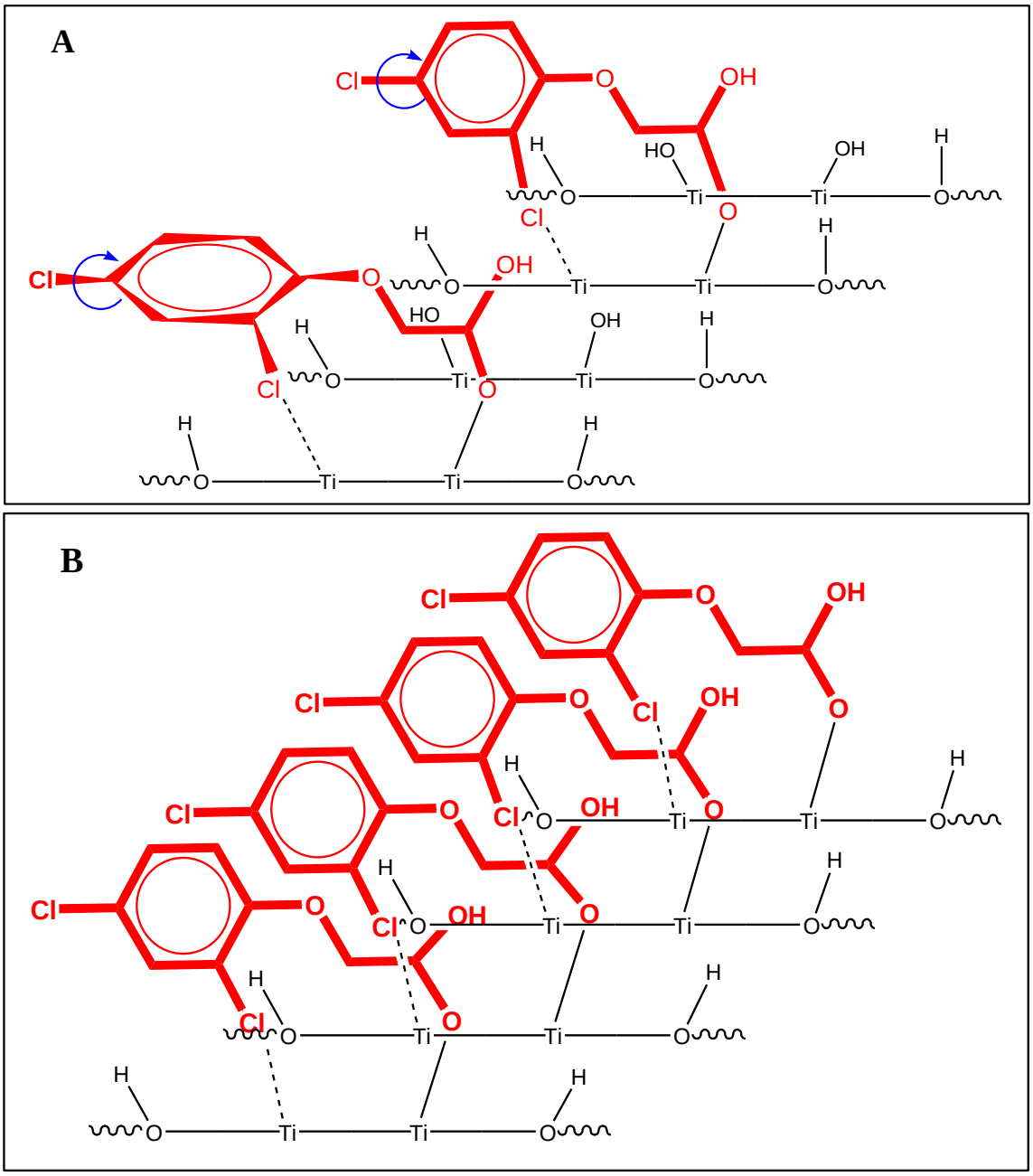

Figure 59: Schematic representation for the adsorption of 2,4-D molecules at an anatase (100) surface. A - At low concentrations (1.4 and 0.5 mmol·L^{-1}). B - At high concentrations (2.7 mmol·L^{-1}).

Assuming that the water molecules adsorbed at the TiO_2 surface are mainly dissociated [52], this water layer can also influence the adsorption. The presence of water on the TiO_2 surface can explain why the spectral signals disappear after certain time. The

expansion of the TiO_2 film, due to the solvation of the particles, causes a desorption of the adsorbed 2,4-D molecules at the upper surface of the layer. Molecules like the 2,4-D cannot occupy the spaces between the TiO_2 particles, due to their huge size. Therefore, the spectral intensity decreases, since the molecules are more distant from the ZnSe crystal, and consequently from the evanescent waves.

The degradation experiments only provide scarce information about the interaction and the changes for the behavior of the pesticide on the TiO_2 surface. For the low concentrated solutions, the spectral signals are almost negligible, and no changes can be observed for the spectral shape. The only exception is the region from 1200 to 900 cm^{-1}, where signals are still observable. The maintenance of these bands is probably correlated to the interaction mode of the aromatic rings with the surface, as already discussed.

The photocatalytic degradation of the system using high 2,4-D concentrations shows only a slight effect on the spectral behavior. Changes of the spectral intensities, as well as shifting or enlargement of the existent bands are almost not present. The most important change was the appearance of a new band at 1458 cm^{-1}. These little changes suggest an ineffective photocatalytic degradation of the 2,4-D molecule under the employed conditions. The new band observed can be assigned to vibrational modes from degradation intermediates, but due to the complex degradation mechanism of 2,4-D [16, 20, 174, 175] the identification of that band is nearly impossible using the techniques employed in this study.

6 Conclusions

The investigation of the interaction between organic molecules and TiO_2 combining the analysis of adsorption isotherms and ATR-FTIR spectroscopy has provided a better understanding of the adsorption process for the different molecules.

Adsorption isotherm indicates that the DCA adsorption does not follow the classical Langmuir model. Different adsorption possibilities and structures can occur. The steady decay of the IR signals assigned to DCA during the equilibration period supports this postulation. To describe that behavior a model has been proposed, this model considers the formation of two adsorption complexes. The first one formed at the beginning of the equilibration, which consists of the interaction between the DCA carboxylate group and the TiO_2 surface forming bidentate or monodentate structures. The second adsorption possibility involves the flip of the DCA molecule on the surface, in such a way that the Cl atoms can interact with the Ti adsorption sites. The new structures are stabilized by interactions with adjacent molecules, which are also adsorbed at the surface. Additionally, these new complexes are able to interact with other DCA molecules in the bulk solution, enabling the formation of a multilayer system. The mathematical model proposed to fitting this adsorption behavior, has been called: modified Langmuir model.

The increase of the pH condition from the solution shows drastically changes for the IR spectra. The pH condition show strongly influence on the distribution of the hydroxyl groups at the TiO_2 surface. The use of different TiO_2 powders does not show huge changes in the adsorption behavior of the organic acid molecules. The spectral bands are not significantly shifted, and new bands cannot be observed. However, for the photocatalytic degradation of DCA the different crystallite size and/or the agglomeration degree of the particles play an important role. New bands can be observed and indicate the presence of new molecules or radicals adsorbed at the TiO_2 surface. These signals result from the formation of new complexes involving other TiO_2 facets. The exposition of these new facets is attributed to the deaggregation, which is caused by the absorption of energy. This energy is provided by the irradiation of the system. Anatase particles have shown higher photocatalytic activity than rutile, in accordance with the literature. Particles with lower particle size show more intense changes in its spectral behavior, which is explained by the deaggregation effect. The use of systems saturated with oxygen does not contribute for a better interaction between the surface

and the molecules. On the other hand, its influence on the photocatalytic systems is remarkable.

Different adsorption mechanisms have been observed for the DCA homologues. AA and TCA adsorbs weakly at the TiO_2 surface. Both molecules show low values for the exchange of the OH groups at the TiO_2 surface. And also for the spectra recorded for the mixtures of the acids only small contributions from both compounds have been observed, especially the AA. MCA was the only molecule that has shown spectral signals after 120 min of equilibration, which suggest a better adsorption at the surface. The intense signals observed in the investigation involving the mixtures and the high number of adsorption sites occupied by the molecule also confirm the higher interaction between MCA and the TiO_2.

The rough sequence for the adsorption affinity of AA and the chlorinated acetic acids: MCA > DCA ≈ TCA > AA. This sequence does not correspond to the dissociation sequence, which indicates the interaction between TiO_2 and the organic acids is influenced by different parameters, e.g., the electronic cloud, or the structures and complexes formed at the surface.

Adsorption of 2,4-D on anatase is strongly affected by pH changes. However, the adsorption kinetics of 2,4-D on TiO_2 reveals a strong dependence from the pesticide concentration. An important structural change is suggested to occur in equilibration at low concentrations. The adsorbed 2,4-D flips from lateral to flat conformation, but with a weak interaction with the surface. Employing high concentrations the system shows a stable conformation, which results from the stabilization of the molecules by interactions with adjacent molecules. These structures form a close packed monolayer at the TiO_2 surface. The photocatalytic degradation of 2,4-D has been only followed by employing high bulk concentration. Slightly spectral changes have been observed during the irradiation time, suggesting low degradation efficiency.

7 References

1. Friedmann, D., Mendive, C., and Bahnemann, D., TiO_2 for water treatment: Parameters affecting the kinetics and mechanisms of photocatalysis. *Applied Catalysis B: Environmental*, **2010**. 99 (3-4): 398-406.

2. Mendive, C.B., Hansmann, D., Bredow, T., and Bahnemann, D., New Insights into the Mechanism of TiO_2 Photocatalysis: Thermal Processes beyond the Electron/Hole Creation. *The Journal of Physical Chemistry C*, **2011**. 115 (40): 19676-19685.

3. Cabral, M.G., Viegas, C.A., Teixeira, M.C., and Sa-Correia, I., Toxicity of chlorinated phenoxyacetic acid herbicides in the experimental eukaryotic model Saccharomyces cerevisiae: role of pH and of growth phase and size of the yeast cell population. *Chemosphere*, **2003**. 51 (1): 47-54.

4. Graymore, M., Stagnitti, F., and Allinson, G., Impacts of atrazine in aquatic ecosystems. *Environment International*, **2001**. 26 (7-8): 483-495.

5. Rodrigues, B.N. and Almeida, F.S., *Guia de herbicidas*. **1998**.

6. Kipopoulou, A.M., Zouboulis, A., Samara, C., and Kouimtzis, T., The fate of lindane in the conventional activated sludge treatment process. *Chemosphere*, **2004**. 55 (1): 81-91.

7. OPAS, *Manual de vigilância da saúde de populações expostas a agrotóxicos.* **1997**, Organizacao Pan-Americana da Saúde Brasília.

8. Esposito, E., Paulillo, S.M., and Manfio, G.P., Biodegradation of the herbicide diuron in soil by indigenous actinomycetes. *Chemosphere*, **1998**. 37 (3): 541-548.

9. Brillas, E., Calpe, J.C., and Cabot, P.L., Degradation of the herbicide 2,4-dichlorophenoxyacetic acid by ozonation catalyzed with Fe^{2+} and UVA light. *Applied Catalysis B-Environmental*, **2003**. 46 (2): 381-391.

10. http://www.irc.nl/page/13219. **2011**.

11. Schottler, S.P. and Eisenreich, S.J., Herbicides in the Great Lakes. *Environmental Science & Technology*, **1994**. 28 (12): 2228-2232.

12. Goolsby, D.A., Thurman, E.M., Pomes, M.L., Meyer, M.T., and Battaglin, W.A., Herbicides and Their Metabolites in Rainfall: Origin, Transport, and Deposition Patterns across the Midwestern and Northeastern United States, 1990-1991. *Environmental Science & Technology*, **1997**. 31 (5): 1325-1333.

13. Hultgren, R.P., Hudson, R.J.M., and Sims, G.K., Effects of Soil pH and Soil Water Content on Prosulfuron Dissipation. *Journal of Agricultural and Food Chemistry*, **2002**. 50 (11): 3236-3243.

14. Garcia-Valcarez, A.I. and Tadeo, J.L., Influence of Soil Moisture on Sorption and Degradation of Hexazinone and Simazine in Soil. *Journal of Agricultural and Food Chemistry*, **1999**. 47 (9): 3895-3900.

15. Bachman, J. and Patterson, H.H., Photodecomposition of the Carbamate Pesticide Carbofuran:Kinetics and the Influence of Dissolved Organic Matter. *Environmental Science & Technology*, **1999**. 33 (6): 874-881.

16. Peller, J., Wiest, O., and Kamat, P.V., Hydroxyl radical's role in the remediation of a common herbicide, 2,4-Dichlorophenoxyacetic acid (2,4-D). *Journal of Physical Chemistry A*, **2004**. 108 (50): 10925-10933.

17. Chu, W., Chan, K.H., Kwan, C.Y., and Lee, C.K., The system design of UV-assisted catalytic oxidation process-degradation of 2,4-D. *Chemosphere*, **2004**. 57 (3): 171-178.

18. Djebbar, K. and Sehili, T., Kinetics of heterogeneous photocatalytic decomposition of 2,4-dichlorophenoxyacetic acid over titanium dioxide and zinc oxide in aqueous solution. *Pesticide Science*, **1998**. 54 (3): 269-276.

19. Singh, H.K. and Muneer, M., Photodegradation of a herbicide derivative, 2,4-dichlorophenoxy acetic acid in aqueous suspensions of titanium dioxide. *Research on Chemical Intermediates*, **2004**. 30 (3): 317-329.

20. Terashima, Y., Ozaki, H., Giri, R.R., Tano, T., Nakatsuji, S., Takanami, R., and Taniguchi, S., Photocatalytic oxidation of low concentration 2,4-D solution with new TiO_2 fiber catalyst in a continuous flow reactor. *Water Science and Technology*, **2006**. 54 (8): 55-63.

21. Spangenberg, D., Moller, U., and Kleinermanns, K., Photooxidation of exhaust pollutants .4. Photocatalytic and thermal decomposition of trichloroacetic acid: Degradation efficiencies and products. *Chemosphere*, **1996**. 33 (1): 43-49.

22. Ellis, D.A., Hanson, M.L., Sibley, P.K., Shahid, T., Fineberg, N.A., Solomon, K.R., Muir, D.C.G., and Mabury, S.A., The fate and persistence of trifluoroacetic and chloroacetic acids in pond waters. *Chemosphere*, **2001**. 42 (3): 309-318.

23. Dvoranova, D., Brezova, V., Mazur, M., and Malati, M.A., Investigations of metal-doped titanium dioxide photocatalysts. *Applied Catalysis B-Environmental*, **2002**. 37 (2): 91-105.

24. Li, Y.X., Me, Y.Z., Peng, S.Q., Lu, G.X., and Li, S.B., Photocatalytic hydrogen generation in the presence of chloroacetic acids over Pt/TiO_2. *Chemosphere*, **2006**. 63 (8): 1312-1318.

25. Malliarou, E., Collins, C., Graham, N., and Nieuwenhuijsen, M.J., Haloacetic acids in drinking water in the United Kingdom. *Water Research*, **2005**. 39 (12): 2722-2730.

26. Reemtsma, T. and Jekel, M., Dissolved organics in tannery wastewaters and their alteration by a combined anaerobic and aerobic treatment. *Water Research*, **1997**. 31 (5): 1035-1046.

27. Lifongo, L.L., Bowden, D.J., and Brimblecombe, P., Photodegradation of haloacetic acids in water. *Chemosphere*, **2004**. 55 (3): 467-476.

28. Mervyn, R., Pesticides - friend or foe? *Water Science and Technology*, **1998**. 37 (8): 19-25.

29. Kim, D.S. and Park, Y.S., Photocatalytic decolorization of rhodamine B by immobilized TiO_2 onto silicone sealant. *Chemical Engineering Journal*, **2006**. 116 (2): 133-137.

30. Malato, S., Blanco, J., Caceres, J., Fernandez-Alba, A.R., Aguera, A., and Rodriguez, A., Photocatalytic treatment of water-soluble pesticides by photo-Fenton and TiO_2 using solar energy. *Catalysis Today*, **2002**. 76 (2-4): 209-220.

31. Muneer, M. and Bahnemann, D., Semiconductor-mediated photocatalyzed degradation of two selected pesticide derivatives, terbacil and 2,4,5-tribromoimidazole, in aqueous suspension. *Applied Catalysis B-Environmental*, **2002**. 36 (2): 95-111.

32. Liu, I., Lawton, L.A., Bahnemann, D.W., and Robertson, P.K.J., The photocatalytic destruction of the cyanotoxin, nodularin using TiO_2. *Applied Catalysis B: Environmental*, **2005**. 60 (3-4): 245-252.

33. Czili, H. and Horvath, A., Photodegradation of chloroacetic acids over bare and silver-deposited TiO_2: Identification of species attacking model compounds, a mechanistic approach. *Applied Catalysis B-Environmental*, **2009**. 89 (3-4): 342-348.

34. Hoffmann, M.R., Martin, S.T., Choi, W.Y., and Bahnemann, D.W., Environmental applications of semiconductor photocatalysis. *Chemical Reviews*, **1995**. 95 (1): 69-96.

35. Ilyas, H., Qazi, I.A., Asgar, W., Awan, M.A., and Khan, Z.U.D., Photocatalytic Degradation of Nitro and Chlorophenols Using Doped and Undoped Titanium Dioxide Nanoparticles. *Journal of Nanomaterials*: 8.

36. Tavares, C.J., Marques, S.M., Lanceros-Mendez, S., Rebouta, L., Alves, E., Barradas, N.P., Munnik, F., Girardeau, T., and Riviere, J.P., N-Doped Photocatalytic Titania Thin Films on Active Polymer Substrates. *Journal of Nanoscience and Nanotechnology*. 10 (2): 1072-1077.

37. Liu, I., Lawton, L.A., Bahnemann, D.W., Liu, L., Proft, B., and Robertson, P.K.J., The photocatalytic decomposition of microcystin-LR using selected titanium dioxide materials. *Chemosphere*, **2009**. 76 (4): 549-553.

38. Ghaly, M.Y., Jamil, T.S., El-Seesy, I.E., Souaya, E.R., and Nasr, R.A., Treatment of highly polluted paper mill wastewater by solar photocatalytic oxidation with synthesized nano TiO_2. *Chemical Engineering Journal*, **2011**. 168 (1): 446-454.

39. Peralta-Zamora, P., Wypych, F., Carneiro, L.M., and Vaz, S.R., Remediation of phenol, lignin and paper effluents by advanced oxidative processes. *Environmental Technology*, **2004**. 25 (12): 1331-1339.

40. de Freitas, A.M., Sirtori, C., and Peralta-Zamora, P., Photoelectrocatalytic degradation of camphor on TiO_2/RuO_2 electrodes. *Environmental Chemistry Letters*, **2011**. 9 (1): 97-102.

41. Abu Tariq, M., Faisal, M., Muneer, M., and Bahnemann, D., Photochemical reactions of a few selected pesticide derivatives and other priority organic pollutants in aqueous

suspensions of titanium dioxide. *Journal of Molecular Catalysis A-Chemical*, **2007**. 265 (1-2): 231-236.

42. Yamazaki, S., Matsunaga, S., and Hori, K., Photocatalytic degradation of trichloroethylene in water using TiO_2 pellets. *Water Research*, **2001**. 35 (4): 1022-1028.

43. Kim, S.B., Hwang, H.T., and Hong, S.C., Photocatalytic degradation of volatile organic compounds at the gas/solid interface of a TiO_2 photocatalyst. *Chemosphere*, **2002**. 48 (4): 437-444.

44. Pecchi, G., Reyes, P., Sanhueza, P., and Villasenor, J., Photocatalytic degradation of pentachlorophenol on TiO_2 solgel catalysts. *Chemosphere*, **2001**. 43 (2): 141-146.

45. Vittadini, A., Casarin, M., and Selloni, A., Chemistry of and on TiO_2-anatase surfaces by DFT calculations: a partial review. *Theoretical Chemistry Accounts: Theory, Computation, and Modeling (Theoretica Chimica Acta)*, **2007**. 117 (5): 663-671.

46. Mendive, C., *Effects of the UV(A) light on chemical reactions at the interface metal oxide / aqueous solution*, in *Department of chemistry*. **2007**, Universidad Nacional de San Martín: San Martin. 244.

47. Ulrike, D., The surface science of titanium dioxide. *Surface Science Reports*, **2003**. 48 (5-8): 53-229.

48. Bahnemann, D., Bockelmann, D., and Goslich, R., Mechanistic studies of water detoxification in illuminated TiO_2 suspensions. *Solar Energy Materials*, **1991**. 24 (1-4): 564-583.

49. Bello, M., *Optimization of the water photodetoxification process by modified and unmodified TiO_2.*, in *Institut für Technische Chemie*. **2009**, Gottfried Wilhelm Leibniz Universität Hannover: Hannover.

50. Feldhoff, A., Mendive, C., Bredow, T., and Bahnemann, D., Direct measurement of size, three-dimensional shape, and specific surface area of anatase nanocrystals. *Chemphyschem*, **2007**. 8 (6): 805-809.

51. *http://www.meinemineraliensammlung.de/victor/goldschmidt/band_7.html*. **2011** [cited 2011 10.08.2011].

52. Mendive, C.B., Bredow, T., Feldhoff, A., Blesa, M.A., and Bahnemann, D., Adsorption of oxalate on anatase (100) and rutile (110) surfaces in aqueous systems: experimental results vs. theoretical predictions. *Physical Chemistry Chemical Physics*, **2009**. 11 (11): 1794-1808.

53. Mendive, C.B., Bredow, T., Feldhoff, A., Blesa, M., and Bahnemann, D., Adsorption of oxalate on rutile particles in aqueous solutions: a spectroscopic, electron-microscopic and theoretical study. *Physical Chemistry Chemical Physics*, **2008**. 10 (14): 1960-1974.

54. Boehm, H.P., Acidic and basic properties of hydroxylated metal oxide surfaces. *Discussions of the Faraday Society*, **1971**. 52: 264-275.

55. Al-Abadleh, H.A. and Grassian, V.H., Oxide surfaces as environmental interfaces. *Surface Science Reports*, **2003**. 52 (3-4): 63-161.

56. Ciambelli, P., Sannino, D., Palma, V., and Vaiano, V., The effect of sulphate doping on nanosized TiO_2 and $MoOx/TiO_2$ catalysts in cyclohexane photooxidative dehydrogenation. *International Journal of Photoenergy*, **2008**: 8.

57. Rudzinski, W., Charmas, R., and Partyka, S., Calorimetric studies of ion adsorption at a water/oxide interface. Effects of energetic heterogeneity of real oxide surfaces. *Langmuir*, **1991**. 7 (2): 354-362.

58. Brown, G.E., Henrich, V.E., Casey, W.H., Clark, D.L., Eggleston, C., Felmy, A., Goodman, D.W., Graetzel, M., Maciel, G., McCarthy, M.I., Nealson, K.H., Sverjensky, D.A., Toney, M.F., and Zachara, J.M., Metal Oxide Surfaces and Their Interactions with Aqueous Solutions and Microbial Organisms. *Chemical Reviews*, **1998**. 99 (1): 77-174.

59. Martin, S.T., Morrison, C.L., and Hoffmann, M.R., Photochemical Mechanism of Size-Quantized Vanadium-Doped TiO_2 Particles. *The Journal of Physical Chemistry*, **1994**. 98 (51): 13695-13704.

60. Nogueira, R.F.P., Trovao, A.G., and Paterlini, W.C., Evaluation of the combined solar TiO_2/photo-Fenton process using multivariate analysis. *Water Science and Technology*, **2004**. 49: 195-200.

61. Malato, S., Blanco, J., Campos, A., Caceres, J., Guillard, C., Herrmann, J.M., and Fernandez-Alba, A.R., Effect of operating parameters on the testing of new industrial titania catalysts at solar pilot plant scale. *Applied Catalysis B: Environmental*, **2003**. 42 (4): 349-357.

62. Zalazar, C.S., Romero, R.L., Martin, C.A., and Cassano, A.E., Photocatalytic intrinsic reaction kinetics I: Mineralization of dichloroacetic acid. *Chemical Engineering Science*, **2005**. 60 (19): 5240-5254.

63. Sakthivel, S., Hidalgo, M.C., Bahnemann, D.W., Geissen, S.U., Murugesan, V., and Vogelpohl, A., A fine route to tune the photocatalytic activity of TiO_2. *Applied Catalysis B: Environmental*, **2006**. 63 (1-2): 31-40.

64. Bahnemann, D.W., Kholuiskaya, S.N., Dillert, R., Kulak, A.I., and Kokorin, A.I., Photodestruction of dichloroacetic acid catalyzed by nano-sized TiO_2 particles. *Applied Catalysis B: Environmental*, **2002**. 36 (2): 161-169.

65. Marugan, J., Aguado, J., Gernjak, W., and Malato, S., Solar photocatalytic degradation of dichloroacetic acid with silica-supported titania at pilot-plant scale. *Catalysis Today*, **2007**. 129 (1-2): 59-68.

66. Marugan, J., Hufschmidt, D., Sagawe, G., Selzer, V., and Bahnemann, D., Optical density and photonic efficiency of silica-supported TiO_2 photocatalysts. *Water Research*, **2006**. 40 (4): 833-839.

67. Enriquez, R., Beaugiraud, B., and Pichat, P., *Mechanistic implications of the effect of TiO_2 accessibility in TiO_2-SiO_2 coatings upon chlorinated organics photocatalytic removal in water*, in *Water Science and Technology*. **2004**. 147-152.

68. Doll, T.E. and Frimmel, F.H., Development of easy and reproducible immobilization techniques using TiO_2 for photocatalytic degradation of aquatic pollutants. *Acta Hydrochimica et Hydrobiologica*, **2004**. 32 (3): 201-213.

69. Bahnemann, D.W., Hilgendorff, M., and Memming, R., Charge carrier dynamics at TiO_2 particles: Reactivity of free and trapped holes. *Journal of Physical Chemistry B*, **1997**. 101 (21): 4265-4275.

70. Chemseddine, A. and Boehm, H.P., A study of the primary step in the photocahemical degradation of acetic acid and chloroacetic acids on a TiO_2 photcatalyst. *Journal of Molecular Catalysis*, **1990**. 60 (3): 295-311.

71. Kraeutler, B. and Bard, A.J., Heterogeneous photocatalytic decomposition of saturated carboxylic acids on titanium dioxide powder. Decarboxylative route to alkanes. *Journal of the American Chemical Society*, **1978**. 100 (19): 5985-5992.

72. Mao, Y., Schoeneich, C., and Asmus, K.D., Identification of organic acids and other intermediates in oxidative degradation of chlorinated ethanes on titania surfaces en route to mineralization: a combined photocatalytic and radiation chemical study. *The Journal of Physical Chemistry*, **1991**. 95 (24): 10080-10089.

73. Menendez-Flores, V.M., Friedmann, D., and Bahnemann, D.W., Durability of Ag-TiO_2 Photocatalysts Assessed for the Degradation of Dichloroacetic Acid. *International Journal of Photoenergy*, **2008**: 11.

74. Ollis, D.F., Hsiao, C.-Y., Budiman, L., and Lee, C.-L., Heterogeneous photoassisted catalysis: Conversions of perchloroethylene, dichloroethane, chloroacetic acids, and chlorobenzenes. *Journal of Catalysis*, **1984**. 88 (1): 89-96.

75. Lindner, M., Bahnemann, D.W., Hirthe, B., and Griebler, W.-D., Solar Water Detoxification: Novel TiO_2 Powders as Highly Active Photocatalysts. *Journal of Solar Energy Engineering*, **1997**. 119 (2): 120-125.

76. Harrick, N.J., Study of Physics and Chemistry of Surfaces from Frustrated Total Internal Reflections. *Physical Review Letters*, **1960**. 4 (5): 224-226.

77. Jung, A.V., Frochot, C., Parant, S., Lartiges, B.S., Selve, C., Viriot, M.L., and Bersillon, J.L., Synthesis of amino-phenolic humic-like substances and comparison with natural aquatic humic acids: A multi-analytical techniques approach. *Organic Geochemistry*, **2005**. 36 (9): 1252-1271.

78. Johnson, S.B., Brown, G.E., Healy, T.W., and Scales, P.J., Adsorption of organic matter at mineral/water interfaces. 6. Effect of inner-sphere versus outer-sphere adsorption on colloidal stability. *Langmuir*, **2005**. 21 (14): 6356-6365.

79. Kallay, N., Dojnovic, Z., and Cop, A., Surface potential at the hematite-water interface. *Journal of Colloid and Interface Science*, **2005**. 286 (2): 610-614.

80. Harju, M., Jarn, M., Dahlsten, P., Nikkanen, J.P., Rosenholm, J.B., and Mantyla, T., Influence of long-term aqueous exposure on surface properties of plasma-sprayed oxides Cr_2O_3 and Cr_2O_3-25 wt% TiO_2. *Journal of Colloid and Interface Science*, **2008**. 326 (2): 403-410.

81. Lana-Villarreal, T., Rodes, A., Perez, J.M., and Gomez, R., A spectroscopic and electrochemical approach to the study of the interactions and photoinduced electron transfer between catechol and anatase nanoparticles in aqueous solution. *Journal of the American Chemical Society*, **2005**. 127 (36): 12601-12611.

82. Gulley-Stahl, H., Hogan, P.A., Schmidt, W.L., Wall, S.J., Buhrlage, A., and Bullen, H.A., Surface Complexation of Catechol to Metal Oxides: An ATR-FTIR, Adsorption, and Dissolution Study. *Environmental Science & Technology*, **2010**. 44 (11): 4116-4121.

83. Mendive, C.B., Blesa, M.A., and Bahnemann, D., The adsorption and photodegradation of oxalic acid at the TiO_2 surface. *Water Science and Technology*, **2007**. 55 (12): 139-145.

84. Hug, S.J. and Bahnemann, D., Infrared spectra of oxalate, malonate and succinate adsorbed on the aqueous surface of rutile, anatase and lepidocrocite measured with in situ ATR-FTIR. *Journal of Electron Spectroscopy and Related Phenomena*, **2006**. 150 (2-3): 208-219.

85. Gong, D.G., Subramaniam, V.P., Highfield, J.G., Tang, Y.X., Lai, Y.K., and Chen, Z., In Situ Mechanistic Investigation at the Liquid/Solid Interface by Attenuated Total Reflectance FTIR: Ethanol Photo-Oxidation over Pristine and Platinized TiO_2 (P25). *Acs Catalysis*, **2011**. 1 (8): 864-871.

86. Mendive, C.B., Bredow, T., Blesa, M.A., and Bahnemann, D.W., ATR-FTIR measurements and quantum chemical calculations concerning the adsorption and photoreaction of oxalic acid on TiO2. *Physical Chemistry Chemical Physics*, **2006**. 8 (27): 3232-3247.

87. Savory, D.M., Warren, D.S., and McQuillan, A.J., Shallow Electron Trap, Interfacial Water, and Outer-Sphere Adsorbed Oxalate IR Absorptions Correlate during UV Irradiation of Photocatalytic TiO_2 Films in Aqueous Solution. *Journal of Physical Chemistry C*, **2011**. 115 (4): 902-907.

88. Carneiro, J.T., Almeida, A.R., Moulijn, J.A., and Mul, G., Cyclohexane selective photocatalytic oxidation by anatase TiO_2: influence of particle size and crystallinity. *Physical Chemistry Chemical Physics*, **2010**. 12 (11): 2744-2750.

89. Dobson, K.D. and McQuillan, A.J., In situ infrared spectroscopic analysis of the adsorption of aromatic carboxylic acids to TiO_2, ZrO_2, Al_2O_3, and Ta_2O_5 from aqueous solutions. *Spectrochimica Acta Part A: Molecular and Biomolecular Spectroscopy*, **2000**. 56 (3): 557-565.

90. Taylor, A.M. and Glover, A.M., Studies in Refractive Index. I and II. *J. Opt. Soc. Am.*, **1933**. 23 (6): 206-215.

91. Taylor, A.M. and Durfee, D.A., Studies in refractive index. III. *J. Opt. Soc. Am.*, **1933**. 23 (8): 263.

92. Harrick, N.J., Surface chemistry from spectral analysis of totally internally reflected radiation. *The Journal of Physical Chemistry*, **1960**. 64 (9): 1110-1114.

93. Fahrenfort, J., Attenuated total reflection: A new principle for the production of useful infra-red reflection spectra of organic compounds. *Spectrochimica Acta*, **1961**. 17 (7): 698-709.

94. Wijnja, H. and Schulthess, C.P., ATR-FTIR and DRIFT spectroscopy of carbonate species at the aged gamma-Al_2O_3/water interface. *Spectrochimica Acta Part a-Molecular and Biomolecular Spectroscopy*, **1999**. 55 (4): 861-872.

95. Arai, Y. and Sparks, D.L., ATR-FTIR spectroscopic investigation on phosphate adsorption mechanisms at the ferrihydrite-water interface. *Journal of Colloid and Interface Science*, **2001**. 241 (2): 317-326.

96. Yoon, T.H., Johnson, S.B., and Brown, G.E., Adsorption of organic matter at mineral/water interfaces. IV. Adsorption of humic substances at boehmite/water interfaces and impact on boehmite dissolution. *Langmuir*, **2005**. 21 (11): 5002-5012.

97. Fredriksson, A., Larsson, M.L., and Holmgren, A., n-Heptyl xanthate adsorption on a ZnS layer synthesized on germanium: An in situ attenuated total reflection IR study. *Journal of Colloid and Interface Science*, **2005**. 286 (1): 1-6.

98. Wang, Z., Larsson, M.L., Grahn, M., Holmgren, A., and Hedlund, J., Zeolite coated ATR crystals for new applications in FTIR-ATR spectroscopy. *Chemical Communications*, **2004** (24): 2888-2889.

99. Warren, D.S. and McQuillan, A.J., Influence of adsorbed water on phonon and UV-induced IR absorptions of TiO2 photocatalytic particle films. *Journal of Physical Chemistry B*, **2004**. 108 (50): 19373-19379.

100. Hug, S.J. and Sulzberger, B., In-situ fourier-transform infrared spectroscopy evidnece for the formtaion of several different surface complexes of oxalate on TiO_2 in the aqueous-phase. *Langmuir*, **1994**. 10 (10): 3587-3597.

101. Roddick-Lanzilotta, A.D. and McQuillan, A.J., An in situ Infrared Spectroscopic Study of Glutamic Acid and of Aspartic Acid Adsorbed on TiO_2: Implications for the Biocompatibility of Titanium. *Journal of Colloid and Interface Science*, **2000**. 227 (1): 48-54.

102. Roncaroli, F. and Blesa, M.A., Kinetics of adsorption of carboxylic acids onto titanium dioxide. *Physical Chemistry Chemical Physics*. 12 (33): 9938-9944.

103. Regazzoni, A.E., Mandelbaum, P., Matsuyoshi, M., Schiller, S., Bilmes, S.A., and Blesa, M.A., Adsorption and photooxidation of salicylic acid on titanium dioxide: A surface complexation description. *Langmuir*, **1998**. 14 (4): 868-874.

104. Rodriguez, R., Blesa, M.A., and Regazzoni, A.E., Surface complexation at the TiO_2 (anatase) aqueous solution interface: Chemisorption of catechol. *Journal of Colloid and Interface Science*, **1996**. 177 (1): 122-131.

105. Weisz, A.D., Rodenas, L.G., Morando, P.J., Regazzoni, A.E., and Blesa, M.A., FTIR study of the adsorption of single pollutants and mixtures of pollutants onto titanium dioxide in water: oxalic and salicylic acids. *Catalysis Today*, **2002**. 76 (2-4): 103-112.

106. Weisz, A.D., Regazzoni, A.E., and Blesa, M.A., ATR-FTIR study of the stability trends of carboxylate complexes formed on the surface of titanium dioxide particles immersed in water. *Solid State Ionics*, **2001**. 143 (1): 125-130.

107. Degussa Technical Bulletin Pigments.56, **1984**.

108. Patterson, A.L., The Scherrer Formula for X-Ray Particle Size Determination. *Physical Review*, **1939**. 56 (10): 978.

109. Gumy, D., Rincon, A.G., Hajdu, R., and Pulgarin, C., Solar photocatalysis for detoxification and disinfection of water: Different types of suspended and fixed TiO_2 catalysts study. *Solar Energy*, **2006**. 80 (10): 1376-1381.

110. Herrmann, M., Kaluza, U., and Boehm, H.P., Über die Chemie der Oberfläche des Titandioxids. IV. Austausch von Hydroxidionen gegen Fluoridionen. *Zeitschrift Fur Anorganische Und Allgemeine Chemie*, **1970**. 372 (3): 308-313.

111. Boehm, H.P. and Herrmann, M., Ueber die Chemie der Oberflaeche des Titandioxids I Bestimmung des Aktiven Wasserstoffs Thermische Entawasserung und Rehydroxilierung. *Zeitschrift Fur Anorganische Und Allgemeine Chemie*, **1967**. 352 (3-4): 156-167.

112. Tao, Z.Y. and Chu, T.W., On the applicability of the Langmuir equation to estimation of adsorption equilibrium constants on a powdered solid from aqueous solution. *Journal of Colloid and Interface Science*, **2000**. 231 (1): 8-12.

113. Lovato, M.E., Martin, C.A., and Cassano, A.E., Degradation of dichloroacetic acid in homogeneous aqueous media employing ozone and UVC radiation. *Photochemical & Photobiological Sciences*, **2011**. 10 (3): 367-380.

114. Kun, R., Szekeres, M., and Dekany, I., Photooxidation of dichloroacetic acid controlled by pH-stat technique using TiO_2/layer silicate nanocomposites. *Applied Catalysis B-Environmental*, **2006**. 68 (1-2): 49-58.

115. Ballari, M.D., Alfano, O.O., and Cassano, A.E., Photocatalytic Degradation of Dichloroacetic Acid. A Kinetic Study with a Mechanistically Based Reaction Model. *Industrial & Engineering Chemistry Research*, **2009**. 48 (4): 1847-1858.

116. Wang, K.P., Guo, J.S., Yang, M., Junji, H., and Deng, R.S., Decomposition of two haloacetic acids in water using UV radiation, ozone and advanced oxidation processes. *Journal of Hazardous Materials*, **2009**. 162 (2-3): 1243-1248.

117. Xu, Z., Zhonglin, C., An, L., Shuqing, Z., He, W., and Lei, Y. Degradation of dichloroacetic acid in acidic solution by nanosized ZnO Catalyzed ozonation. in *2010 International Conference on Challenges in Environmental Science and Computer Engineering (CESCE 2010)*. **2010**. Wuhan, China: IEEE Computer Society.

118. Sagawe, G., Satuf, M.L., Brandi, R.J., Muschner, J.P., Federer, C., Alfano, O.M., Bahnemann, D., and Cassano, A.E., Analysis of Photocatalytic Reactors Employing the Photonic Efficiency and the Removal Efficiency Parameters: Degradation of Radiation Absorbing and Nonabsorbing Pollutants. *Industrial & Engineering Chemistry Research*, **2010**. 49 (15): 6898-6908.

119. Castillo, N.C., Ding, L., Heel, A., Graule, T., and Pulgarin, C., On the photocatalytic degradation of phenol and dichloroacetate by $BiVO_4$: The need of a sacrificial electron acceptor. *Journal of Photochemistry and Photobiology A-Chemistry*, **2010**. 216 (2-3): 221-227.

120. Robert, D., Parra, S., Pulgarin, C., Krzton, A., and Weber, J.V., Chemisorption of phenols and acids on TiO_2 surface. *Applied Surface Science*, **2000**. 167 (1-2): 51-58.

121. Hilgendorff, M., *Untersuchungen zur Bedeutung der Adsorption in der Photokatalyse*, in *Physikalische Chemie*. **1995**, Universität Hannover: Hannover. 173.

122. Stumm, W., Sigg, L., and Sulzberger, B., *Chemistry of the solid-water interface: processes at the mineral-water and particle-water interface in natural systems*. **1992**: Wiley.

123. Duval, J., Lyklema, J., Kleijn, J.M., and van Leeuwen, H.P., Amphifunctionally electrified interfaces: Coupling of electronic and ionic surface-charging processes. *Langmuir*, **2001**. 17 (24): 7573-7581.

124. Yates, D.E., Levine, S., and Healy, T.W., Site-binding model of the electrical double layer at the oxide/water interface. *Journal of the Chemical Society, Faraday Transactions 1: Physical Chemistry in Condensed Phases*, **1974**. 70: 1807-1818.

125. Krimm, S., The infrared spectra of complex molecules, Vol. 1 (3rd ed.), L. J. Bellamy, Halsted Press, a division of John Wiley & Sons, Inc., New York, **1975**, 433 pp.

126. Bellamy, L.J., The infrared spectra of complex molecules. *Journal of Polymer Science: Polymer Letters Edition*, **1976**. 14.

127. Joung, S.K., Amemiya, T., Murabayashi, M., and Itoh, K., Adsorbed species on TiO_2 associated with the photocatalytic oxidation of trichloroethylene under UV. *Journal of Photochemistry and Photobiology A-Chemistry*, **2006**. 184 (3): 273-281.

128. Segarra, X. **2010**: Theoretical calculations performed by Xavier Segarra, University of Valencia, Spain.

129. Spinner, E., The vibration spectra of some substituted acetate ions. *Journal of the Chemical Society (Resumed)*, **1964**: 4217-4226.

130. Abdullah, M., Low, G.K.C., and Matthews, R.W., Effects of common inorganic anions on rates of photocatalytic oxidation of organic-carbon over illumintated titanium-dioxide. *Journal of Physical Chemistry*, **1990**. 94 (17): 6820-6825.

131. Bekbolet, M., Boyacioglu, Z., and Ozkaraova, B., The influence of solution matrix on the photocatalytic removal of color from natural waters. *Water Science and Technology*, **1998**. 38 (6): 155-162.

132. Mohamed, H.H., Mendive, C.B., Dillert, R., and Bahnemann, D.W., Kinetic and Mechanistic Investigations of Multielectron Transfer Reactions Induced by Stored Electrons in TiO_2 Nanoparticles: A Stopped Flow Study. *Journal of Physical Chemistry A*, **2011**. 115 (11): 2139-2147.

133. Mendive, C.B., Bahnemann, D.W., and Blesa, M.A., Microscopic characterization of the photocatalytic oxidation of oxalic acid adsorbed onto TiO_2 by FTIR-ATR. *Catalysis Today*, **2005**. 101 (3-4): 237-244.

134. Roncaroli, F. and Blesa, M.A., Kinetics of adsorption of carboxylic acids onto titanium dioxide. *Physical Chemistry Chemical Physics*, **2010**. 12 (33): 9938-9944.

135. Bamba, D., Atheba, P., Robert, D., Trokourey, A., and Dongui, B., Photocatalytic degradation of the diuron pesticide. *Environmental Chemistry Letters*, **2008**. 6 (3): 163-167.

136. Venyaminov, S.Y. and Prendergast, F.G., Water (H_2O and D_2O) Molar Absorptivity in the 1000-4000 cm^{-1} Range and Quantitative Infrared Spectroscopy of Aqueous Solutions. *Analytical Biochemistry*, **1997**. 248 (2): 234-245.

137. *CRC Handbook of Chemistry and Physics*, Vol. 88th Edition. **2007**: CRC Press.

138. Max, J.J. and Chapados, C., Infrared spectroscopy of aqueous carboxylic acids: Malic acid. *Journal of Physical Chemistry A*, **2002**. 106 (27): 6452-6461.

139. Mattsson, A. and Osterlund, L., Adsorption and Photoinduced Decomposition of Acetone and Acetic Acid on Anatase, Brookite, and Rutile TiO_2 Nanoparticles. *Journal of Physical Chemistry C*, **2010**. 114 (33): 14121-14132.

140. Backes, M.J., Lukaski, A.C., and Muggli, D.S., Active sites and effects of H_2O and temperature on the photocatalytic oxidation of 13C-acetic acid on TiO_2. *Applied Catalysis B: Environmental*, **2005**. 61 (1-2): 21-35.

141. Rotzinger, F.P., Kesselman-Truttmann, J.M., Hug, S.J., Shklover, V., and Gratzel, M., Structure and Vibrational Spectrum of Formate and Acetate Adsorbed from Aqueous Solution onto the TiO_2 Rutile (110) Surface. *The Journal of Physical Chemistry B*, **2004**. 108 (16): 5004-5017.

142. El-Maazawi, M., Finken, A.N., Nair, A.B., and Grassian, V.H., Adsorption and Photocatalytic Oxidation of Acetone on TiO_2: An in Situ Transmission FT-IR Study. *Journal of Catalysis*, **2000**. 191 (1): 138-146.

143. Committee, A.o.L.S.S.D.W. and Committee, N.R.C.C.o.L.S.S.D.W., *Drinking water and health*. **1980**: National Academy of Sciences.

144. Gines, J.M., PerezMartinez, J.I., Arias, M.J., Moyano, J.R., Morillo, E., RuizConde, A., and SanchezSoto, P.J., Inclusion of the herbicide 2,4-dichlorophenoxyacetic acid (2,4-D) with beta-cyclodextrin by different processing methods. *Chemosphere*, **1996**. 33 (2): 321-334.

145. Goyne, K.W., Chorover, J., Zimmerman, A.R., Komarneni, S., and Brantley, S.L., Influence of mesoporosity on the sorption of 2,4-dichlorophenoxyacetic acid onto alumina and silica. *Journal of Colloid and Interface Science*, **2004**. 272 (1): 10-20.

146. Silverstein, R.M., Webster, F.X., and Kiemle, D.J., *Spectrometric identification of organic compounds*. **2005**: John Wiley & Sons.

147. Herrmann, M. and Boehm, H.P., Über die Chemie der Oberfläche des Titandioxids. II. Saure Hydroxylgruppen auf der Oberfläche. *Zeitschrift Fur Anorganische Und Allgemeine Chemie*, **1969**. 368 (1-2): 73-86.

148. Flaig-Baumann, R., Herrmann, M., and Boehm, H.P., Über die Chemie der Oberfläche des Titandioxids. III. Reaktionen der basischen Hydroxylgruppen auf der Oberfläche. *Zeitschrift Fur Anorganische Und Allgemeine Chemie*, **1970**. 372 (3): 296-307.

149. Vasudevan, D. and Stone, A.T., Adsorption of 4-Nitrocatechol, 4-Nitro-2-Aminophenol, and 4-Nitro-1,2-Phenylenediamine at the Metal (Hydr)Oxide/Water Interface: Effect of Metal (Hydr)Oxide Properties. *Journal of Colloid and Interface Science*, **1998**. 202 (1): 1-19.

150. Koretsky, C.M., Sverjensky, D.A., and Sahai, N., A model of surface site types on oxide and silicate minerals based on crystal chemistry: Implications for site types and densities, multi-site adsorption, surface infrared spectroscopy, and dissolution kinetics. *American Journal of Science*, **1998**. 298 (5): 349-438.

151. Roncaroli, F. and Blesa, M.A., Kinetics of adsorption of oxalic acid on different titanium dioxide samples. *Journal of Colloid and Interface Science*. 356 (1): 227-233.

152. Pettibone, J.M., Cwiertny, D.M., Scherer, M., and Grassian, V.H., Adsorption of organic acids on TiO_2 nanoparticles: Effects of pH, nanoparticle size, and nanoparticle aggregation. *Langmuir*, **2008**. 24 (13): 6659-6667.

153. Krysa, J., Waldner, G., Mest'ankova, H., Jirkovsky, J., and Grabner, G., Photocatalytic degradation of model organic pollutants on an immobilized particulate TiO_2 layer - Roles of adsorption processes and mechanistic complexity. *Applied Catalysis B-Environmental*, **2006**. 64 (3-4): 290-301.

154. Duckworth, O.W. and Martin, S.T., Surface complexation and dissolution of hematite by C-1-C-6 dicarboxylic acids at pH=5.0. *Geochimica Et Cosmochimica Acta*, **2001**. 65 (23): 4289-4301.

155. Scaranto, J., Charmet, A.P., Stoppa, P., and Giorgianni, S., Vinyl halides adsorbed on TiO_2 surface: FTIR spectroscopy studies and ab initio calculations. *Journal of Molecular Structure*, **2005**. 741 (1-3): 213-219.

156. Ivanova, I. **2010**, Experiments performed by Irina Ivanova at the Leibniz Universität Hannover: Hannover.

157. Maçôas, E.M.S., Khriachtchev, L., Fausto, R., and Räsänen, M., Photochemistry and Vibrational Spectroscopy of the Trans and Cis Conformers of Acetic Acid in Solid Ar. *The Journal of Physical Chemistry A*, **2004**. 108 (16): 3380-3389.

158. Takeuchi, M., Martra, G., Coluccia, S., and Anpo, M., Investigations of the structure of H_2O clusters adsorbed on TiO_2 surfaces by near-infrared absorption spectroscopy. *Journal of Physical Chemistry B*, **2005**. 109 (15): 7387-7391.

159. Wang, C.Y., Pagel, R., Dohrmann, J.K., and Bahnemann, D.W., Antenna mechanism and deaggregation concept: novel mechanistic principles for photocatalysis. *Comptes Rendus Chimie*, **2006**. 9 (5-6): 761-773.

160. Hufschmidt, D., Bahemann, D., Testa, J.J., Emilio, C.A., and Litter, M.I., Enhancement of the photocatalytic activity of various TiO_2 materials by platinisation. *Journal of Photochemistry and Photobiology A-Chemistry*, **2002**. 148 (1-3): 223-231.

161. Brunella, M.F., Diamanti, M.V., Pedeferri, M.P., Di Fonzo, F., Casari, C.S., and Bassi, A.L., Photocatalytic behavior of different titanium dioxide layers. *Thin Solid Films*, **2007**. 515 (16): 6309-6313.

162. Daneshvar, N., Salari, D., Niaei, A., and Khataee, A.R., Photocatalytic degradation of the herbicide erioglaucine in the presence of nanosized titanium dioxide: Comparison and modeling of reaction kinetics. *Journal of Environmental Science and Health Part B-Pesticides Food Contaminants and Agricultural Wastes*, **2006**. 41 (8): 1273-1290.

163. Zhang, J.L., Xu, H.S., Chen, H.J., and Anpo, M., Study on the formation of H_2O_2 on TiO_2 photocatalysts and their activity for the photocatalytic degradation of X-GL dye. *Research on Chemical Intermediates*, **2003**. 29 (7-9): 839-848.

164. Lindner, M., Theurich, J., and Bahnemann, D.W., Photocatalytic degradation of organic compounds: Accelerating the process efficiency. *Water Science and Technology*, **1997**. 35 (4): 79-86.

165. Liao, L.-F., Lien, C.-F., and Lin, J.-L., FTIR study of adsorption and photoreactions of acetic acid on TiO_2. *Physical Chemistry Chemical Physics*, **2001**. 3 (17): 3831-3837.

166. Nakamoto, K., *Infrared and Raman Spectra of Inorganic and Coordination Compounds: Theory and applications in inorganic chemistry*. **2009**: Wiley.

167. Araujo, P.Z., Mendive, C.B., Rodenas, L.A.G., Morando, P.J., Regazzoni, A.E., Blesa, M.A., and Bahnemann, D., FT-IR-ATR as a tool to probe photocatalytic interfaces. *Colloids and Surfaces A-Physicochemical and Engineering Aspects*, **2005**. 265 (1-3): 73-80.

168. Tauchert, E., Ivanova, I., Atitar, F., and Mendive, C. **2010**: Photocatalytic degradation of acetic acid and chlorinated acids in batch system, unpublished work. Hannover.

169. Parra, S., Olivero, J., and Pulgarin, C., Relationships between physicochemical properties and photoreactivity of four biorecalcitrant phenylurea herbicides in aqueous TiO_2 suspension. *Applied Catalysis B-Environmental*, **2002**. 36 (1): 75-85.

170. Hansen, R.S. and Craig, R.P., The Adsorption of Aliphatic Alcohols and Acids from Aqueous Solutions by Non-porous Carbons. *The Journal of Physical Chemistry*, **1954**. 58 (3): 211-215.

171. Stafford, U., Gray, K.A., Kamat, P.V., and Varma, A., An in situ diffuse reflectance FTIR investigation of photocatalytic degradation of 4-chlorophenol on a TiO_2 powder surface. *Chemical Physics Letters*, **1993**. 205 (1): 55-61.

172. Zhou, J., Dag, S., Senanayake, S.D., Hathorn, B.C., Kalinin, S.V., Meunier, V., Mullins, D.R., Overbury, S.H., and Baddorf, A.P., Adsorption, desorption, and dissociation of benzene on TiO_2(110) and Pd/TiO_2(110): Experimental characterization and first-principles calculations. *Physical Review B*, **2006**. 74 (12): 11.

173. Orlov, A., Watson, D.J., Tikhov, W.M., and Lambert, R.M., Interactions of 4-chlorophenol with TiO_2 polycrystalline surfaces: A study of environmental interfaces by NEXAFS, XPS, and UPS. *Langmuir*, **2007**. 23 (19): 9551-9554.

174. Giri, R.R., Ozaki, H., Takanami, R., and Taniguchi, S., Heterogeneous photocatalytic ozonation of 2,4-D in dilute aqueous solution with TiO_2 fiber. *Water Science and Technology*, **2008**. 58 (1): 207-216.

175. Peller, J., Wiest, O., and Kamat, P.V., Mechanism of hydroxyl radical-induced breakdown of the herbicide 2,4-Dichlorophenoxyacetic acid (2,4-D). *Chemistry - A European Journal*, **2003**. 9 (21): 5379-5387.

8 Appendix

8.1 Additional data

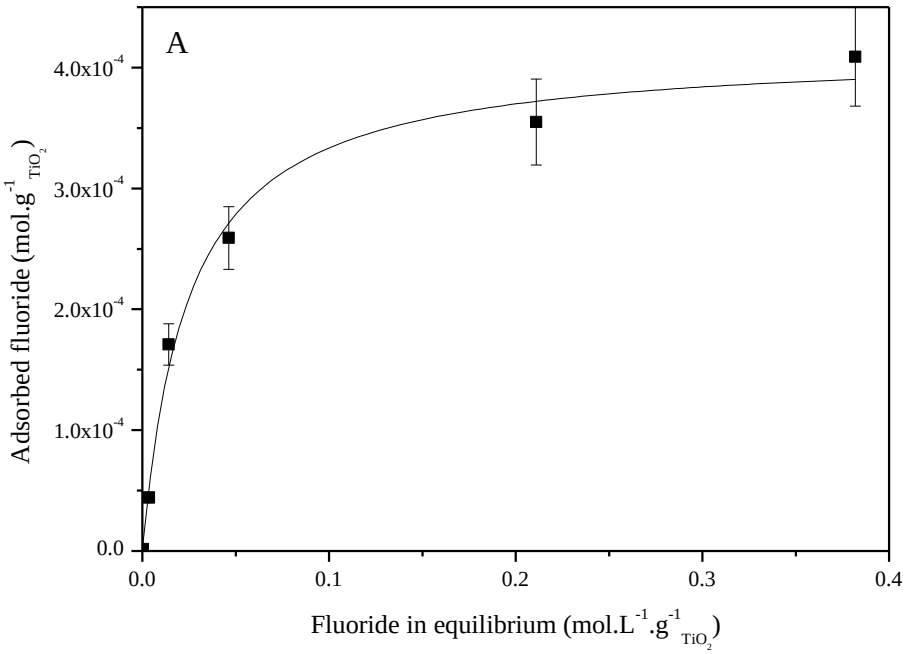

Figure 60: Adsorption isotherm for fluoride anions on anatase (PC500) powder. Dots are the experimental data and the line is the fitting curve obtained from the Langmuir isotherm model.

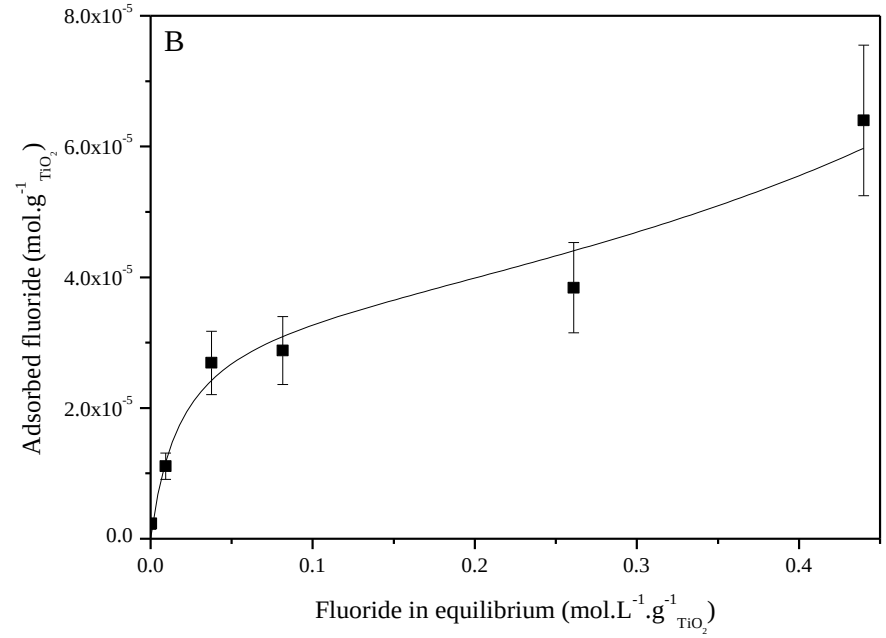

Figure 61: Adsorption isotherm for fluoride anions on rutile (R15) powder. Dots are the experimental data and the line is the fitting curve obtained from the BET isotherm model.

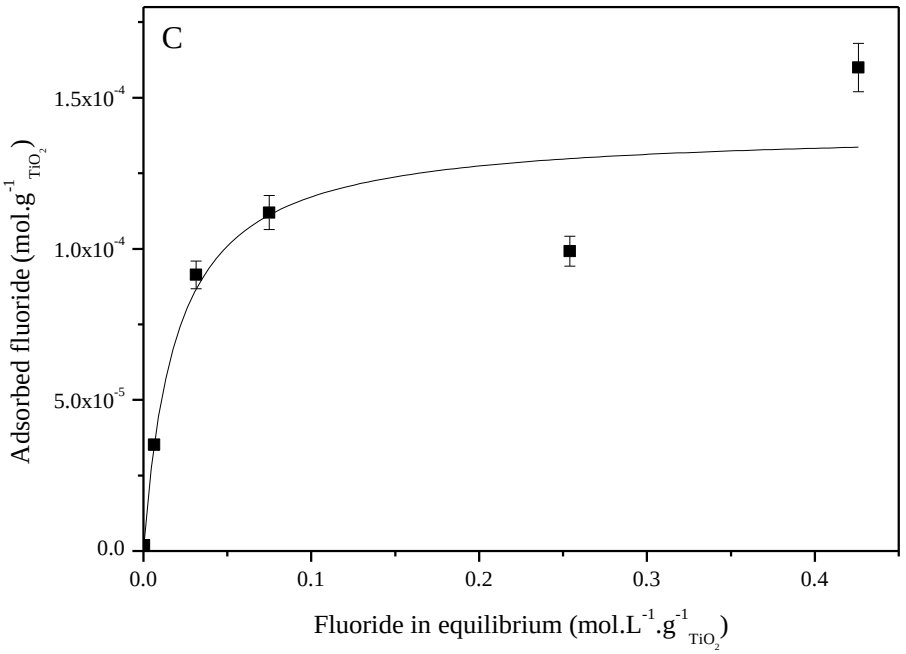

Figure 62: Adsorption isotherm of fluoride anions on P25 powder. Dots are the experimental data and the line is the fitting curve obtained from the Langmuir isotherm model.

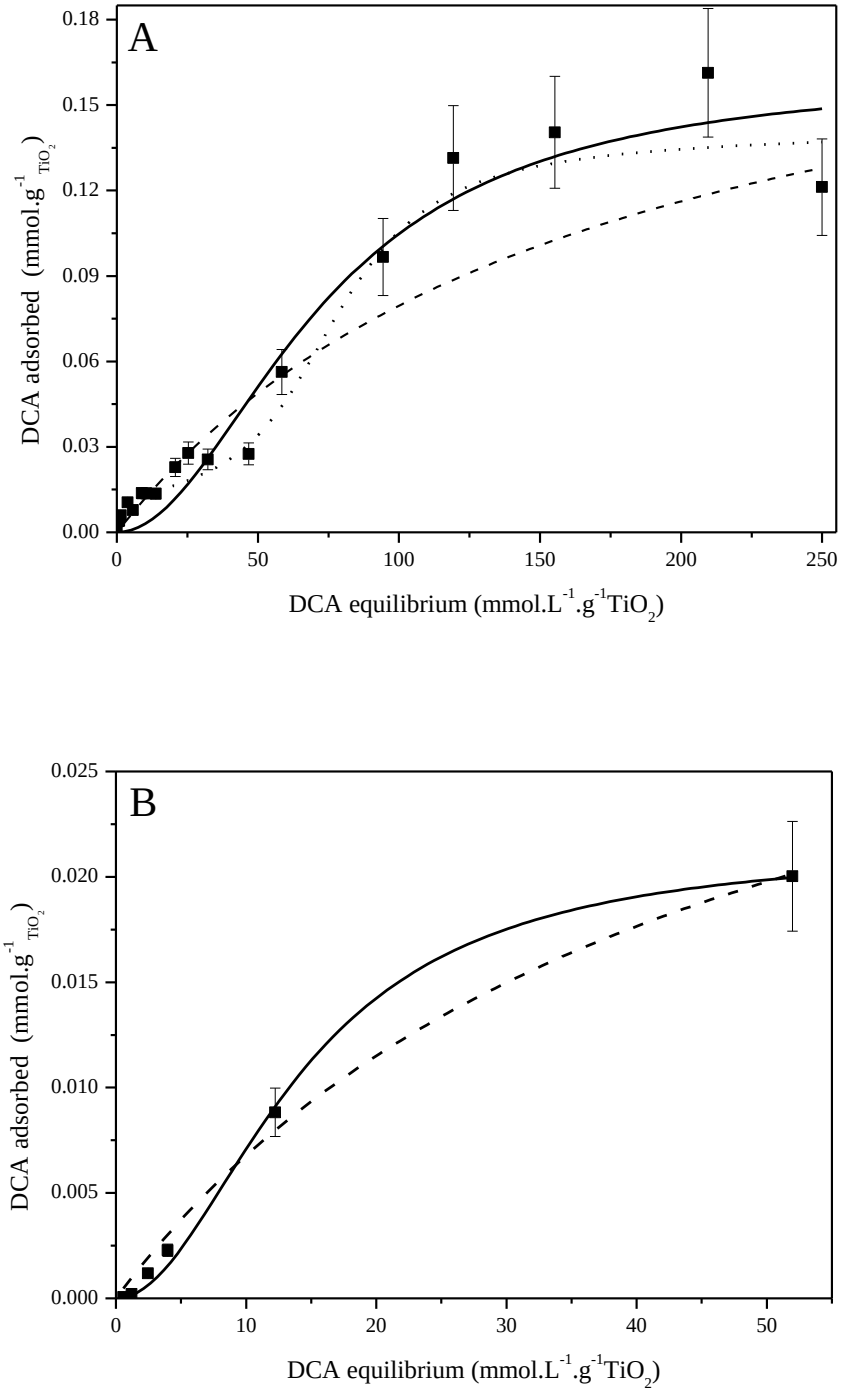

Figure 63: A - DCA (pH 3.0) adsorption isotherm on P25. The black line is the fitting to the modified Langmuir isotherm equation, the dashed line is the fitting to the Langmuir isotherm equation, and the pointed line is the fitting to the BET isotherm equation. B - DCA (pH 9.0) adsorption isotherm on PC500. The black line is the fitting to the modified Langmuir isotherm equation, and the dashed line is the fitting to the Langmuir isotherm equation.

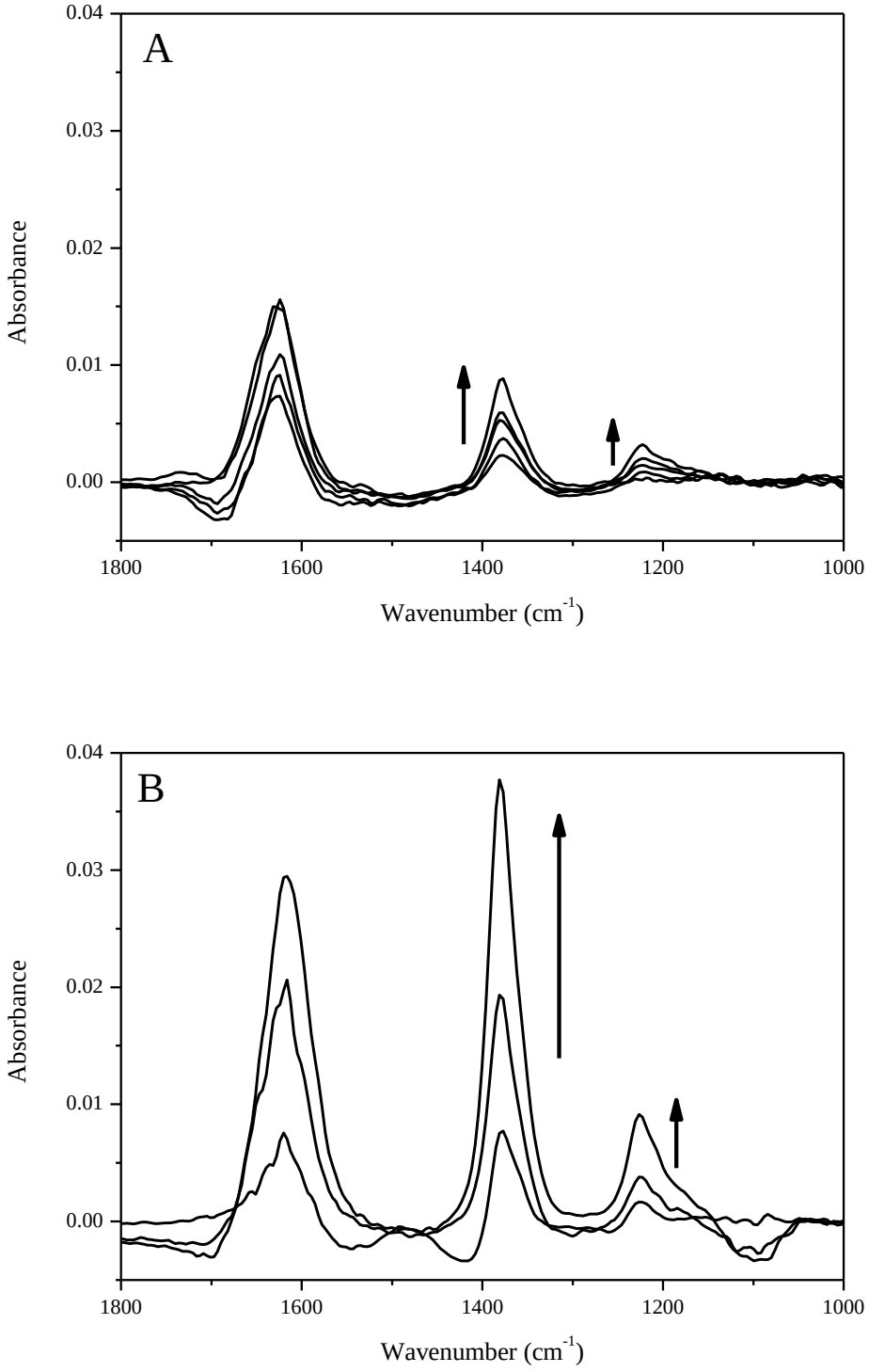

Figure 64: A - ATR-FTIR spectra of DCA (different concentrations), pH 4.0 in 10.0 mmol·L^{-1} KNO_3: on a ZnSe crystal (1.0, 2.0, 3.0, 5.0 and 10.0 mmol·L^{-1}), taken after 15 min. Arrows in the figures indicate the direction of the spectral changes with increase of the concentration. B - ATR-FTIR spectra of DCA (different concentrations), at pH 4.0 in 10.0 mmol·L^{-1} KNO_3: on a PC500 film (0.5, 1.0 and 2.0 mmol·L^{-1}) taken after 15 min. Arrows in the figures indicate the direction of the spectral changes with increase of the concentration.

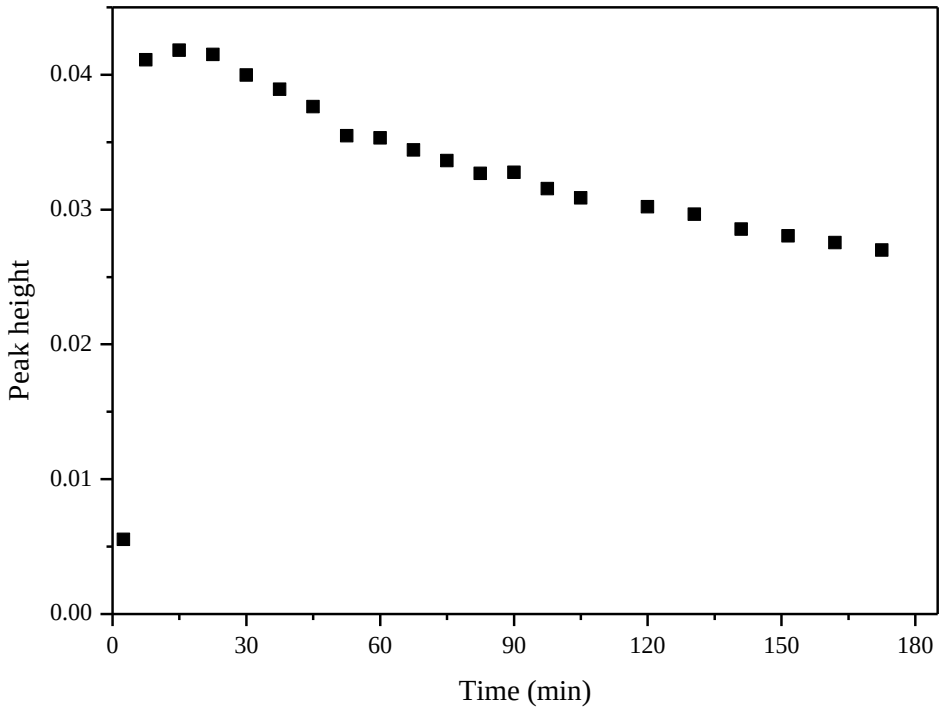

Figure 65: Evolution of the peak height from the ATR-FTIR spectral band centered at 1381 cm^{-1} for DCA (20.0 $mmol \cdot L^{-1}$) solution at pH 4.0 on a TiO_2 (PC500) film in 10.0 $mmol \cdot L^{-1}$ KNO_3.

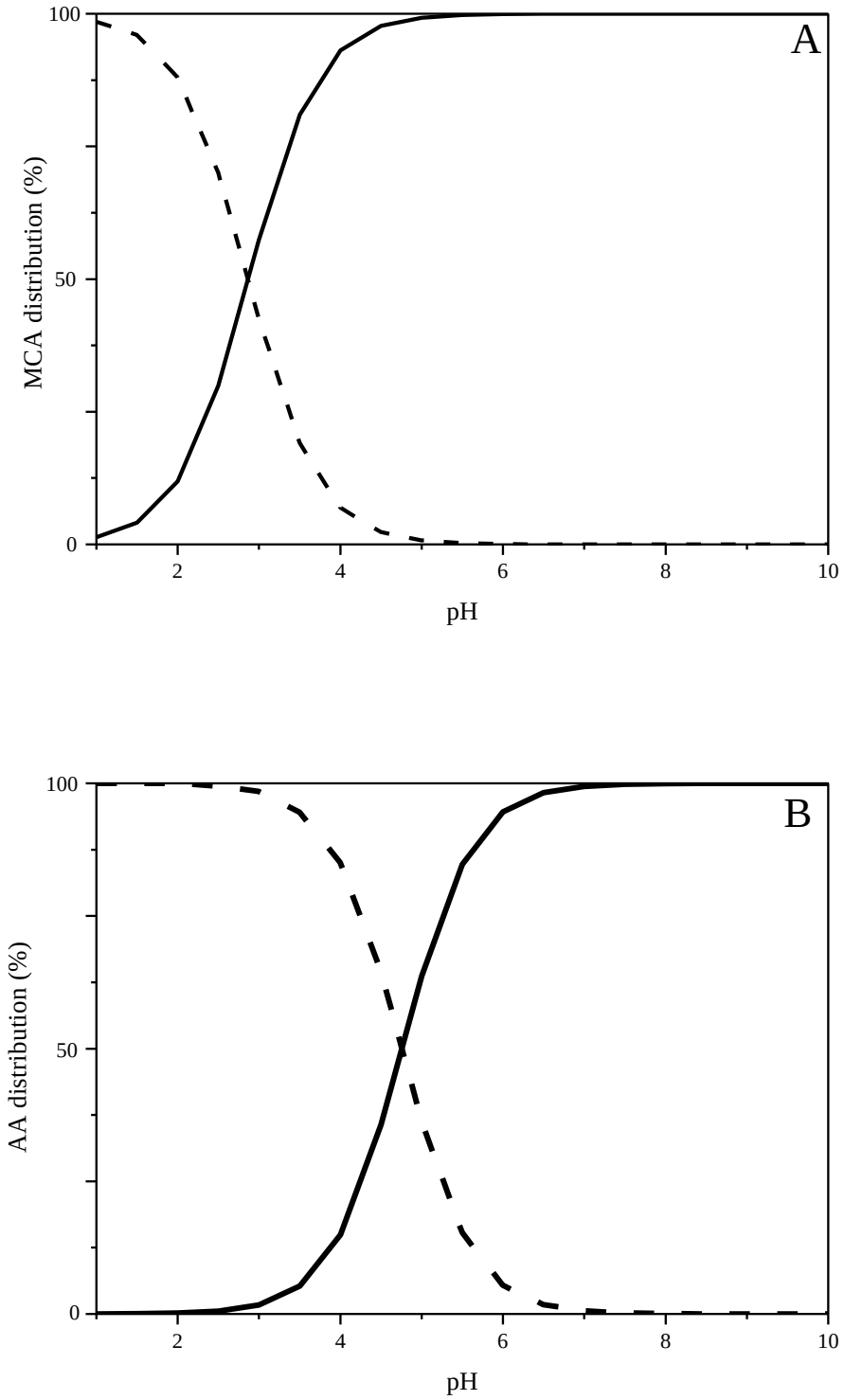

Figure 66: A - Distribution of monochloroacetic acid (– –) and monochloroacetate (——) as a function of the pH condition, calculated based upon its dissociation constant, pK_a = 2.87 [137]. B - Distribution of AA (– –) and AA^- (——) as a function of the pH condition, calculated based upon its dissociation constant, pK_a = 4.75 [137].

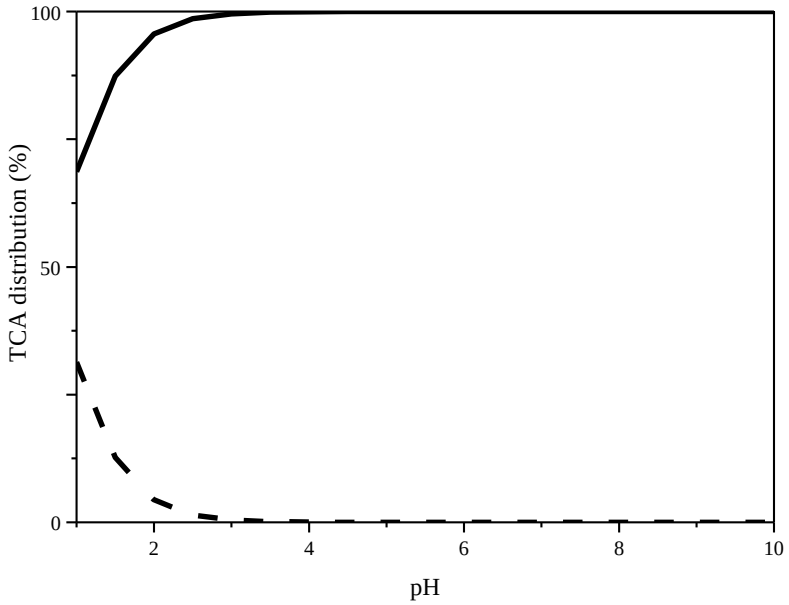

Figure 67: Distribution of TCA (– –) and TCA^- (——) as a function of the pH condition, calculated based upon its dissociation constant, $pK_a = 0.7$ [137].

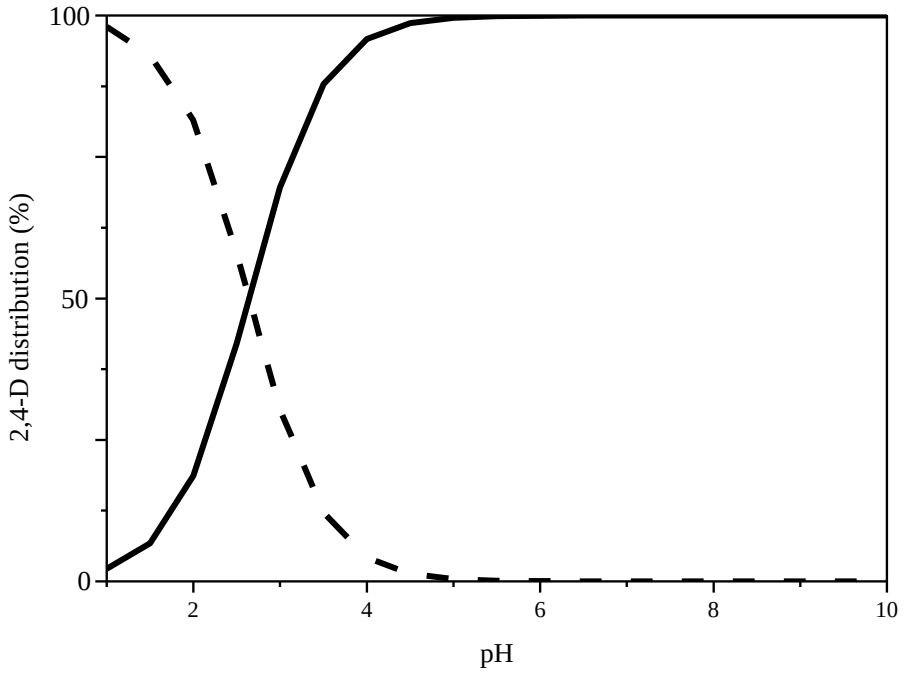

Figure 68: Distribution of 2,4-Dichlorophenoxyacetic acid (– –) and 2,4-Dichlorophenoxyacetate (——) as a function of the pH condition, calculated based upon its dissociation constant.

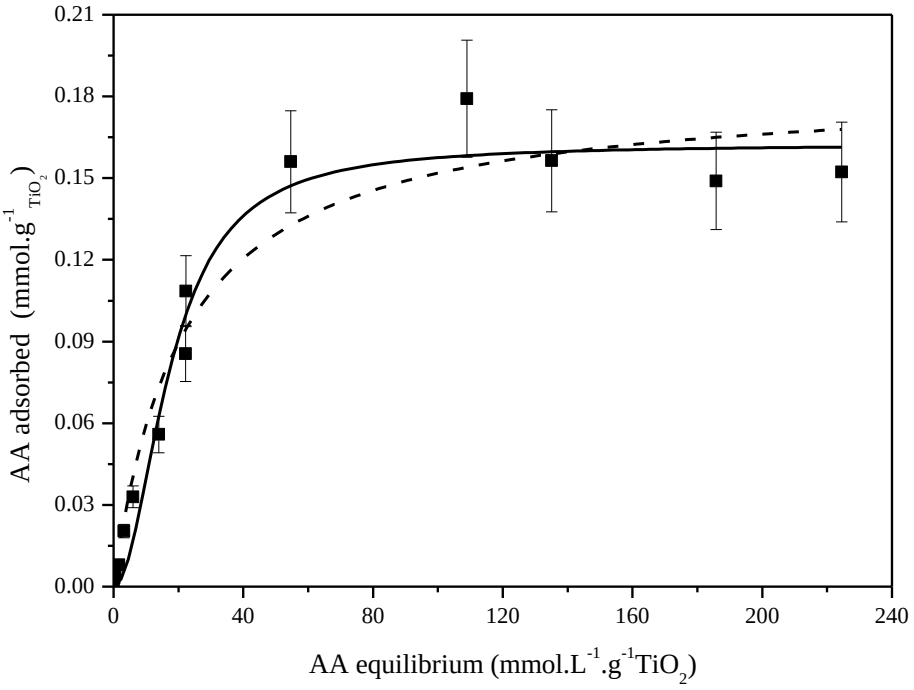

Figure 69: Acetic acid (pH 3.0) adsorption isotherm on PC500. The black line is the fitting to the modified Langmuir isotherm equation, and the dashed line is the fitting to the Langmuir isotherm equation.

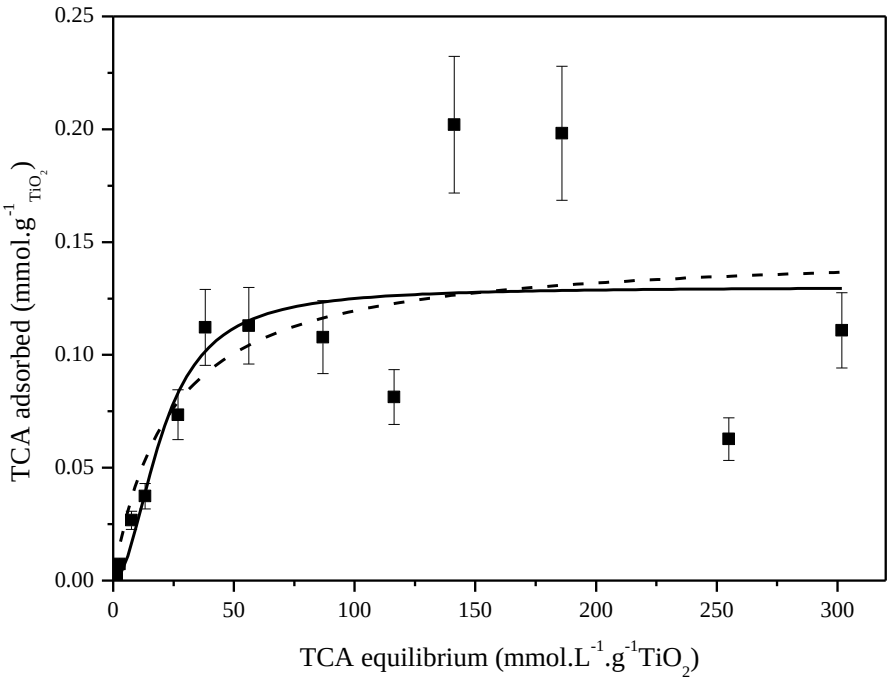

Figure 70: Trichloroacetic acid (pH 3.0) adsorption isotherm on PC500. The black line is the fitting to the modified Langmuir isotherm equation, and the dashed line is the fitting to the Langmuir isotherm equation.

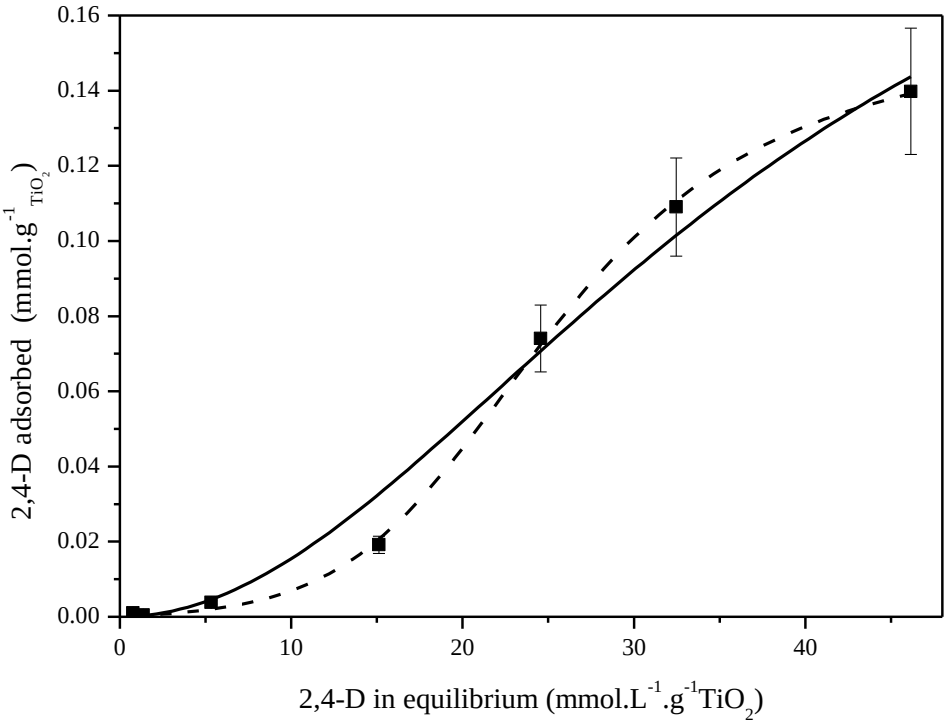

Figure 71: 2,4-D (pH 2.9) adsorption isotherm on PC500. The black line is the fitting to the modified Langmuir isotherm equation, and the dashed line is the fitting to the BET isotherm equation.

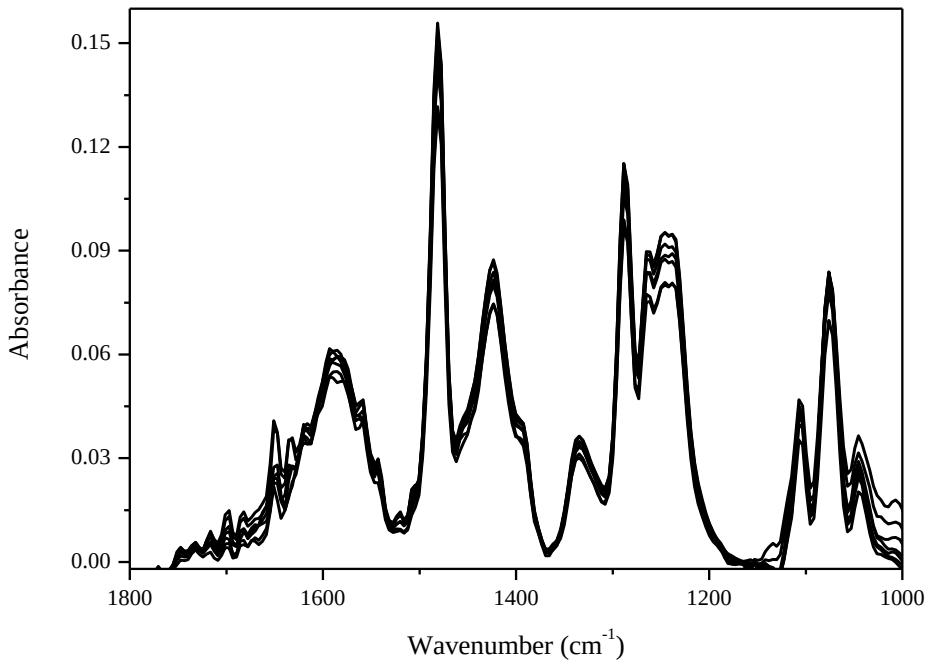

Figure 72: Evolution of ATR-FTIR spectra for an anatase TiO_2 film (PC500) 2.7 mmol·L^{-1} 2,4-D solution at pH 2.9 in 10.0 mmol·L^{-1} KNO_3. The spectra have been taken after 10, 15, 30, 60 and 120 min of equilibration.

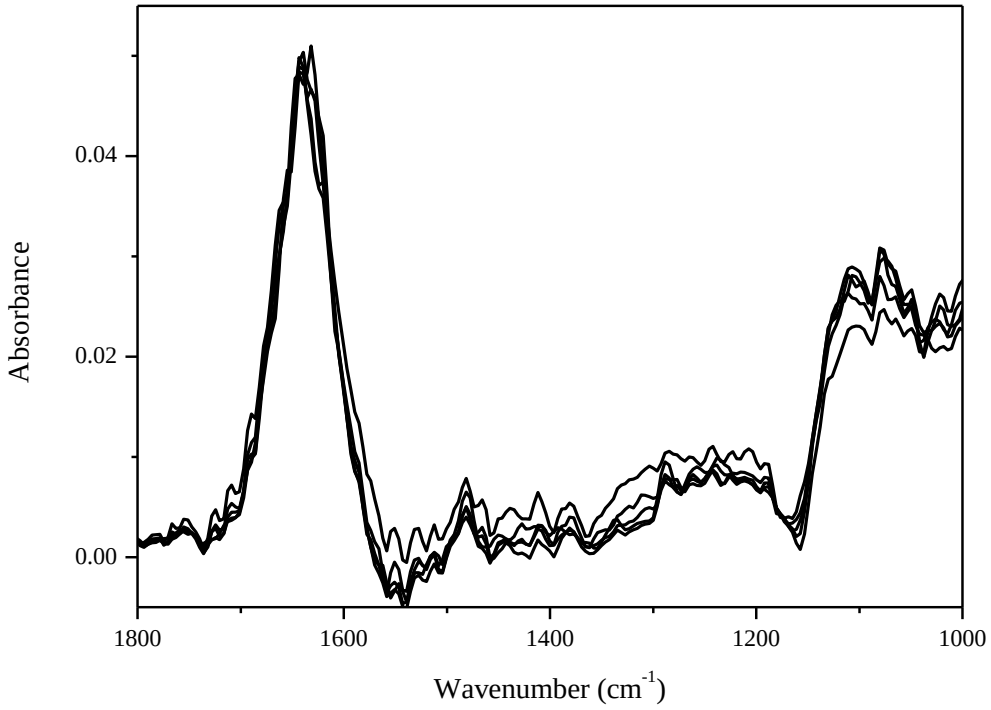

Figure 73: Evolution of ATR-FTIR spectra for an anatase TiO_2 film (PC500) in 0.5 mmol·L^{-1} 2,4-D solution at pH 2.9 in 10.0 mmol·L^{-1} KNO_3. The first spectrum has been taken after 90 min dark-equilibration, the following spectra were taken 30, 45, 60 and 90 min after starting the UV irradiation (with a light intensity of 1.0 mW·cm^{-2}).

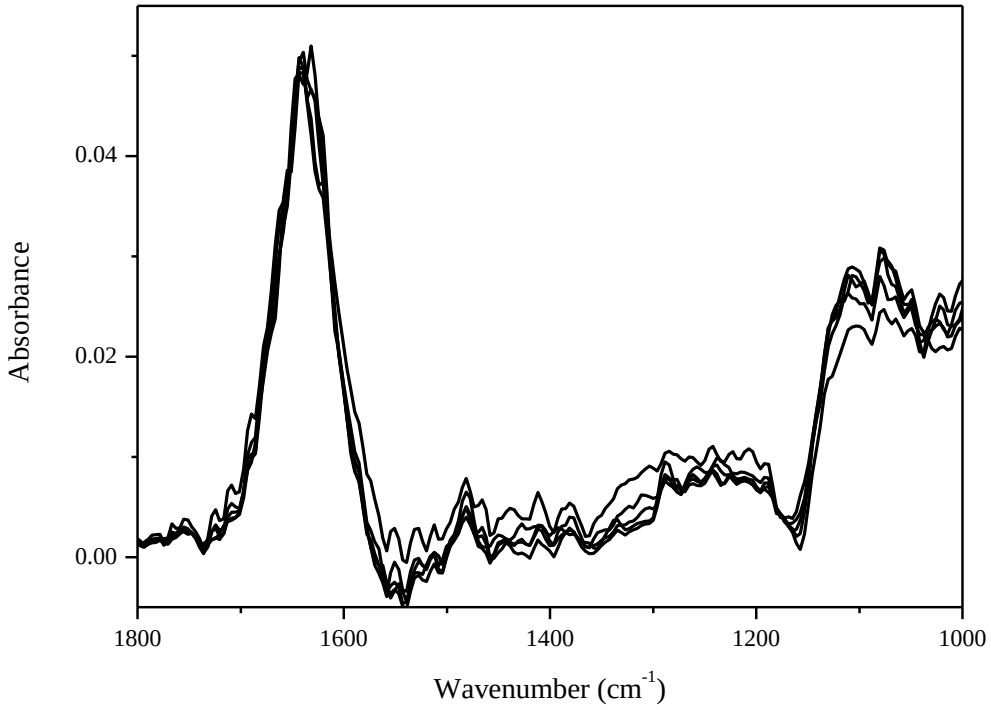

Figure 74: Evolution of the ATR-FTIR spectra for an anatase TiO_2 film (PC500) in 0.5 mmol·L^{-1} 2,4-D solution at pH 2.9 in 10.0 mmol·L^{-1} KNO_3. The first spectrum has been taken after 90 min dark-equilibration, the following spectra were taken 30, 45, 60, and 90 min after starting the UV irradiation (with a light intensity of 1.0 mW·cm^{-2}).

Curriculum Vitae

Personal Profile

Elias Tauchert

born the 1st of March 1982 in Cunha Porã - Brazil.

Private Address: Haltenhoffstr. 22, D-30167, Hannover, Germany.

Email: eliascdtauchert@yahoo.com.br.

04/2007-03/2012	**PhD student** in chemistry at the Institute for technical chemistry - Leibniz Universität Hannover. Main fields: Photocatalysis and surface. Supervisor: Prof. Dr. Detlef Bahnemann.
12/2006-03/2007	**German course (DSH-1)** - Carl Duisberg Centrum in Köln, Germany.
05/2006-11/2006	preparation for the PhD - Brazil (Bureaucratic procedures and language course)
05/2004-04/2006	**Master of Science - Main topic: Analytical Chemistry** Universidade Federal do Paraná, Curitiba, PR - Brazil. Supervisor: Prof. Dr. Patricio Peralta-Zamora.
02/2000-03/2004	**Bachelor in Chemistry - Note: 0,817** - Universidade Federal do Paraná, Curitiba, PR - Brazil.
1997-1999	**High school -** Colégio Estadual N. Sª da Salete, Maravilha, SC - Brazil.